DIAGNOSIS OF INTER TURN SHORT CIRCUIT FAULT IN PERMANENT MAGNET SYNCHRONOUS MACHINES

by

Yuan Qi

APPROVED BY SUPERVISORY COMMITTEE:

_____

Dr. Bilal Akin, Chair

_____

Dr. Babak Fahimi

_____

Dr. Ghanshyamsinh Gohil

_____

Dr. Mehrdad Nourani

DIAGNOSIS OF INTER TURN SHORT CIRCUIT FAULT IN PERMANENT MAGNET SYNCHRONOUS MACHINES

by

YUAN QI, MS

DISSERTATION

Presented to the Faculty of

The University of Texas at Dallas

in Partial Fulfillment

of the Requirements

for the Degree of

DOCTOR OF PHILOSOPHY IN

ELECTRICAL ENGINEERING

THE UNIVERSITY OF TEXAS AT DALLAS

December 2018

ACKNOWLEDGMENTS

I would like to express my appreciation to my committee chair, Dr. Bilal Akin, for the continuous encouragement, patient guidance and insightful advice during my PhD studies. Not only did his immense knowledge help me in writing this dissertation but also his great personality supported me to overcome the obstacles in my research career. It was an honor for me to be a PhD student under his supervision.

Beside my advisor, I would like to thank the rest of my dissertation committee members: Dr. Mehrdad Nourani, Dr. Babak Fahimi and Dr. Ghanshyamsinh Gohil, for their profound comments and helpful suggestions.

I would like to give special thanks to the former and current administrative assistants, who provide extraordinary support for studying and working in the electrical engineering department.

I am grateful to Dr. Mohsen Zafarani, Dr. Emine Bostanci and Mr. Vignesh Gurusamy for their contributions in this research. In addition, I thank my fellow lab mates, Dr. Yijiang Jia, Dr. Bohang Zhu, Dr. Qicheng Huang, Dr. Zhuangyao Tang, Dr. Xiong Li, Dr. Serkan Dusmez, Dr. Syed Huzaif Ali, Dr. Taner Goktas, Mr. Enes Ugur, Mr. Shi Pu, Mr. Fei Yang, Mr. Chi Xu, Mr. Kudra Baruti and Mr. Feyzullah Erturk, for their kind help in my PhD studies. Furthermore, I would like to thank Mr. Yaoxin Qian and Mr. In Chul Jang from Schlumberger Technology Corporation for their support to this research.

Last but not the least; I would like to thank my family: my deepest appreciation goes to my wife and my parents, who provide me with moral and emotional support in my life.

October 2018

DIAGNOSIS OF INTER TURN SHORT CIRCUIT FAULT IN PERMANENT MAGNET SYNCHRONOUS MACHINES

Yuan Qi, PhD
The University of Texas at Dallas, 2018

Supervising Professor: Dr. Bilal Akin

Inter turn short circuit (ITSC) fault is one of the most common faults in permanent magnet synchronous machines (PMSM). ITSC fault has limited impact on system performance in early stages, but it can turn into several failures without proper treatment. Therefore, it is important to characterize ITSC fault of PMSM and develop reliable fault diagnosis algorithms. In the past few years, many studies proposed different kinds of ITSC fault detection algorithms, such as motor current signature analysis, parameter identifications, real-time estimators and searching coils. Recently, the study about ITSC fault mitigation algorithms has drawn more attentions due to its potential of extending the fault machine lifetime. Instead of immediate replacement, the fault machine can operate with proper control techniques, which can prevent the deterioration of existing ITSC fault and reduce the risk of system total failure. This technique is essential to mission and cost critical systems, which are unable to replace the fault machine immediately. By applying fault mitigation algorithms, the fault machine can still operate until the next available maintenance for replacement. However, the precise and reliable mitigation algorithm requires a good understanding of ITSC fault condition, particularly the number of shorted turns and short circuit current. The number of shorted turns is the key parameter used in modeling the ITSC fault

machine. The short circuit current is the main reason that causes damage on insulation material. A reliable mitigation method should be able to limit the short circuit current in a safety range. However, it is impossible to measure the short circuit current in real application. Therefore, it requires short circuit current estimation method in order to provide a feedback for evaluating the performance of ITSC fault mitigation algorithms. In this study, the characterization of ITSC fault is analyzed in detail at first. Following that, a parameter identification method is provided to estimate the number of shorted turns at standstill condition. At last, a short circuit current estimation algorithm is developed based on back electromotive force (back-EMF) estimation.

TABLE OF CONTENTS

LIST OF FIGURES

LIST OF TABLES

CHAPTER 1

INTRODUCTION

1.1 Background

In the few decades, permanent magnet synchronous machine (PMSM) has been widely used in many applications due to its inherent advantages, such as high efficiency, high power and torque density. The increasing usage of PMSMs raises significant concerns of system reliability, especially for cost and safety critical system. A machine fault can greatly affect the system performance, cause unexpected interruptions and even turn into catastrophic failure. Therefore, it is essential to have reliable fault detection algorithms.

One of the most common faults is ITSC fault, which is caused by insulation failure between two nearby turn in one coil. As the demand of power and torque density rising intensively, the PMSM is more likely to be exposed to higher thermal, electrical and mechanical stresses, which can potentially increase the possibility of insulation failure. Since ratio between number of shorted turn and total number of turns in one phase is usually small, the fault machine may maintain the performance with little changes. However, the short circuit current can increase significantly, due to the uncontrolled permanent magnet excitation and low impedance of circulating loop. The excessive short circuit current can generate localized heat, which can further increase the thermal stress on the insulation material nearby. If ITSC fault is treated properly, it can be expanded by involving more conductors and ultimately turns into phase-to-phase, phase-to-ground short circuit fault and even open circuit fault, which can cause motor tripped over.

Many studies have been published with aiming at ITSC fault detection algorithms, including motor current signature analysis, parameter identification based method, combined motor variables,

search coils and mechanical outputs. Beyond that, some studies focus on developing ITSC fault mitigation algorithms which can be used for extending fault machine lifetime. It is essential for the mission critical system, where unexpected stop is extremely expensive.

However, the short circuit current is not analyzed adequately due to the difficulty of measurement. It is the key component that makes the most contributions to the deterioration of ITSC fault. By monitoring the short circuit current, the ITSC fault severity can be observed directly. More importantly, the short circuit current estimation lays a foundation of fault mitigation algorithms . It can be used to evaluate the performance of mitigation algorithms that are designed to suppress or limit the short circuit current. Instead of tuning blindly, it is possible to tune the mitigation algorithms based on the estimation results with higher accuracy and efficiency.

1.2 Literature Review of ITSC Fault Diagnosis[1]

Several methods and fault indexes are proposed in the literature to detect and identify the drive system faults. In the proposed methods, actual and reference values of various machine variables, estimated electric parameters, torque ripple, instantaneous power, vibration spectrum and induced voltage in search coils are used as fault indicators. Presented results in the previous section evidently show the variations in the machine flux density distribution, machine variables, machine parameters and torque output in case of an ITSC fault. Furthermore, studies tend to combine various fault indicators to improve the accuracy of fault decision and minimize false alarms. In addition to fault diagnosis and classification, the fault severity assessment is the next essential step

[1] ©2018 IEEE Reprinted with permission from M. Zafarani, E. Bostanci, Y. Qi, T. Goktas and B. Akin, "Inter-turn Short Circuit Faults in Permanent Magnet Synchronous Machines: An Extended Review and Comprehensive Analysis," in *IEEE Journal of Emerging and Selected Topics in Power Electronics*, vol. 6, no. 4, pp. 2173-2191, Dec. 2018.

in health management process. Depending on the machine type, certain responses to impending faults and corresponding amplitudes should be classified to obtain fault severity index. Unlike diagnosis techniques, the fault severity assessment has not been studied in detail for PM motors, and there is a huge room for research to set a meaningful motor specific threshold and minimize false alarms. In this section, a comprehensive literature review on the ITSC diagnosis methods is presented. Diagnosis methods are categorized under 6 groups based on the used fault indicator(s).

1.2.1 Phase Currents Based Diagnosis Methods

The motor current signature analysis (MCSA) is the most popular technique that is used by several researchers to monitor the machine conditions. Stator current sequences and the impact of different faults on these components are investigated in studies such as [1], [2]. It has been also applied to detect short circuit faults in PMSM by defining different fault patterns for steady state and transient conditions. In most of these analyses, different signal processing approaches such as wavelet [3], Hilbert–huang [4] or fast Fourier transforms (FFT) [5] are deployed to analyze the effect of the fault on the stator current.

In [6] and [7], a matrix system based on the linear model of an IPM type BLDC machine and a fault detection algorithm for three types of faults including ITSC dynamic eccentricity (DEF) and combination of these two faults that is a hybrid fault (HF) are presented. The SITF and DEF create additional harmonics in the stator current, which follow the patterns given in (1.1) and (1.2), respectively.

$$f_{SITF} = (2k-1)\, f_f \tag{1.1}$$

$$f_{DEF} = (2k)\, f_f \tag{1.2}$$

where k is an integer value, f_f is the fundamental frequency, f_{SITF} and f_{DEF} are the harmonics appearing in the stator current spectrum due to SITF and DEF, respectively. Combination of these two faults creates both harmonics in the spectrum as shown in (1.3);

$$f_{HF} = f_{SITF} + f_{DEF} \tag{1.3}$$

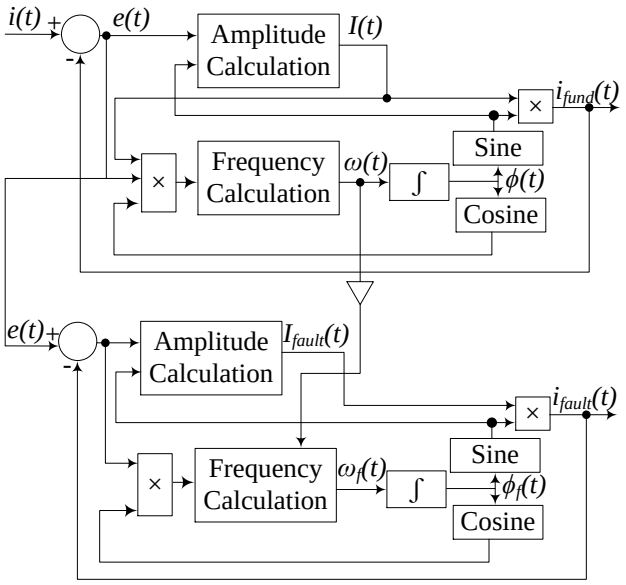

Figure 1.1. Block diagram representing the new fault detection algorithm in [8].

In order to extract the fault waveform out of the main current signal during transient operation, an algorithm shown in Figure 1.1 is presented in [8]. In this algorithm, the stator current is split into two parts as the fundamental and the rest of the harmonics, which can be noise, transient disturbance and all other harmonics. These two components analyzed to detect different faults including demagnetization, static eccentricity and ITSC.

Effect of the ITSC fault on the stator current and electromagnetic torque of an axial flux PM motor is investigated in [9]. It is shown that the harmonics in stator current due to the short circuit fault have the pattern given in (1.4);

$$f_{ISC} = f_s\left(n \pm \frac{2k+1}{p}\right) \quad (1.4)$$

where p is the number of pole pair, n=1,3,5,.. and k is an integer value. Additionally, transient analysis using wavelet transformation of the stator current is used to investigate the effect of the ITSC on the current. In [10], current harmonics of the faulty phase are analyzed under three ITSC conditions and it is shown that 9th current harmonic arise during the fault and it does not vary with the fault level.

Two types of faults in a PM motor including the ITSC and inverter switch open faults are investigated in [11], [12]. It is shown that both faults excite the second order harmonic in the *q*-axis current. Through a practical algorithm, it is possible to detect any of those two faults and identify the fault type based on the dc offset and harmonic spectrum of the *q*-axis current. Similarly, the second harmonic of the *q*-axes current is used to detect ITSC fault in [13], [14]. It is shown that by increasing the level of fault, the RMS of faulty phase current increases. In [15], two methods including MCSA and extended park's vector analysis (EPVA) are used to detect ITSC fault. The main focus of the MCSA based method is also the 2nd harmonic component of *q-axis* current. Additionally, the park transformation of the stator current is used to detect the fault through EPVA.

A novel frequency pattern and competent criterion are introduced to recognize ITSC fault in a PMSM [16]. It is shown that the signatures appear in the air-gap flux density due to the ITSC follow the frequency pattern given in (1.5).

$$f_{Field} = \left(1 \pm \frac{2K_{sa}}{P}\right) f_s \quad (1.5)$$

where P is number of pole pairs and K_{sa} is a constant value. Effect of the ITSC on the stator current

is also investigated and additional phase current harmonics with the frequency pattern given in (1.6) are determined.

$$f_{Current} = \left(1 \pm \frac{2K_{sa}+1}{P}\right) f_s \tag{1.6}$$

Empirical mode decomposition (EMD) is also used to analyze the stator current for short circuit fault detection [17]. The stator current can be decomposed as a set of intrinsic mode functions, which are analyzed by quadratic time-frequency distributions and generate fault signatures. This method can be applied on both steady state and transient conditions. Moreover, PM synchronous wind generator is analyzed in [18] with Hilbert-Huang Transform (HHT). It provides early inter turn insulation degradation and the minimum intensity degree can be detected is 0.1488%. In [19] and [20], the wavelet packet decomposition is used for ITSC. The performance of short-time Fourier transform (STFT) and undecimated discrete wavelet transform (UDWT) are evaluated in the insulation failure diagnosis of PM machines [21]. Multiple signal processing methods, such as STFT, UDWT, and Wigner and Choi-Williams distribution, are examined for different types of fault in [22]. Additionally, two categorization algorithms, linear discriminate analysis and k-means analysis, are applied in classification of short circuit fault. In [23], a novel fault diagnosis method for ITSC fault is presented based on the trust region algorithm applied to phase currents. It is shown that this algorithm is able to estimate ITSC ratio within a short time.

The artificial intelligence methods, such as artificial neutral network (ANN), have been widely used to monitor the motor condition, recently. An ANN based pattern recognition method proposed in [24] is used to detect the ITSC and its severity in PMSMs by utilizing both 1st and 3rd current harmonics. However, factors affecting the 3rd current harmonic content such as winding connections of the machine and the supply unbalance are not taken into account. ANN-based

method utilizing by particle swarm optimization for parameter optimization is proposed by Nyanteh et al. for real time identification of rapid changes in the supply current due to short circuits in machine windings [25]. Another ANN-based detection method monitoring the zero current-sequence component is used to determine the actual fault severity by an online optimization algorithm in [26]. In another study, negative current sequence is detected by using a deformed flux model [27].

A simple fault index calculated by the total of the absolute phase current amplitude differences is introduced in [28]. Unlike traditional methods using FFT to calculate the fundamental component and a diagnosis approach in rotational reference frame with few calculation steps and a simple low-pass filter is applied. Similarly, there are other diagnosis studies using difference between the measured and estimated phase currents. A PSO algorithm is used for ITSC ratio in [29] and difference between estimated current and measured current is used with a state observer used to estimate *d-q* currents in [30].

The motor current signature analysis is the most common method for ITSC fault detection. Since the motor current is available in most motor drive systems and single component discrete Fourier transforms doesn't require too many instruction cycles, it is relatively easy to implement the frequency analysis of motor current. Furthermore, some signatures, like 3^{rd} harmonics of phase current and 2^{nd} harmonics of q-axis current, do not depend on the winding topology. Therefore, in order to reduce the difficulty of the implementation on unknown PMSMs, these kinds of methods can be used for ITSC detection.

Time-frequency analyses such as EMD, HHT, STFT, UDWT and wavelet packet decomposition are able to detect impending faults during transient state since they have faster response time than

the frequency analysis. In some certain situations, they require immediate detection of inter turn short circuit fault and the time-frequency analysis would be a better choice than frequency analysis. However, in time-frequency analysis, the effect of winding topologies is not clear and further research is needed.

It is also worth to mention that the operating point dependent effect of the current controllers on the phase currents is a challenge for all MCSA algorithms. Short time elimination or compensation of the current controllers can be beneficial if only phase currents are available for ITSC diagnosis.

1.2.2 Parameter Estimation Based Diagnosis Methods

Machine parameters such as induced back-EMF, inductances and machine saliency are monitored in parameter based fault diagnosis methods to detect the presence and intensity of the fault. In most of the proposed methods, initial conditions or threshold values are usually predefined through the measurements or simulations. In [31], two fault diagnosis methods are proposed for an electric vehicle drive system. The first one is an online strategy based on the back-EMF negative sequence that is estimated by an iterative observer, which can be executed on a microcontroller for practical applications. Since the proposed online method is not able to detect the fault at low rotational speed operations, its performance is improved by an offline diagnosis technique.

Since the ITSC fault directly affects the stator windings, some studies focus on the characteristics of electrical parameters under short circuit fault condition. In [32], the variations in the incremental inductance is used to detect the ITSC fault by considering the saturation. This value decreases during the saturation and further reduces when the short circuit fault occurs. Several types of PM machines are tested and k-Nearest Neighbor method is introduced to classify the short circuit and the eccentricity faults. An impedance based modeling is presented for an IPM type BLDC in In

[33]. The input current, back-EMF, circulating current, flux density distribution, torque and motor performance are analyzed based on this model. A resulting diagnosis algorithm using the input impedance as an indicator is proposed in [34]. An off-line diagnosis method that focuses on distinguishing ITSC fault from eccentricity fault is proposed in [35]. Both of these faults affect the impedance and cause unbalance of stator windings. However, the impedance variations have different patterns regarding the saturation effect. PM machine parameters including inductance, resistance and back-EMF constant are estimated in [36] and [37]. This method can be applied for different fault locations in the slot with the consideration of winding distribution and leakage fluxes. Similarly, the phase resistance and inductance of a surface mounted PMSM are analyzed under insulation failure in [38] and [39], and a finite element based phase variable model of a PMSM is proposed for analyzing the machine parameters with respect to the fault location and number of faulty turns [40]. Electric parameter based diagnosis is also applied on multi-phase PM machine such as in [41]. A dynamic inductance based fault diagnosis that has superior performance compared to linear models is proposed in [42].

Online diagnosis algorithms based high frequency (HF) signal injection method are proposed in [43] and [44]. As shown in Figure 1.2, low magnitude HF sinusoidal voltage signals in α-β reference frame are superimposed on the fundamental voltage references and the machine saliency component is detected from the measured current. The estimated online saliency is used as the indicator of the stator winding fault. Another condition monitoring method based on the pulsating-type voltage injection is presented in [45]. In this approach, a pulse voltage is applied on *d*-axis and induced current ripple is used to monitor the *d*-axis inductance change under ITSC fault. This method is immune to the saliency harmonics and valid under both normal operation and standstill

conditions. Likewise, in [46], PMSM saliency is calculated by indirect flux detection and on-line reactance measurement (INFORM) methods, which is also valid from standstill condition to full speed operation.

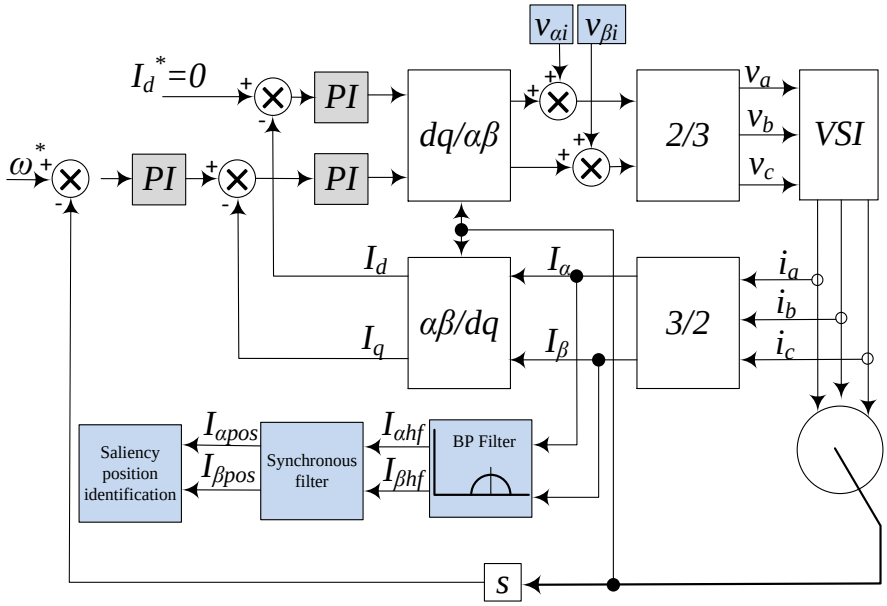

Figure 1.2. Implementation of the condition monitoring scheme in [84].

In ITSC fault condition, the electrical parameters including back-EMF, inductance and resistance change due to fault are used as the fault indicator. One advantage of the parameter based method is the ease of implementation. Since most of the drive systems deploy self-commissioning algorithms for control purpose, the initial conditions of the parameters including non-linear phenomenon are already known. There are many parameter identification and estimation tools which can be used for this purpose as long as they provide sufficiently accurate results to distinguish the fault cases. Similar to the MCSA method, discernment of ITSC fault and other fault types is possible since they share similar fault signatures. For instance, in demagnetization fault condition, we observe similar signatures on the back-EMF for both inter turn short circuit fault

and demagnetization. Thus, further investigation is needed to discern the impending faults signatures. Another common approach is using inductance as fault indicator. In off-line algorithms, using inductance as short circuit fault precursor can help distinguishing ITSC from other types of fault such as eccentricity or demagnetization faults and it is relatively less dependent on stator winding configuration.

1.2.3 Voltage Based Diagnosis Methods

As the analysis results presented in section II reveal, the zero sequence voltage components (ZSVCs) can also be used in the short circuit diagnosis when the neutral point of the PM machine is available. In [47], the ZSVC is analyzed on both stationary and transient conditions with Fourier transformation and HHT, respectively. The amplitude of the fundamental harmonic is used in the HHT and a severity index is created based on its linear relationship with rotational speed. Likewise, the ITSC fault of a five phase PMSM is studied by means of the analysis of ZSVC in [48]. A severity estimation based on amplitude and initial phase of zero sequence current is developed. An online inter-turn fault detection technique that considers star and delta connections is proposed in [49]. To this end, expressions for ZSVC and zero sequence current component (ZSCC) are presented for star and delta connections, respectively and a fault index is introduced based on the calculated short circuit current. It is claimed that the proposed method is able to detect short circuit fault, and identify the fault severity and the faulty phase. Neutral voltage-based detection method is applied to various stator short circuit faults is analyzed in [50] for parallel strand connections and it is stated that this method can be use the detect phase imbalance but not to identify the type of the short circuit.

The imbalance in the reference phase voltages v_a*, v_b*and v_c*, which are adjusted by the controller

to compensate the asymmetrical fault effects is used as another fault indicator. A new index based on the variations in the voltage references is defined to detect ITSC fault [51]. In [52], the second harmonics in the reference *d-q* voltage v_d* and v_q* in rotating reference frame are used as the indicators of the insulation failure fault. Similarly, the *q*-axis reference voltage command is analyzed by continuous wavelet transformation (CWT) for ITSC fault diagnosis in [53]. In [54] and [55], a new online monitoring of ITSC fault of a non-sinusoidal back-EMF PMSM considering the changes in the reference voltages based on the structure distance between an extended park model and a faulty machine model is introduced. The fault detection algorithm estimates the new set of PMSM parameters based on the new input variables by using a recursive least square algorithm and the structure distance is determined by comparing the new estimated parameters and those values calculated through the model. CWT is also used for incipient ITSC fault diagnosis in [56]. The incipient ITSC fault describes the transient state from disconnected faulty turns to fully connected faulty turns. It represents the stage after the insulation material is broken and before the broken stator windings are fully connected. By using CWT, it is possible to capture the voltage change during this transient state.

The voltage signature analysis is similar to current signature analysis, except the challenges in sensing through low-pass filters and isolation elements. Since the fault signature is usually small compared to the output voltage, it is a challenge to detect signatures with limited resolution of general purpose ADCs. The symmetrical component analysis is one of the most common tools used for intern-turn short detection where unbalanced windings increase the zero sequence components in three phase system. In star connected systems with neutral point, ZSVC can be used as indictor; where in delta connected winding ZSCC is preferred.

1.2.4 Search Coil Based Diagnosis Methods

Search coil is a tool that is used to detect fault, and define its location and type. In [57], three search coils are wound around stator teeth and the induced voltages in each coil are measured and analyzed to detect the ITSC fault. Similarly, terminal voltage of search coils in 2-phase and 3-phase PM machines are evaluated and used as the indicator of the short circuit fault in [58]. Lee et al. presented an algorithm based on the induced voltage across the detection coils for diagnosis of ITSC fault in a BLDC motor [59]. In [60], electromagnetic field model is applied for the motor modeling and used for calculating MMF and flux of the tooth. Similarly, Yao Da et al. applied search coils for electro-magnetic signature analysis of various faults including ITSC in [61].

Using search coil or flux sensors are very reliable methods to detect the inter turn short circuit fault. By monitoring the flux, the short circuit can be easily detected and the fault position is located. Dealing with winding configuration dependency and fault type discernment is also relatively easier using search coils. However the search coil method is invasive, requires special installation procedure and increases the difficulty of machine design.

1.2.5 Mechanical Outputs Based Diagnosis Methods

Though not very common, vibration monitoring is also used to detect machine faults in some studies. Two piezoelectric sensors are installed on the stators external surface to detect inter-turn short and open circuit faults through mechanical oscillation in [62]. It is shown that these failures create additional components on the mechanical vibration spectrum, which are proposed as proper fault detection indexes. Similarly, the vibration spectrum is analyzed to diagnose the partial demagnetization and ITSC fault in [63]. Boileau et al. proposed to use mechanical power spectrum

for ITSC diagnosis, arguing that this parameter will be eventually affected in case of an ITSC fault independent of the controller type [64].

Vibration analysis is the best option for mechanical faults and can be used for electrical faults as well due to fault related torque oscillations. However, it is very sensitive to environmental disturbance and external vibrations which may significantly affect the accuracy of the fault analysis. Both vibration and mechanical power output related detection methods require additional sensors, which increases the fault detection implementation cost

1.2.6 Mixed Variables Based Diagnosis Methods

Combination of different fault signatures is also used to further improve the reliability of the fault decisions. In [65], the effects of different severity levels on the stator current and ZSVC of a five phase PMSM are investigated. The fundamental and 3^{rd} harmonic contents of ZSVC and the 5^{th} stator current component are introduced as proper fault indicators. It is shown that the amplitude of those signatures increase with the fault intensity. However, these analyses are restricted only to the rated operating point. Similarly, a fault diagnostic method based on the analysis of the 3^{rd} harmonic content of stator current and the DC value of the ZSVC is proposed in [66] for a 3-phase SMPMSM. The harmonics determined as the fault precursors are traced by applying Vold–Kalman filtering order tracking (VKF-OT) method. The suitability of the proposed method under transient conditions is validated experimentally.

Harmonic content of motor phase currents and voltages are monitored and a Linear Discrimination Analysis (LDA) is implemented to distinguish static eccentricity, demagnetization and short circuit faults and their severity in [67]. One of the interesting conclusions is the negative effect of the temperature on fault detection accuracy.

A new index based on combined space vector given in (1.7) is introduced in [68], [69], [70] to detect ITSC fault in a five phase PMSM. This index is also used to distinguish the ITSC fault from other fault types such as magnet demagnetization, static and dynamic eccentricity faults.

$$\vec{D} = \vec{v}_{\alpha\beta}.\vec{v}_{\alpha 2\beta 2} \quad (1.7)$$

It is found that, the dc and $2f_s$ components are the two signatures that are affected more than other frequencies in case of a short circuit fault.

In [71] and [72], a combination of stator current and vibration noise frequency spectrums is used to diagnose ITSC fault in a 10-pole/12-slot PM motor. Correlation analysis is used to combine the two signals to a signal called fusion waveform. The fusion result is proven to show the fault feature more obviously than the stator current and the vibration signal.

The fault response on voltage, current and torques are theoretically analyzed using a hybrid wavelet packet transform (WPT) and ANN based methods to detect the stator electrical faults in [3]. The proposed hybrid method can detect the stator fault without any signal processing technique and do not depend on any machine parameter. Another ANN-based method proposed in [73] targets to monitor the ratio of the magnitudes of third harmonic and fundamental components of phase currents and supply voltage for ITSC detection.

In [53], continuous wavelet transformation method is used to analyze the electromagnetic torque and the phase voltage summation. The features of the fault at different rotational speeds are extracted from the torque waveform and voltage phase summation, which are used as the fault indicators.

The combination multiple methods are mainly based on the current signature and voltage signature analysis. The artificial index created in the combined methods provides better sensitivity. In some

practical applications, accelerometers and flux sensors are also used to support the fault decision; especially for mechanical and magnet related faults to obtain more accurate results. In many cases, combining the corresponding signatures in different variables can significantly improve the reliability of the fault analysis.

1.3 Aims of the Study

The main objectives of the proposed study can be summarized as following:

- To analyze and characterize PMSM current behavior under different condition, including different number of shorted turns, fault resistance, speed and load conditions.
- To develop an algorithm of number of shorted turns estimation at stand still condition.
- To develop an algorithm of short circuit current estimation in on-line condition.

1.4 Structure of the Dissertation

The chapter arrangement is given in the following:

- After the brief introduction given in this chapter, the comprehensive analysis of the PMSM current signature under ITSC fault is presented In Chapter 2. It focuses on the short circuit current and 3^{rd} harmonics in phase current under different working conditions, including different number of shorted turns, fault resistance, speed and load conditions.
- In Chapter 3, an algorithm of estimating number of shorted turns for PMSM is proposed. The advantage of proposed method is no need of tests on existing or manually made ITSC fault PMSM. The number of shorted turns can be calculated by a standstill test with the knowledge of machine parameters.

- In Chapter 4, the short circuit current estimation algorithm is proposed with knowledge of number of shorted turns. The short circuit current is calculated by the voltage variation on back-EMF, which are obtained by a proportional−integral (PI) observer.
- In Chapter 5, a brief summary of this dissertation is presented.

CHAPTER 2

ANALYSIS OF PMSM CURRENT SIGNATURE UNDER ITSC FAULT[2]

2.1 Background

Previous studies provide various models in order to understand the behavior of short circuit fault from different perspectives [1], [16], [35], [74]. In order to analyze the effect of the winding configurations, analytical models are developed through deformed flux models and symmetrical components for both series and parallel windings [1], [75]. For the machines with multi-strand winding, [76] proposes a practical model and suggests that the multi-strand winding machine has better performance and less apparent fault features. The multi-phase fractional slot concentrated winding PM machines is analyzed in [77]. It is shown that by adopting two adjacent coils per phase, PM machines exhibit better magnetic isolation but yields worse performance during the mitigation. Another analytical model for both star and delta connection windings is presented in [49] which introduces the calculation of zero sequence components to detect inter turn short circuit fault.

Improving the model accuracy by introducing more details constitutes another set of discussions in the literature. For example, [78] proposes a predictive model by considering the fault location inside slot. It reveals that, for a concentrated winding machine with the same number of shorted turns, the short circuit current increases as the fault location approaches to slot opening. The spatial harmonics of back-EMF has influence on the current behavior as well [79]. By considering the

[2] ©2018 IEEE Reprinted with permission from Y. Qi, E. Bostanci, V. Gurusamy and B. Akin, "A Comprehensive Analysis of Short-Circuit Current Behavior in PMSM Interturn Short-Circuit Faults," in *IEEE Transactions on Power Electronics*, vol. 33, no. 12, pp. 10784-10793, Dec. 2018.

spatial harmonics, the proposed model verifies the 5th and 7th harmonics of the phase current and improves the accuracy of the fault assessment. In order to achieve higher accuracy in the models, FEA is combined with the phase variable model in [40]. The rotor position dependent parameters, like inductance, back-EMF and cogging torque are calculated in FEA and saved in look-up tables. In real-time simulation, those parameters are retrieved according to the rotor position. Due to the high short circuit currents, the thermal effect becomes a critical factor, thus a transient thermal model of inter turn short circuit machine is proposed in [80].

Some of the studies directly focus on the signature analysis. Following a stator turn fault, 2nd harmonic pops-up in two-axis stationary reference frame back EMF [31]. In order to use this feature, an extended state observer (ESO) is integrated with second-order generalized integrator for back-EMF estimation and fault detection. In [81] and [11], q-axis current signatures are evaluated under fault conditions. The authors indicate that the inter turn short circuit fault introduce 2nd harmonics into the q-axis current. Regarding the fault impact on the performance, an analytical model based on winding function is proposed in [82]. The results show that the inter turn short circuit introduces asymmetrical back-EMF and the short circuit current becomes higher than rated current, which in turn damage the windings. Since the damage is caused by the overcurrent of the shorted turns, the fault severity should be defined by the amplitude of short circuit current. Among the above studies, the fault severity is generally defined as the number of shorted turns, but the resistance in short circuit path is not taken into account adequately. As well known, the decrease in fault resistance is considered as the degradation of insulation material and the number of shorted turns determines the induced voltage in the shorted windings due to the electromagnetic coupling.

Therefore, it is essential to understand the dependency of short circuit current level to both these parameters.

This study presents a comprehensive short circuit current analysis and addresses the contact resistance effect in particular through FEA based equivalent circuit model. The circulating current behavior in the shorted turns is analyzed for various numbers of turns and fault resistance combinations. It's found that, there exist a relatively complex relationship between short circuit current versus the number of shorted turns and fault resistance. Thus the fault severity cannot be simply defined by the number of shorted turns without considering the short circuit contact resistance. The parameters of the FEA based equivalent circuit model are obtained from 2D FEA simulation. Since the short circuit current is extremely high, the inductance saturation is incorporated into the calculations. The inductance matrix is derived with different current levels at different rotor positions and incorporated into the equivalent circuit model as multi-dimensional lookup tables. In order to take loop responses into account, the model is run through field oriented control (FOC) under closed speed and current loops. The study is further extended to the harmonics analysis. The 3rd harmonics of phase current is often used to identify the fault severity in certain circumstances. However, in this study, it's been revealed that the 3rd harmonic analysis is not a reliable option to distinguish the fault severity level.

2.2 FEA Based Equivalent Circuit Model

The proposed FEA based equivalent circuit model includes two independent simulations as depicted in Figure 2.1. At the first stage, 2D FEA simulation is executed to obtain the machine inductance and back-EMF. The machine model in FEA includes machine geometry and magnetic characteristics of the materials. The 2-D cross-section view of the 8-pole PM test machine is given

in Figure 2.1. As shown in this figure, there are 21 slots and 18 turns in each slot. The stator winding is double layer fractional-slot overlapping concentrated winding. Each phase has 7 coils in series and each coil has 9 turns. In the simulation, the three phase windings are excited by three current sources, which are controlled manually in rotating reference frame. In order to mimic the inter turn fault condition, certain number of turns are disconnected from the three phase winding and excited by an independent current sources. By performing a sweep of current in the shorted turns, electrical angle, d-axis and q-axis current, the inductance matrix are obtained. Similarly, back-EMF look-up tables are generated through electrical angle sweeps at certain speeds.

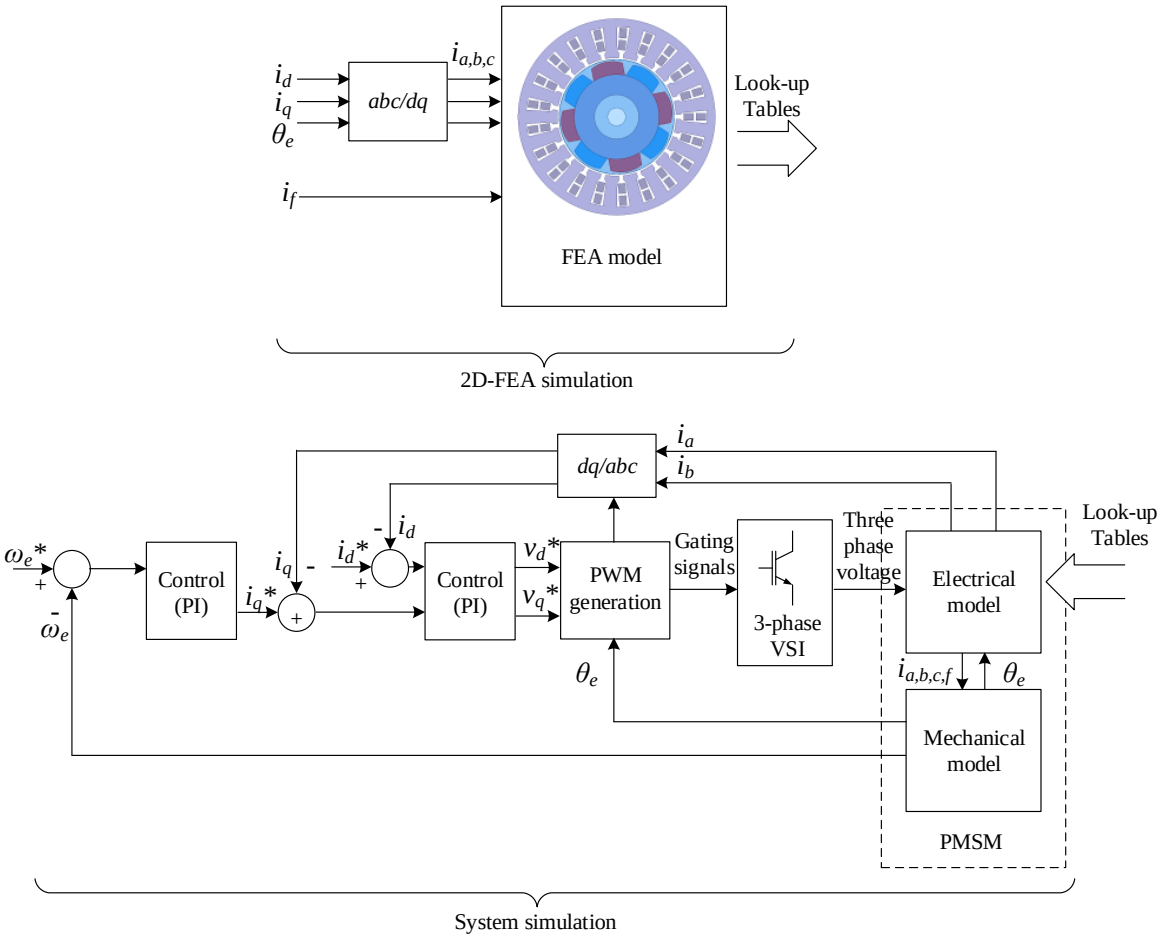

Figure 2.1. Block diagram of proposed FEA based equivalent circuit model.

The next step is the real time simulation, including the schematic of FOC and the model of PMSMs. According to [76], torque ripple rises when the inter turn short circuit fault happens. Therefore, speed loop is included in the system for simulating the mechanical response as well. It is worth to mention that, the real time simulation and FEA simulation can be performed simultaneously, which is named as co-simulation. However, co-simulation requires very large computational resource and significant execution time. Therefore, the proposed method divides the co-simulation into two asynchronous simulations and links them by look-up tables.

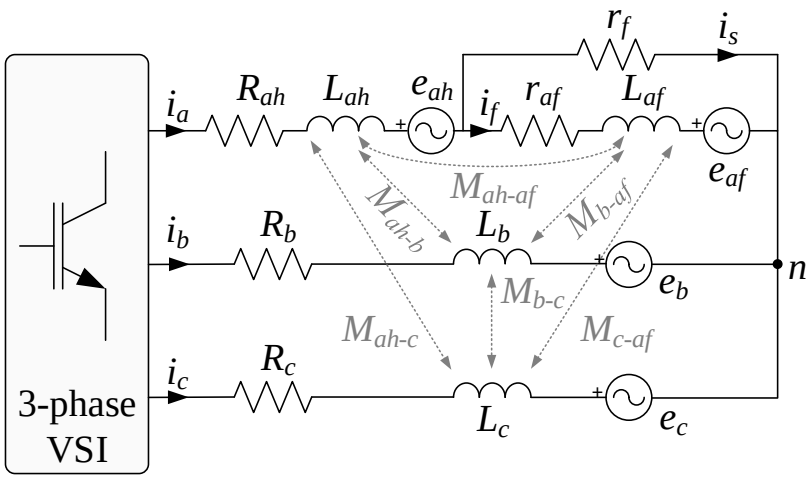

Figure 2.2. The electrical model of PMSM with inter turn short fault.

The equivalent circuit model of the PM machine in real time simulation is given in Figure 2.2. The resistance of the short path cannot be perfectly zero and hence a fault resistance r_f is introduced into in this model. In this case, the current in the circulating path is divided to two different components. One is the short circuit current i_s, which flows in the short path; and the other one is the fault current i_f, which is the current in the shorted turns.

Based on Figure 2.2, the voltage equations of the stator winding can be derived in

$$\mathbf{v}_{abcf} = \mathbf{R}_s \mathbf{i}_{abcf} + \mathbf{L}_s \frac{d}{dt}\mathbf{i}_{abcf} + \mathbf{e}_m \quad (2.1)$$

where,

$$\mathbf{v}_{abcf} = \begin{bmatrix} v_{ah} & v_{bn} & v_{cn} & v_{af} \end{bmatrix}^T$$

$$\mathbf{i}_{abcf} = \begin{bmatrix} i_a & i_b & i_c & i_f \end{bmatrix}^T$$

$$\boldsymbol{\lambda}_m = \begin{bmatrix} \lambda_{ah} & \lambda_b & \lambda_c & \lambda_{af} \end{bmatrix}^T$$

$$\mathbf{e}_m = \begin{bmatrix} e_{ah} & e_b & e_c & e_{af} \end{bmatrix}^T$$

$$\mathbf{r}_s = \begin{bmatrix} R_{ah} & 0 & 0 & 0 \\ 0 & R_b & 0 & 0 \\ 0 & 0 & R_c & 0 \\ 0 & 0 & 0 & R_{af} \end{bmatrix}$$

$$\mathbf{L}_s = \begin{bmatrix} L_{ah} & M_{ah-b} & M_{ah-c} & M_{ah-af} \\ M_{ah-b} & L_b & M_{b-c} & M_{b-af} \\ M_{ah-c} & M_{b-c} & L_c & M_{c-af} \\ M_{ah-af} & M_{b-af} & M_{c-af} & L_{af} \end{bmatrix}$$

The voltage on the fault resistance is given in (2.2).

$$R_f i_s = R_{af} i_f + L_{af} \frac{di_f}{dt} + M_{ah-af} \frac{di_a}{dt} + M_{b-af} \frac{di_b}{dt} + M_{c-af} \frac{di_c}{dt} + e_{af} \quad (2.2)$$

The mechanical model of PMSM can be developed by the torque equation, which is given in (2.3)

$$T_e = \frac{P}{2} \mathbf{i}_{abcf}^T \frac{d\boldsymbol{\lambda}_m}{d\theta_e} = \frac{P}{2} \mathbf{i}_{abcf}^T \frac{\mathbf{e}_m}{\omega_e} \quad (2.3)$$

Since the test motor is surface mount PMSM, only electromagnetic torque is modeled as the torque output.

2.3 Short Circuit Current and Fault Current Analysis

According to the literature, the severity of inter turn short circuit fault is usually defined as the number of shorted turns. Since e_f is proportional to the number of shorted turns, the induced voltage of short circuit path increases when the severity increases. Due to the low impedance of the circuit, the short circuit current i_s increases dramatically in this case. Moreover, as the number of shorted turns increases, the difference between the remaining healthy winding and other healthy winding become more obvious. It leads to the system unbalance increases.

However, referring to the equation (2.2), the fault resistance r_f is also an important factor which affects the behavior of the short circuit current. Thus, we can reorganize (2.2) by substituting i_f into i_a and i_s ,

$$\left(r_f + r_{af}\right)i_s + L_{af}\frac{di_s}{dt} = r_{af}i_a + L_{af}\frac{di_a}{dt} + M_{ah-af}\frac{di_a}{dt} + M_{b-af}\frac{di_b}{dt} + M_{c-af}\frac{di_c}{dt} + e_{af} \quad (2.2.4)$$

and substitute all variables into vectors as follows:

$$\left(r_f + r_{af} + j\omega_e L_{af}\right)\vec{\mathbf{I}}_s = \left(r_{af} + j\omega_e L_{af} + j\omega_e M_{ah-af}\right)\vec{\mathbf{I}}_a + j\omega_e M_{b-af}\vec{\mathbf{I}}_b + j\omega_e M_{c-af}\vec{\mathbf{I}}_c + \vec{\mathbf{e}}_{af} \quad (2.5)$$

Consider a PM machine with multi-coils in one phase, the sum of L_{af} and $M_{ah\text{-}af}$ can be simplified as,

$$L_{af} + M_{ah-af} = \frac{N_s^2}{N_h^2}L_{a1} + \frac{N_s\left(N_h - N_s\right)}{N_h^2}L_{a1} + \frac{N_s}{N_h}M_{a1-a} = \frac{N_s}{N_h}\left(L_{a1} + M_{a1-a}\right) = \frac{N_s}{N_c N_h}L_a \quad (2.6)$$

where L_{a1} is the self-inductance of coil a1, $M_{a1\text{-}a}$ is the mutual inductance between coil a1 and other phase A coils and L_a is the self-inductance of phase A winding. Similarly, the mutual inductance is given by,

$$M_{af-b} = \frac{N_s}{N_c N_h} M_{a-b} \quad (2.7)$$

$$M_{af-c} = \frac{N_s}{N_c N_h} M_{a-c} \quad (2.8)$$

If the mutual inductance between the shorted turns and other phase windings are assumed identical, the equation (2.5) can be simplified to,

$$\left(R_f + R_{af} + j\omega_e L_{af}\right)\vec{\mathbf{I}}_s = \eta\left(R_a + j\omega_e L_s\right)\vec{\mathbf{I}}_a + \vec{\mathbf{e}}_{af} \quad (2.9)$$

where a fault index is defined as $\eta = \frac{N_s}{N_c N_h}$ and L_s is the synchronous inductance.

One can notice that the right part of the equation (9) represents the phase current and the back-EMF of shorted turns. During inter turn short circuit fault, the short circuit current is proportional to change in torque output and the back-EMF is proportional to the operating speed. Therefore, with the same r_f and N_s, the short circuit current i_s is depends on the motor speed and torque in the same direction.

Since the sum of L_{af} and $M_{ah\text{-}af}$, r_{af}, $M_{b\text{-}af}$, $M_{c\text{-}af}$ and e_{af} are all proportional to N_s, the induced voltage in the circulating path is proportional to the number of shorted turns, as shown in the right hand part of (9). This conclusion belongs to the previous studies. However, referring to (9), the short circuit current i_s is also related to r_f, r_{af} and $j\omega_e L_{af}$, which are the impedance components of the short circuit path. According to (9), the fault resistance r_f has no relationship with N_s, whereas r_{af} is proportional to the number N_s and L_{af} is proportional to the N_s^2. Therefore, when the number of shorted turns increases, predicting the behavior of short circuit current is not straightforward process. Based on the r_f change, it can be categorized into three scenarios, which are given below.

- *A1.* Fault resistance r_f is extremely large so that there is little current flowing through r_f. It can be considered as healthy condition.
- *A2.* Fault resistance r_f is close to the faulty turns impedance $(r_{af} + j\omega_e L_{af})$. In this case, the short circuit current behavior is dependent on number of shorted turns and the motor speed at the same time. At low speed, the reactance is small and the current increases as N_s increases. However, at high speed, the reactance part could be much greater than the resistance part. Therefore, in this case when N_s increases and the short circuit current decreases.
- *A3.* Fault resistance r_f is much smaller than the shorted turns impedance $(r_{af} + j\omega_e L_{af})$. In this scenario, the dominant part is the shorted turns impedance $(r_{af} + j\omega_e L_{af})$. Referring to (2.5) and (2.6), when the number of shorted turns increases, the short circuit current decreases. This case can be considered as the ideal short circuit fault.

The fault current i_f also plays an important role in inter turn short circuit fault. The difference between i_f and i_s is that the i_s is flowing through the short path, which constitute relatively small area; however i_f is still flowing in the shorted turns spreading through the slots. Thus, it is possible that the fault can further spread to nearby healthy coils and create multiple short circuit faults with large fault current in the shorted turns.

Referring to (2.5), the fault current can be given in.

$$-\left(R_f + R_{af} + j\omega_e L_{af}\right)\vec{\mathbf{I}}_f = -R_f\vec{\mathbf{I}}_a + j\omega_e M_{ah-af}\vec{\mathbf{I}}_a + j\omega_e M_{b-af}\vec{\mathbf{I}}_b + j\omega_e M_{c-af}\vec{\mathbf{I}}_c + \vec{\mathbf{e}}_{af} \quad (2.10)$$

Similar to the analysis of is, the fault current if can also be categorized into three scenarios, with the change of r_f.

- *B1.* Fault resistance r_f is extremely large. Referring to (2.10), the fault current i_f is close to phase current i_a. This is the healthy condition.
- *B2.* Fault resistance r_f is close to the value of $\left|\vec{\mathbf{e}}_{af}/\vec{\mathbf{I}}_a\right|$, as shown in Figure 2.3. In this case, the variation of i_f is dependent on the operation conditions. If the phase shift of phase current and the variation of mutual inductance under faulty condition are neglected, the voltage vector of mutual inductance can be simplified to one vector with 90° phase shift with respect to the back-EMF vector. In Figure 2.3, they are shown as $jX\,\vec{\mathbf{I}}_a$. $\overrightarrow{\mathbf{V}_f}$ represents the term of $-\left(r_f + r_{af} + j\omega_e L_{af}\right)\vec{\mathbf{I}}_f$. L_{af} is relatively small in this scenario and hence its effect can be neglected. The variation in the number of turns has the same effect as the speed change.
    - *a.* Figure 2.3 (a) shows the variation of $\vec{\mathbf{V}}_f$ at different speeds. As the speed increases, $\vec{\mathbf{V}}_f$ switches from $\vec{\mathbf{V}}_{f-ls}$ to $\vec{\mathbf{V}}_{f-hs}$. It first decreases and then increases and there exists a minimum point at certain speed.
    - *b.* Figure 2.3 (b) gives the variation of $\vec{\mathbf{V}}_f$ at different torque levels. In this case, as the torque increase, $\vec{\mathbf{V}}_f$ switches from $\vec{\mathbf{V}}_{f-lt}$ to $\vec{\mathbf{V}}_{f-ht}$. It first decreases and then increases and there exists a minimum point with certain torque.
- According to the vector diagram shown in Figure 2.3, the amplitude of if can be approximated as follows,
- $$\left|\vec{\mathbf{I}}_f\right| = \frac{\sqrt{\left(R_f\left|\vec{\mathbf{I}}_a\right| - \vec{\mathbf{e}}_{af}\right)^2 + \left(X\left|\vec{\mathbf{I}}_a\right|\right)^2}}{\left(R_f + R_{af} + j\omega_e L_{af}\right)} \quad (2.11)$$

- According to (2.11), the amplitude of i_f is a function of speed and phase current. If the parameters in (2.11) are approximated by the results of 2-D FEA simulation for a case, where fault resistance is 1.0 Ohm and 5 turns are shorted, then if amplitude can be depicted as in Figure 2.4. One can notice that the fault current if doesn't change linearly neither with the speed nor torque conditions. There are minimum operation conditions for the fault current.

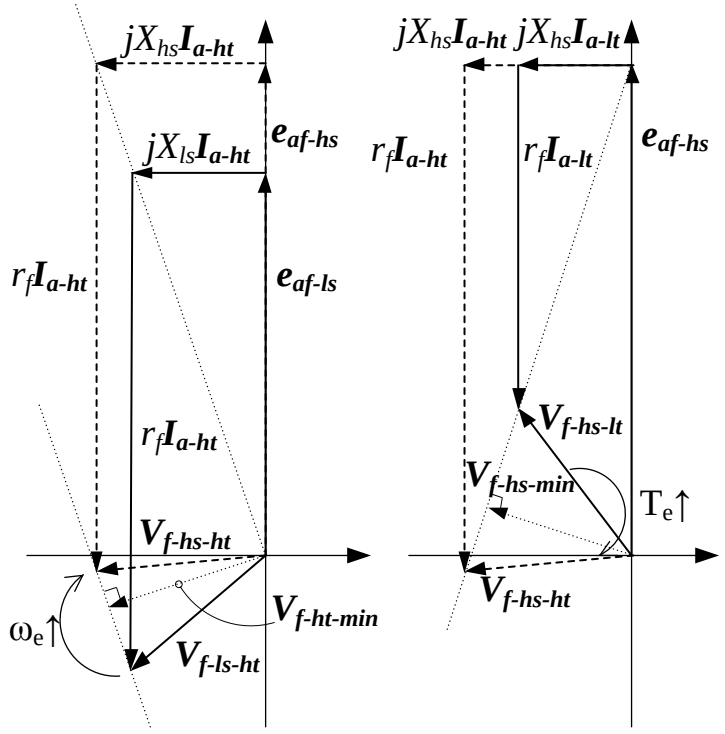

Figure 2.3. Vector diagram of $\boldsymbol{V_f}$ at different operation conditions, (a) speed change, (b) torque change.

- *B3.* Fault resistance r_f is much smaller than the value of $\left|\vec{\mathbf{e}}_{af}/\vec{\mathbf{I}}_a\right|$. In this case, the current in the short path is dominated by short circuit current i_s. However, compared to (2.10),

equation (2.5) reverses the vector $r_f \vec{\mathbf{I}}_a$ and extends the vector $jX \vec{\mathbf{I}}_a$, which is similar to Figure 2.3 (a). Thus, in this scenario, the amplitude of i_s is always greater than i_f and this difference is proportional to the phase current.

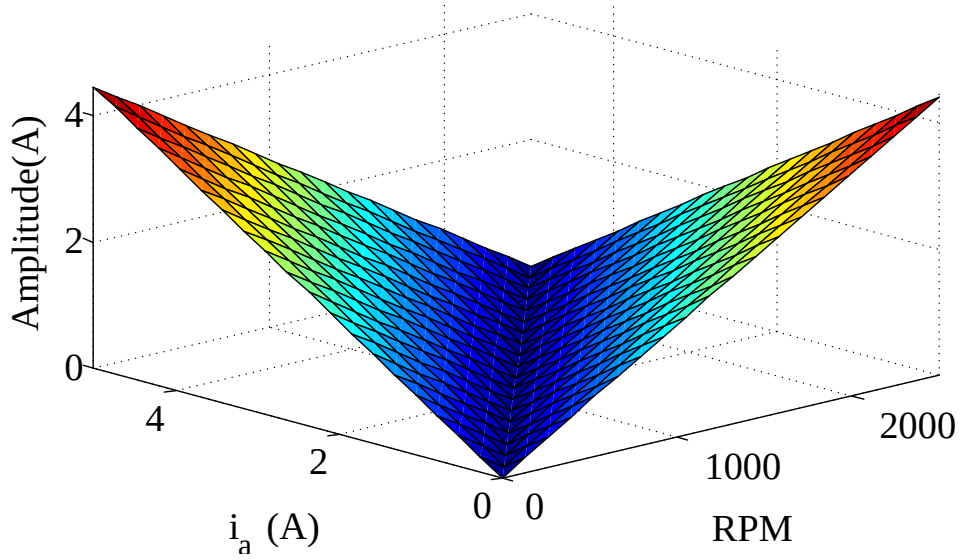

Figure 2.4. Fault current i_f, 1.0 ohm fault resistance and 5 shorted turns.

2.4 Validation in FEA Based System Simulation

In order to fully understand the behavior of inter turn short circuit fault, the FEA based equivalent circuit model has been created for an 8-pole surface mounted PMSM. The parameters of the test motor are given in Table 2.1.

The motor inductance and back-EMF parameters are calculated via 2-D FEA simulation in ANSYS Maxwell. The back-EMF waveform is calculated at 1000 rpm and the inductances are calculated through current and rotor position sweep. Since this study focuses on the steady state condition, in the FEA simulation the d-axis current is fixed to zero. The sweep of q-axis current and fault current are set from 0 to 6 ampere and -200 to 200 ampere, respectively. The sweep of

rotor position is from 0 to 360° of electrical angle. Eventually, for each inductance, a four dimensional look-up table is created.

Table 2.1. Machine parameters

Power	2.0 kW	Torque Constant	0.378 Nm/A peak
Speed	8000 rpm	L_d	0.0021 H
Current	7.03 A peak	L_q	0.00221 H
Poles	8	Torque Constant (FEA)	0.363 Nm/A peak
Inertia	50.5×10^{-6} kgm^2	L_d (FEA)	0.0018294 H
Static Friction	0.1 Nm	L_q (FEA)	0.0018392 H

The real time simulation of FEA based equivalent circuit model is developed in ANSYS Simplorer. A voltage source inverter is used to drive the motor at 10 kHz switching frequency. The load torque ranges from 0.5 Nm to 1.5 Nm and speed ranges from 1500 rpm to 10500 rpm. During the simulations, the test motor is shorted by 1 turn, 2 turns and 5 turns in one coil and the fault resistance is set to 0 Ohm, 0.1 Ohm, 1.0 Ohm and 5.0 Ohm.

The simulation results of short circuit current is are given in Figure 2.5 to Figure 2.9. From Figure 2.5 to 2.8 it is shown that as the fault resistance r_f increases, the current decreases. The ideal short circuit fault scenario is given in Figure 2.5. It can be seen that the short circuit current can be as high as 130 ampere with 0 Ohm fault resistance. With 5 Ohm fault resistance, the current level reduces to the acceptable range, which is below the rated current. In Figure 2.5, the 1 turn shorted machine has larger is than the other two cases, which is consistent with the discussions in *A3*. On the contrary, this phenomenon is reversed with 0.1 Ohm and higher fault resistance shown in

Figure 2.6. The highest current is observed in 5 turns shorted machine. This result is consistent in case *A2*. An example at 10500 rpm with 1.5 Nm torque is given in Figure 2.9. One can see that the amplitude of is consistently increases as the fault resistance r_f decreases. On the other hand, with higher fault resistance, such as 0.1 Ohm, 1.0 Ohm and 5.0 Ohm, the amplitude of is increases as the fault number of shorted turns increases. However, the behavior of is reverses in the 0 Ohm fault resistance scenario, where the amplitude of is decreases when the number of shorted turns N_s increases.

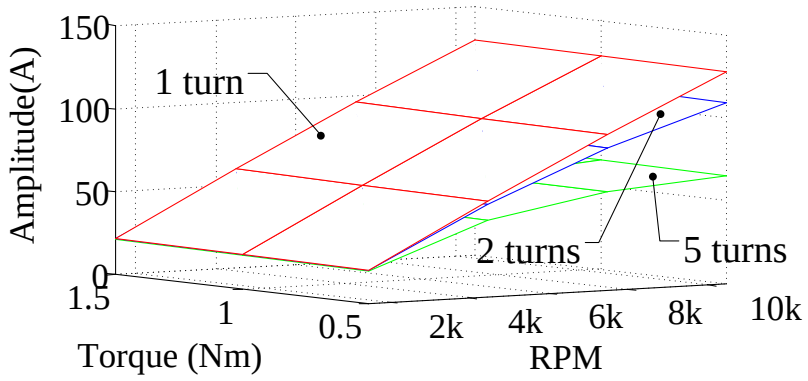

Figure 2.5. RMS value of short circuit current i_s with 0 Ohm r_f.

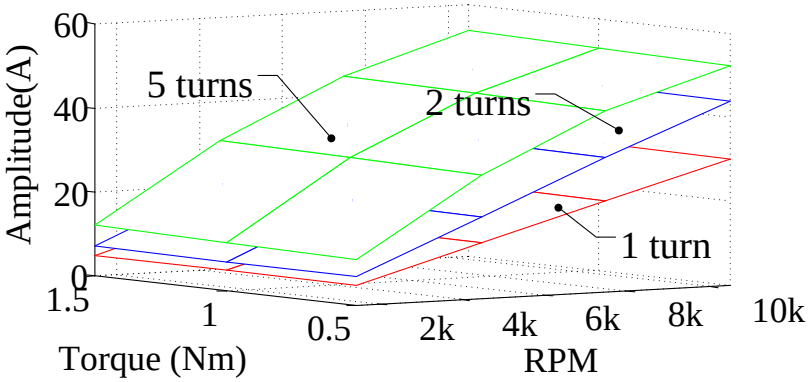

Figure 2.6. RMS value of short circuit current i_s with 0.1 Ohm r_f.

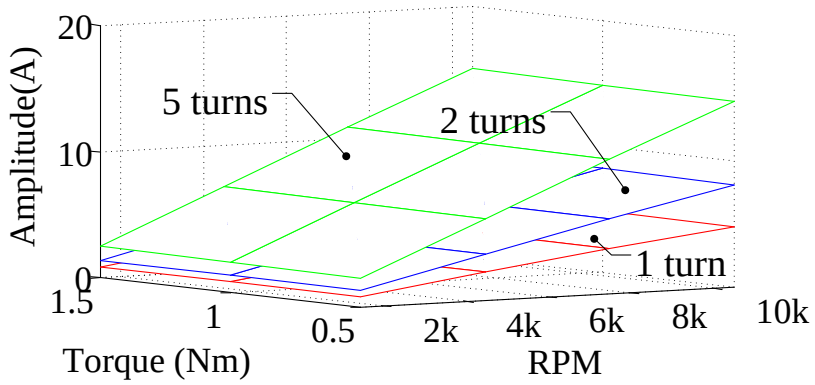

Figure 2.7. RMS value of short circuit current i_s with 1.0 Ohm r_f.

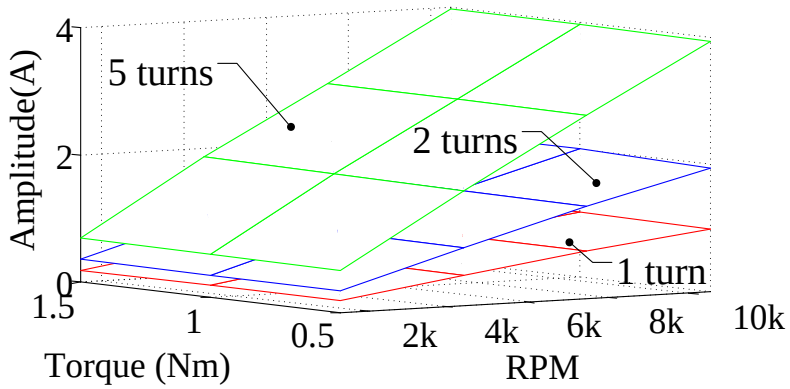

Figure 2.8. RMS value of short circuit current i_s with 5.0 Ohm r_f.

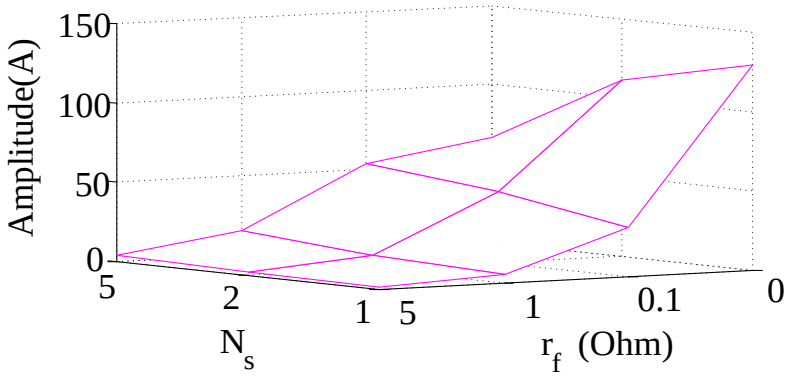

Figure 2.9. RMS value of short circuit current i_s at 10500 rpm with 1.5 Nm torque.

The fault current i_f plots are given in Figure 2.10 to Figure 2.14. Figure 2.10 shows the current behavior described in *B3*, where i_f increases as the speed increases. Since the fault resistance is 0 when N_s increases, the current level drops, same as the short circuit current i_s. With higher fault resistance, the current level increases associated with the number of shorted turns in the same direction as shown in Figure 2.11, 2.12 and 2.13. In Figure 2.12, one can notice that at 1500 rpm and 1.5 Nm torque, 1 turn shorted case has higher current level than 2 turns shorted case. This is described in *B2.a* and the vector diagram is given in Figure 2.3(a). The decrease in the number of shorted turns causes the induced back-EMF drop and then the voltage vector $\vec{\mathbf{V}}_f$ extend. Therefore, the fault current increases. In Figure 2.13, the current in 1 turn and 2 turns shorted machine shows the same behavior detailed in case *B1*. However, the current of 5 turns shorted machine exhibits similar behavior to case *B2*. In the zoomed figure - Figure 2.14, one can see that the 5 turns shorted machine exhibits the same behavior depicted in Figure 2.4, where the highest current appears at the reverse extremes of torque and speed.

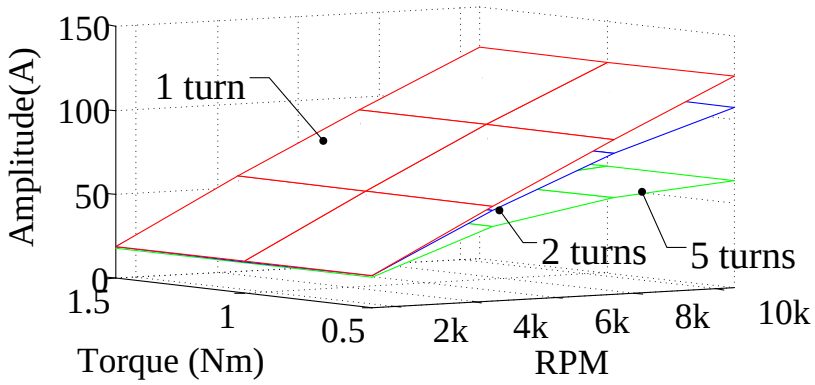

Figure 2.10. RMS value of fault current i_f with 0 Ohm r_f.

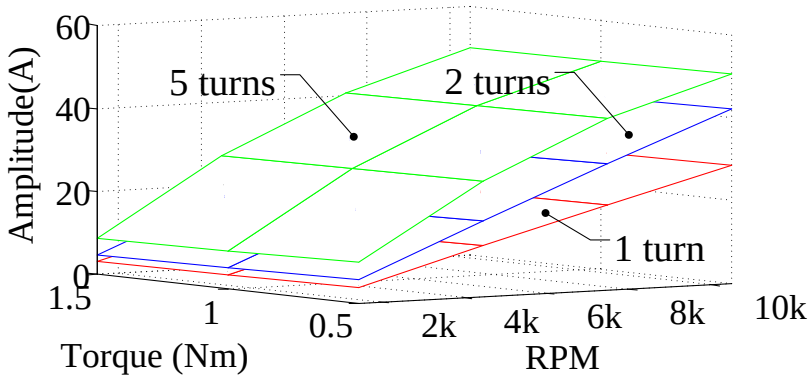

Figure 2.11. RMS value of fault current i_f with 0.1 Ohm r_f.

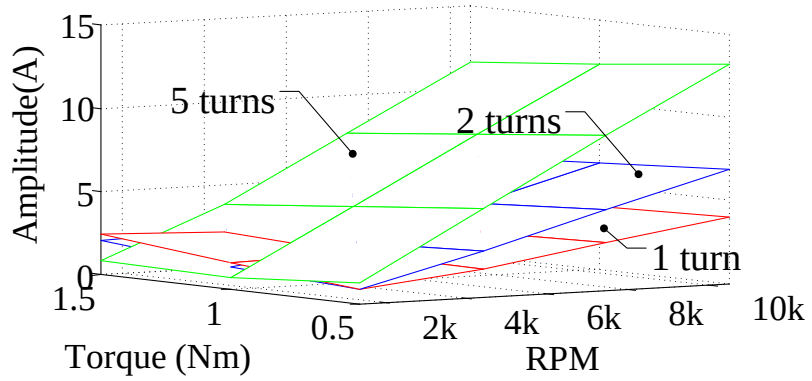

Figure 2.12. RMS value fault current i_f with 1.0 Ohm r_f.

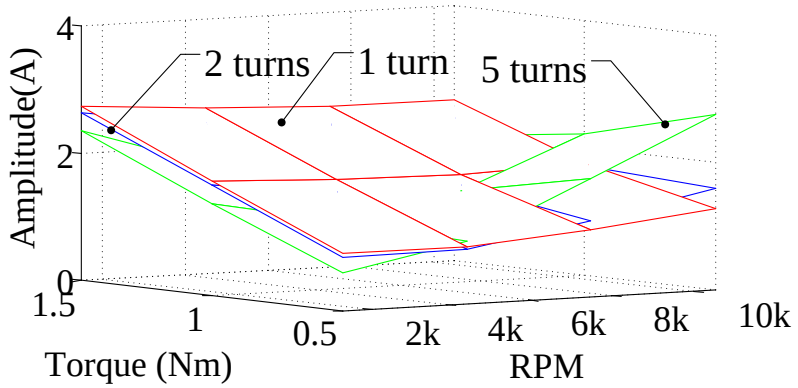

Figure 2.13. RMS value of fault current i_f with 5.0 Ohm r_f.

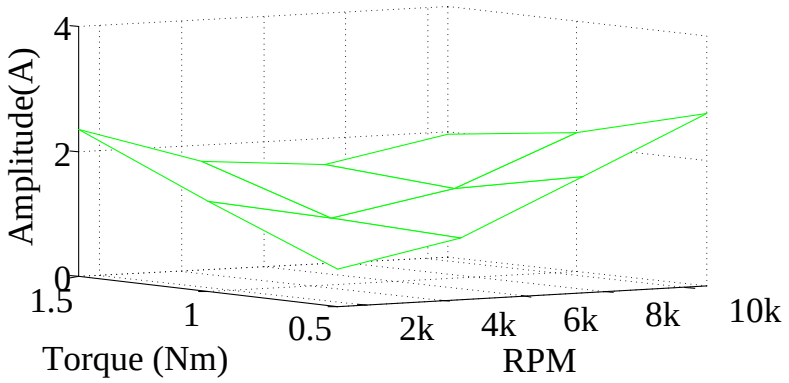

Figure 2.14. Zoomed plot of 5 turn shorted case with 5.0 Ohm r_f.

The harmonic analysis results are given in Figure 2.15 to Figure 2.19. It can be seen that the 3rd harmonics component consistently increases as the number of shorted turns increases; and the 3rd harmonic component consistently decreases when the fault resistance increases. However, the 3rd harmonic result doesn't exhibit a consistent relationship between the short circuit current, number of turns and fault resistance. For instance, 3rd harmonic analysis results at 10500 rpm with 1.5 Nm torque is given in Figure 2.19. Here, it's shown that the 3rd harmonic and changes linearly with respect to the number of shorted turns fault resistance. However, in Figure 2.9, the short circuit current level doesn't change linearly with the number of shorted turns. As the number of shorted turn increases, the current level decreases at 0 Ohm fault resistance and increases with higher fault resistances. It means that the 3rd harmonic component is consistent with the variation of the number of shorted turns but it may not reflect the change in short circuit current level, especially when the fault resistance is low. In brief, the 3rd harmonics can be used to distinguish the number of shorted turns. However, since the fault resistance and shorted turns impedance are hard to estimate, it cannot be used to define the severity and predict short circuit current level.

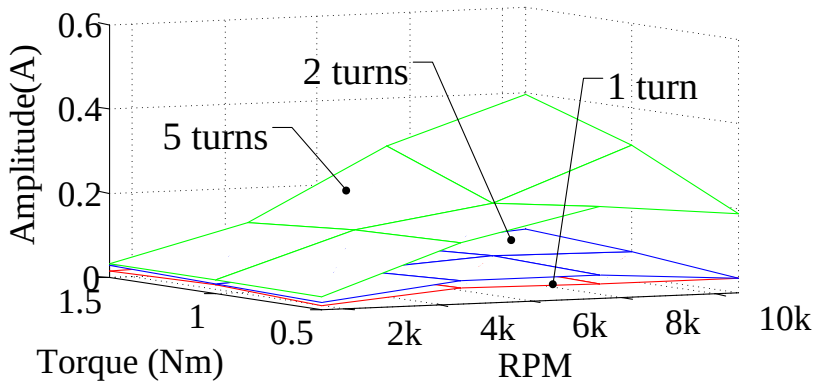

Figure 2.15. Amplitude of 3rd harmonics component in phase current with 0 Ohm r_f.

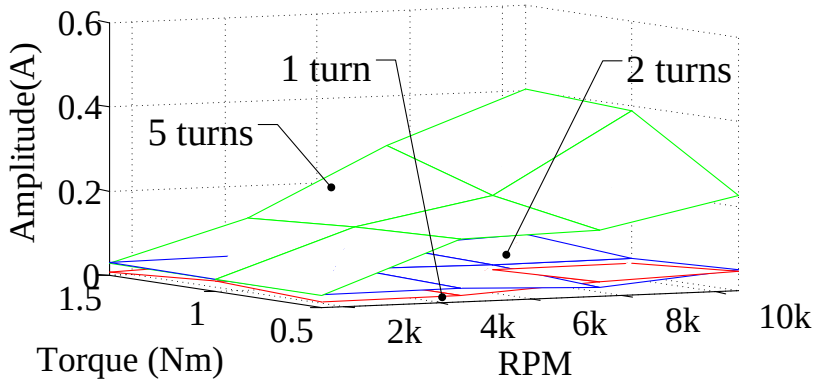

Figure 2.16. Amplitude of 3rd harmonics component in phase current with 0.1 Ohm r_f.

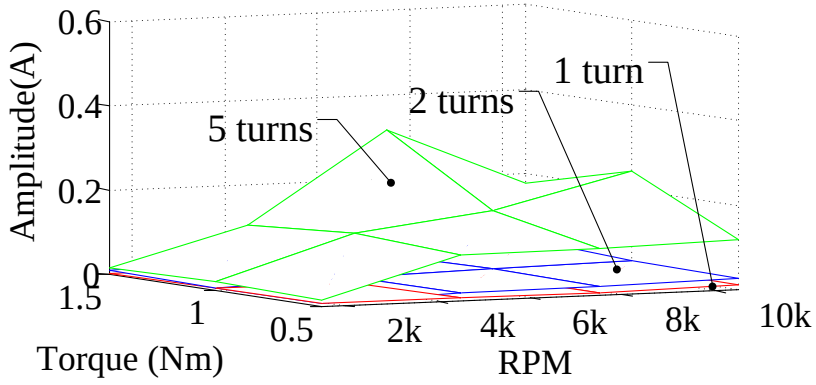

Figure 2.17. Amplitude of 3rd harmonics component in phase current with 1.0 Ohm r_f.

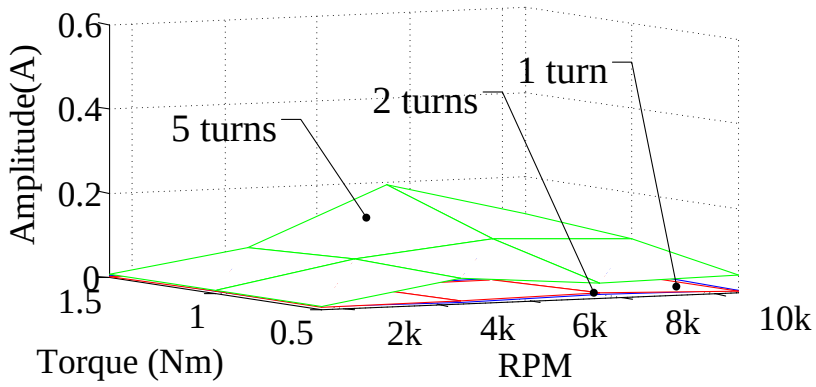

Figure 2.18. Amplitude of 3rd harmonics component in phase current with 5.0 Ohm r_f.

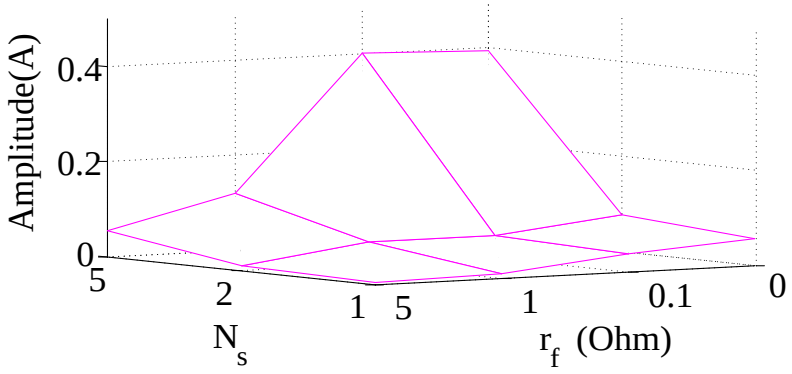

Figure 2.19. Amplitude of 3rd harmonics component in phase current at 10500 rpm with 1.5 Nm torque.

Compared to regular simulations, using look up table doesn't increase the simulation time remarkably. Based on the laboratory setup, there is only about 5% difference. However, obtaining look up tables in FEA simulation may take long time, which depends on the computational capabilities of the setup. Since, this step is a one-time simulation performed once at the very beginning, all of the real time simulations can benefit from look-up table with negligible overhead.

Experiment Validation

The Experiment setup is shown in Figure 2.20. A 2.5 kW motor drive is used which is equipped with TMS320F28335 MCU running at 10 kHz switching frequency. The actual test PMSM is the

same as the one used in simulation models. In order to mimic the inter turn short circuit fault, taps are extracted from one coil in phase B to create 1 turn, 2 turns and 5 turns inter turn shorted circuit fault. Various power resistors are used to mimic the fault resistance. The inherent resistance of the tabs and current acquisition setup is measured as 0.1 Ohms which is the default fault resistance. The short circuit currents are measured by external current transducers and stored in PC via the NI USB-6351 multifunction I/O device. The sampling frequency of current measurement is set to 50 kHz. During the experiment, the three phase current and short circuit current are sampled for 2 s at 50 kHz and processed in MATLAB to calculate corresponding signature amplitudes. The machine is loaded by hysteresis dynamometer which has 1.49×10^{-3} kgm^2 inertia. Due to safety reasons, motor operations are limited to 1200 rpm and 1.5 Nm, which are far below the rated operating point. In the experiment, the motor is tested at 600, 900 and 1200 rpm with 0.5, 1.0 and 1.5 Nm load. In order to validate the proposed model, the real time simulation under the same operation conditions is carried out at the same time. The experimental results and the corresponding simulation results are given from Figure 2.21 to Figure 2.39. The inherent resistance of the taps and current acquisition setup is around 0.1 Ohm, which is close to the impedance of shorted turns. Therefore, the ideal short circuit fault cannot be achieved in the experiments. In order to mimic imperfect short circuit faults, the shorted turns are connected in series with different power resistors, which represents the additional fault (contact) resistance.

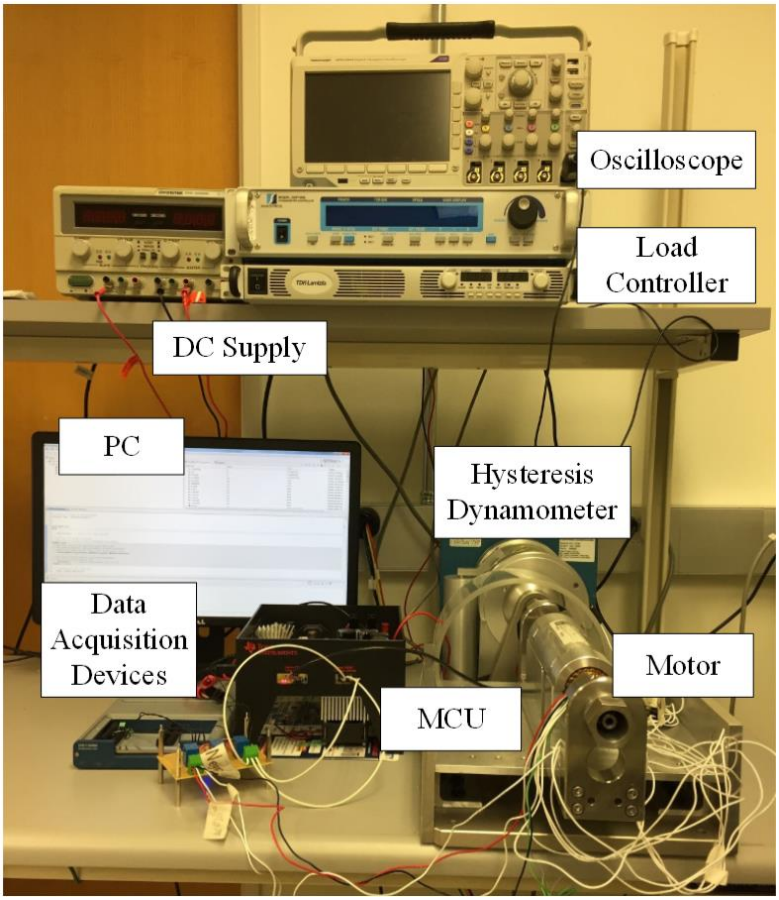

Figure 2.20. Experiment setup.

The results of short circuit current is are given in Figure 2.21 to Figure 2.26. It can be seen that the short circuit current is beyond 10 ampere, which is almost 2 times of the rated current. The short circuit current decreases when the fault resistance r_f increases. The results of fault current i_f are given in Figure 2.27 and Figure 2.32. With 0 Ohm power resistor, the fault current if is still much larger than the rated current. As the fault resistance increases, if approaches to the phase current value. The harmonic analysis results are given in Figure 2.33 and Figure 2.38. With 0 Ohm power resistor, the 3rd harmonic variation for different number of shorted turns is obvious. As the fault resistance increase, the fault is further mitigated, and at the same time, the 3rd harmonic components are suppressed.

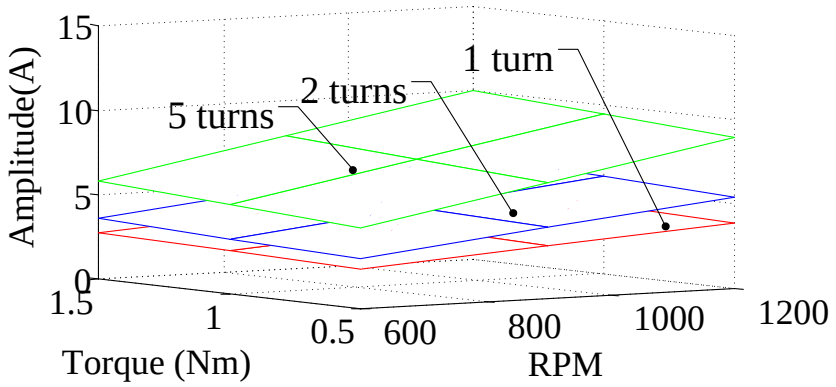

Figure 2.21. Simulation results: RMS value of short circuit current i_s with 0 Ohm resistor.

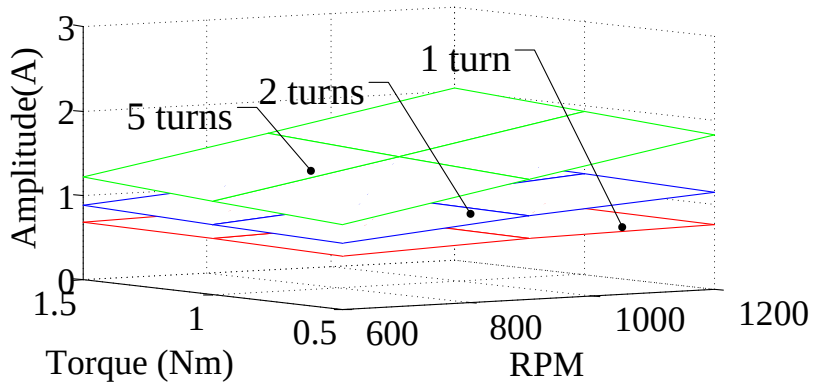

Figure 2.22. Simulation results: RMS value of short circuit current i_s with 1.0 Ohm resistor.

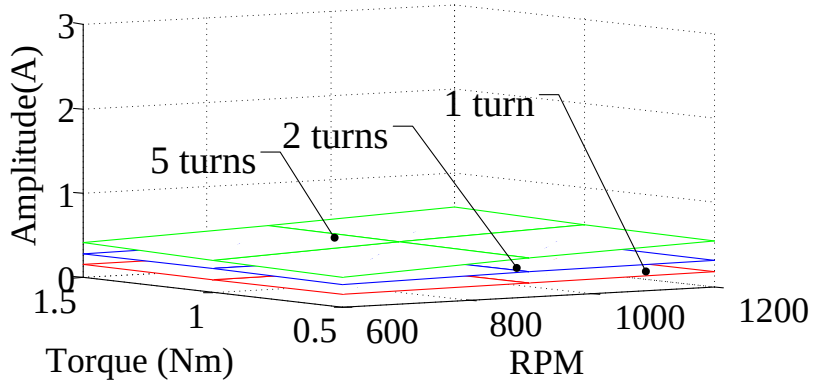

Figure 2.23. Simulation results: RMS value of short circuit current i_s with 5.0 Ohm resistor.

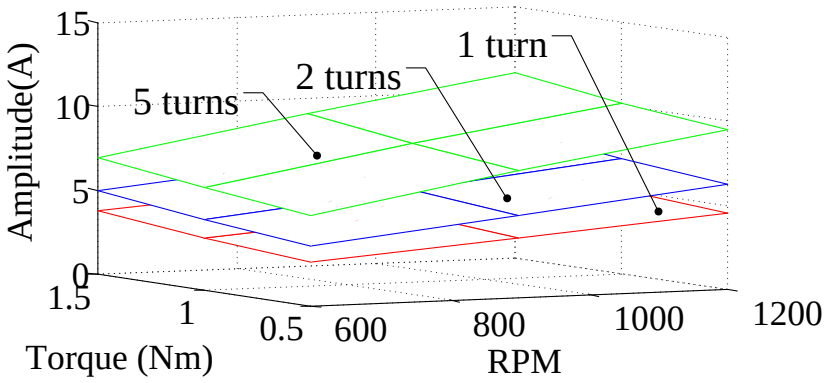

Figure 2.24. Experimental results: RMS value of short circuit current i_s with 0 Ohm resistor.

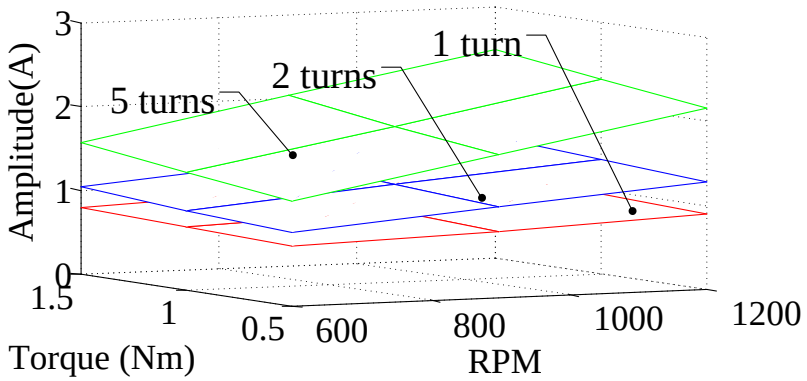

Figure 2.25. Experimental results: RMS value of short circuit current i_s with 1.0 Ohm resistor.

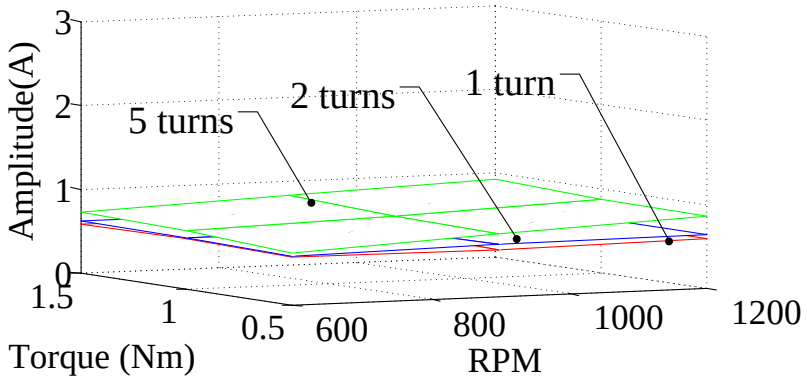

Figure 2.26. Experimental results: RMS value of short circuit current i_s with 5.0 Ohm resistor.

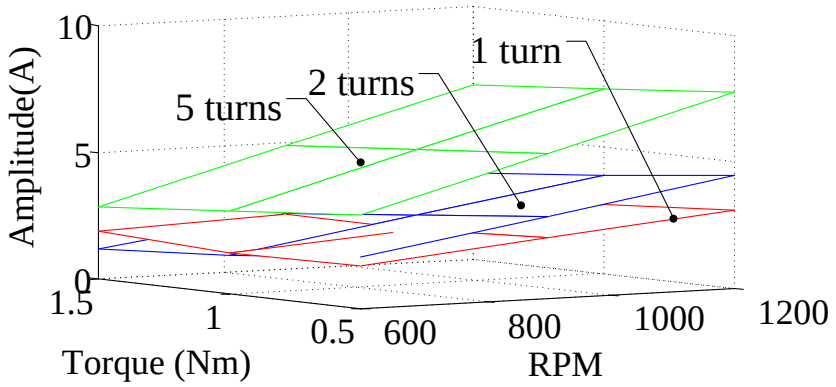

Figure 2.27. Simulation results: RMS value of faulty turns i_f with 0 Ohm resistor.

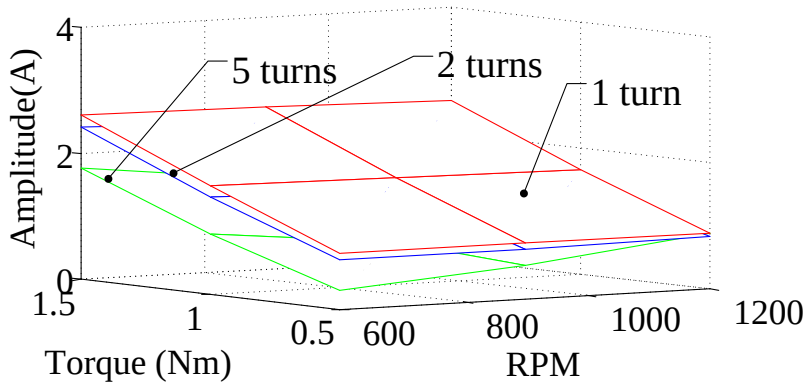

Figure 2.28. Simulation results: RMS value of faulty turns i_f with 1.0 Ohm resistor.

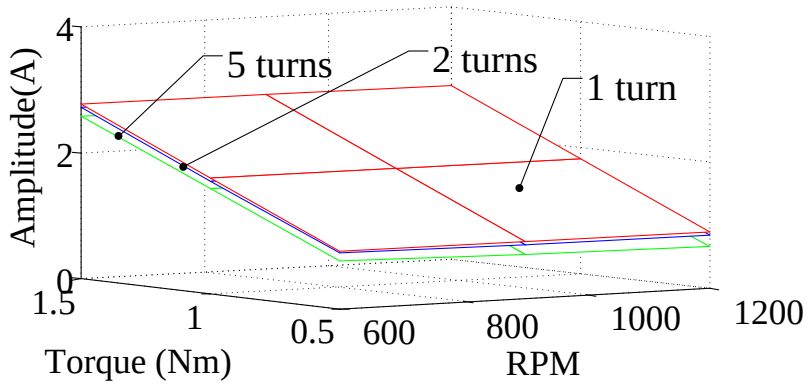

Figure 2.29. Simulation results: RMS value of faulty turns i_f with 5.0 Ohm resistor.

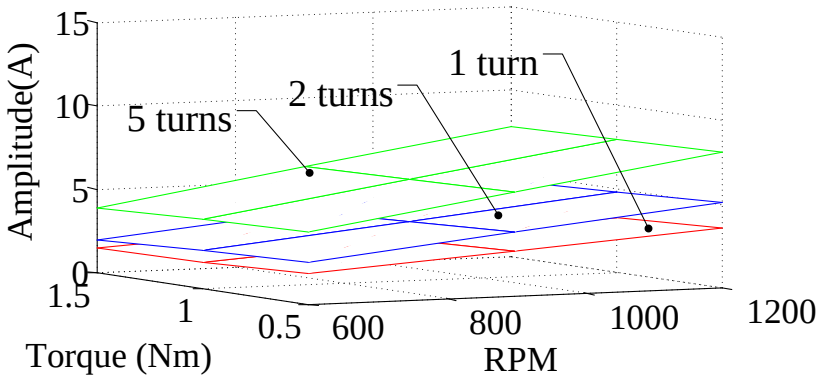

Figure 2.30. Experimental results: RMS value of faulty turns i_f with 0 Ohm resistor.

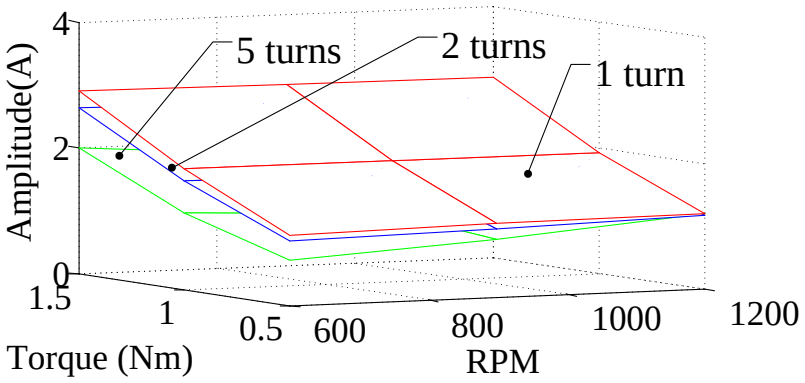

Figure 2.31. Experimental results: RMS value of faulty turns i_f with 1.0 Ohm resistor.

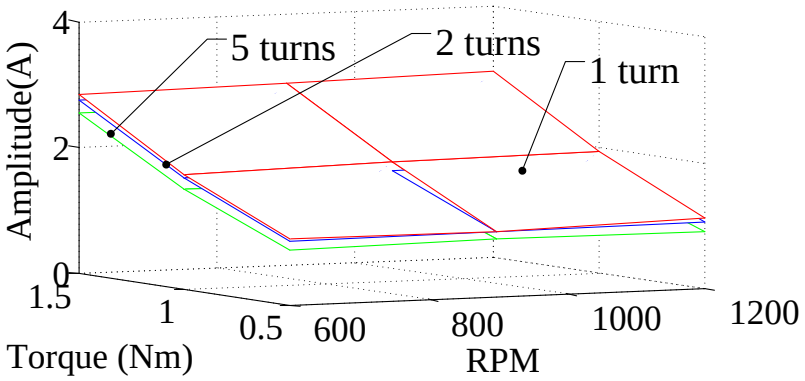

Figure 2.32. Experimental results: RMS value of faulty turns i_f with 5.0 Ohm resistor.

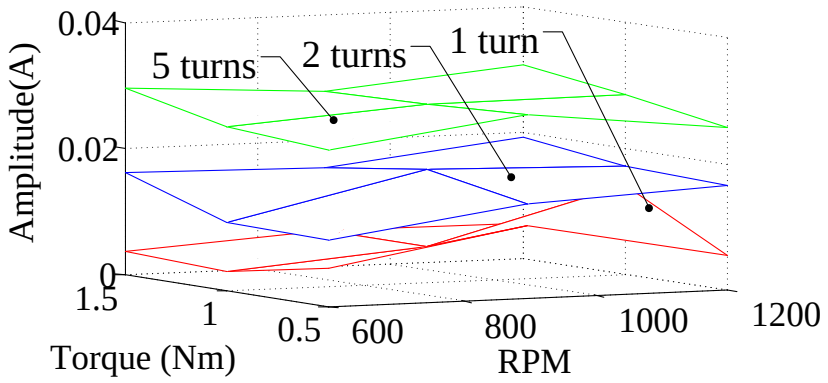

Figure 2.33. Simulation results of 3rd harmonics in phase current with 0 Ohm resistor.

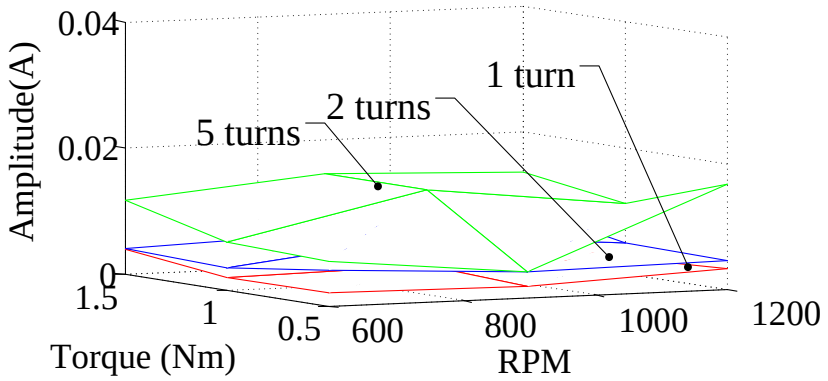

Figure 2.34. Simulation results of 3rd harmonics in phase current with 1.0 Ohm resistor.

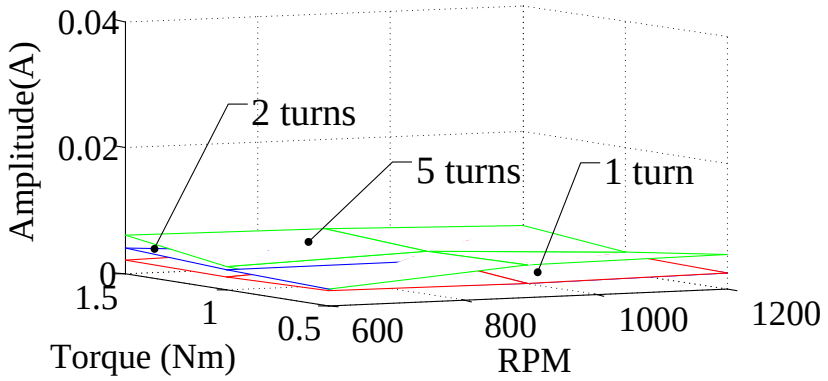

Figure 2.35. Simulation results of 3rd harmonics in phase current with 5.0 Ohm resistor.

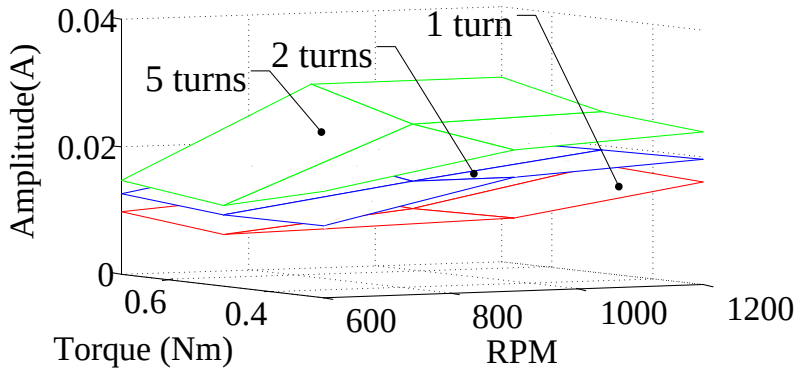

Figure 2.36. Experimental results of 3rd harmonics in phase current with 0 Ohm resistor.

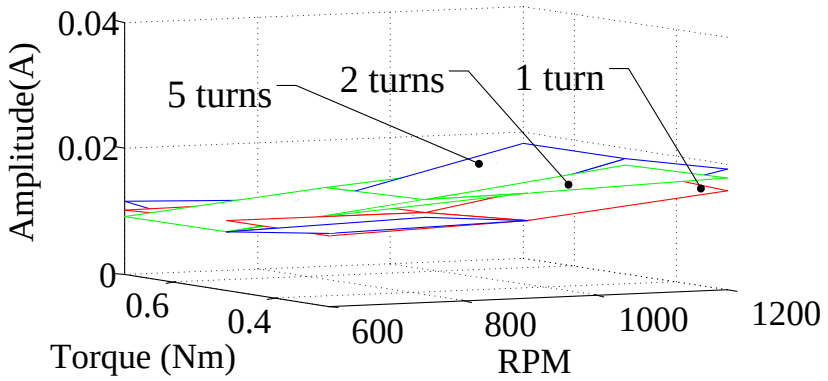

Figure 2.37. Experimental results of 3rd harmonics in phase current with 1.0 Ohm resistor.

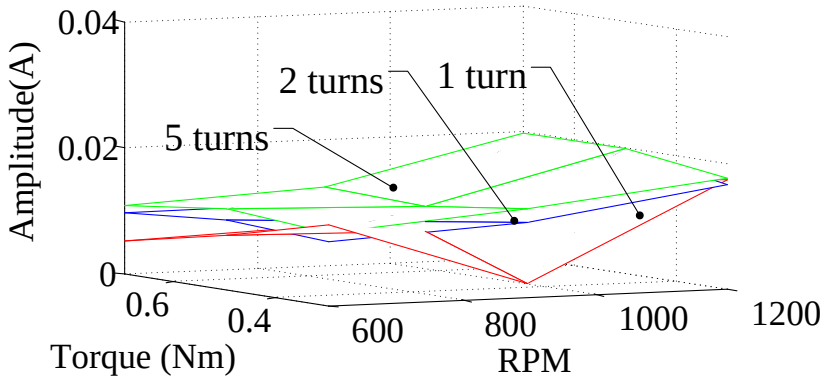

Figure 2.38. Experimental results of 3rd harmonics in phase current with 5.0 Ohm resistor.

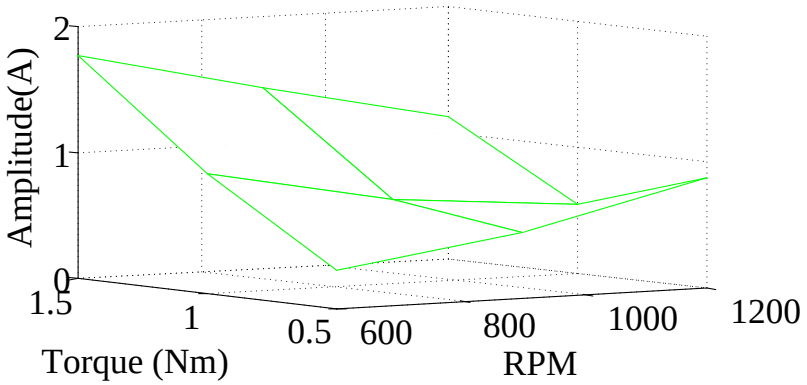

(a)

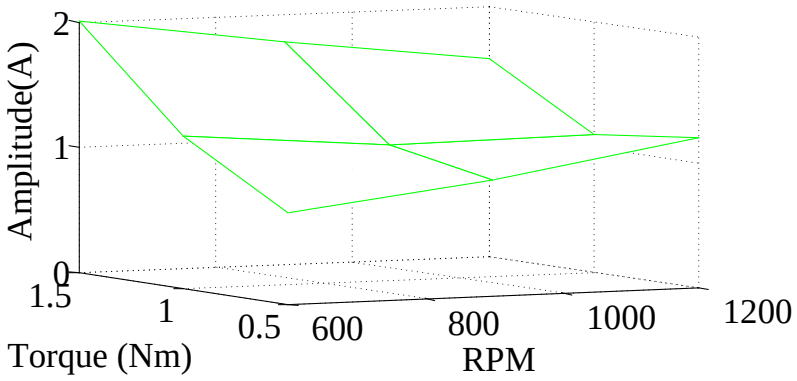

(b)

Figure 2.39. RMS value of fault current i_f with 5 turns shorted and r_f =1.0 Ohm. (a) simulation results, (b) Experimental results.

In the above figures, there are slight differences between simulation and experimental results. This can be caused by several reasons including vibrations, noise, magnet demagnetization and mechanical parameter discrepancies, i.e. inertia and viscous damping factors. Furthermore, 2-D FEA simulations skip the end winding effect, which contributes to these differences as well. However, these differences between simulations and experiments are in a tolerable range and the results have shown the same trend in current variation at different conditions which support the main goal of this study.

2.5 Conclusion

This study presents investigation of short circuit current behavior in PMSM with inter turn short circuit fault under different fault scenarios. Different from previous studies, the fault resistance in the short path is taken into account which is essential for true short circuit fault analysis and remarkably changes the results. There are three key findings in this study:

- The fault severity is directly related with the amplitude of the short circuit current. Therefore, the fault severity is inversely proportional to fault resistance. On the other hand, the number of shorted turns is not always directly proportional to the fault severity. Depending on the fault resistance, number of turns can be directly or inversely proportional to the short circuit current amplitude.
- The current in the shorted turns is combination of short circuit current and phase current. It is dominated by short circuit current when fault resistance is low, and dominated by phase current when fault resistance is high. Thus, depending on the fault resistance, this current share drastically changes between these two scenarios. As the fault evolves and the fault resistance is between two extremes, the current of the shorted turns increases with increasing speed at low torque conditions. However, this relationship is reversed when the load torque is high. Thus the highest fault current situation occurs at the reverse extremes of torque and speed. In real application, based on this analysis, the fault current can be mitigated by selecting proper operation conditions.
- The results from 3rd harmonic analysis show that this component can be used to predict the number of shorted turns during the fault condition. However, it doesn't reveal the

change in short circuit current when the fault resistance is low. Hence, the results from harmonic analysis aren't reliable enough to detect fault severity.

Based on the presented analysis, it can be concluded that the relationship between number of shorted turns and short circuit current level depends on the fault resistance as well. In other words, the fault severity may not be directly equal to number shorted turns. Therefore, this study indicates the need for a new fault severity detection method which can predict the short circuit current accurately. Furthermore, the proposed simulation method can be used to determine the safe operating area (SOA) for faulty machine. Using the same simulation procedure, the safe operating area can be obtained for various operation scenarios where the short circuit current remains in the safe range with zero fault resistance (worst case). In real applications, following a precise identification of number of shorted turns, the faulty machine can be forced to work in SOA with limited speed and torque till the earliest possible maintenance.

CHAPTER 3

ESTIMATION OF NUMBER OF SHORTED TURNS IN ITSC FAULT[3]

3.1 Background

In industrial application, the fault diagnosis algorithm can be categorized into model-based fault diagnosis, signal-based fault diagnosis, knowledge-based fault diagnosis, and hybrid fault diagnosis [83]. For ITSC fault in PMSM, the detection approaches are mainly developed upon signal analysis, including the analysis current, voltage and flux, and model-based analysis, such as parameter variation and back-EMF estimator [84]. The most common method is the motor current signature analysis (MCSA), which identifies the fault by obtaining specific current harmonics via fast Fourier Transform (FFT) [6] [16]. Instead of FFT, the time-frequency analysis, like wavelet analysis [20], [21], [22] [53], short time Fourier Transform (STFT) [21] [22], Hilbert-Huang Transform (HHT) [18] and Wigner-Ville distributions [17], are also applied in the fault detection algorithms for non-stationary state. Some other diagnosis algorithms are developed based on the unbalanced three phase variable model of faulty PMSM. Using the advantage of unbalance, the methods based on symmetrical component analysis are introduced in [49] and [1], where the zero sequence and negative sequence components are used as the fault indicators, respectively. It's known that, the shorted turns reduce the back-EMF, which can be used as the fault indicator. In [31], an extended state observer with second order generalized integrator is designed to observe the back-EMF variation. Furthermore, in [80], a thermal-based estimator is developed for monitoring the unbalanced back-EMF in the faulty machine. Since the short circuit fault reduces

[3] ©2018 IEEE [in Press] Reprinted with permission from Y. Qi, E. Bostanci, M. Zafarani, and B. Akin, "Severity Estimation of Inter Turn Short Circuit Fault for PMSM," in *IEEE Transactions on Industrial Electronics* [in Press].

the equivalent stator winding impedance, a few methods are proposed based on the parameter analysis such as input impedance measurement [34]. The input impedance is calculated by the input voltage and phase current and it reflects the variation in stator winding impedance and back-EMF. A diagnosis method based on high frequency signal injection is given in [45]. In this algorithm, high frequency pulsating voltage signals are injected in rotating reference frame. Due to the change in electrical parameters under fault condition, the current response of the superimposed signal changes accordingly. The artificial neutral network is also applied in the field of ITSC fault diagnosis. In [25], particle swarm optimization (PSO) is used to optimize the ANN weight values during the training process. In [3], a hybrid wavelet package transform (WPT) and ANN based detection algorithm is proposed and tested for both line-fed and inverter-fed IPM machines. Both of the algorithm have shown high accuracy and fast response. However, obtaining a well trained ANN model might be a challenge in real application. The real time diagnosis methods are highly dependent on the motor operating conditions. Therefore, it will be easily affected by the load and speed oscillations. In order to overcome this drawback, off-line diagnosis methods used to monitor the motor at start-up are proposed. For instance, in [35] and [85], diagnosis methods are developed based on the parameter identification of self-commissioning procedures. The stator winding impedance is selected as the fault precursor by taking saturation effects into account.

According to the literature, the characteristics of ITSC fault signatures are directly related to the number of shorted turns [1], [16], [17], [30], [31], [35], [45], [49], [80] and [85]. The amplitude of the signatures increases as the number of shorted turns increases. However, this relationship is too generic to determine the severity of the faulty machines. Furthermore, it is not a straightforward

task to obtain this information in practical applications. In order to figure out the relationship between the fault signature behavior and the number of shorted turns, comprehensive experimental analysis is needed to generate sufficient data for training purpose. On the other hand, the estimation of the shorted turns number analyzed in this study plays an important role in post-fault operation. First, it provides a straightforward description of the damage caused by ITSC fault. Secondly, the number of shorted turns is usually considered as an unknown parameter whereas it is critical in the dynamic fault models. Thus, following the ITSC fault identification, the state space representation of faulty PMSM can be obtained by approximating the number of shorted turns and resistance between shorted nodes. It lays foundation of short circuit current estimation, which is the key element for the fault severity [86]. If the short circuit current can be estimated in real time, the safe operating area of the fault motor can be obtained [28]. Moreover, it can also be used to develop precise mitigation algorithms for suppressing the short circuit current [78], [87].

This study proposes an algorithm to estimate the number of shorted turns in PMSMs based on standstill parameter identification. Using the proposed algorithm, the number of shorted turns in a faulty machine can be obtained directly. As one of the key advantages, this method doesn't require off-line experimental tests to find the relationship between fault signatures' amplitudes and number of shorted turns. Building an ITSC prototype machine for fault characterization is usually expensive and time consuming process. This approach eliminates the need for prototype and hence significantly simplifies the fault characterization. Furthermore, it lays a solid foundation for next steps, like real-time estimation of short circuit current, optimization of mitigation methods and determination of safe operating area.

3.2 Three Phase Equivalent Circuit Model with ITSC

The three phase equivalent circuit model is introduced in [49] and [78]. In order to improve the accuracy, a non-linear circuit model is proposed in [42], where the parameters are obtained through experimental flux linkage measurements. It is also used for ITSC fault analysis in induction machines [88] and [89]. In this study, in order to simply the analysis, the proposed algorithms is analyzed with linear three phase equivalent circuit model mentioned in previous section. However, the simulation verification is performed with nonlinear machine model which is supported by the FEA simulation, including saturation and spatial harmonics

The equivalent circuit model of the stator winding can be described as in (3.1). In order to simplify the expression, the subscription are changed from the expression of three phase to stator side. As a result, the unaffected phase winding can have identical symbol for all parameters.

$$\begin{bmatrix} v_{an} \\ v_{bn} \\ v_{cn} \\ 0 \end{bmatrix} = \begin{bmatrix} R_{sh} & 0 & 0 & R_{sf} \\ 0 & R_s & 0 & 0 \\ 0 & 0 & R_s & 0 \\ -R_f & 0 & 0 & R_{sf}+R_f \end{bmatrix} \begin{bmatrix} i_a \\ i_b \\ i_c \\ i_f \end{bmatrix} + \begin{bmatrix} L_{ssh}+M_{sh-sf} & M_{sh-s}+M_{s-sf} & M_{sh-s}+M_{s-sf} & L_{ssf}+M_{sh-sf} \\ M_{sh-s} & L_{ss} & M_s & M_{s-sf} \\ M_{sh-s} & M_s & L_{ss} & M_{s-sf} \\ M_{sh-sf} & M_{sh-s} & M_{sh-s} & L_{ssf} \end{bmatrix} \frac{d}{dt} \begin{bmatrix} i_a \\ i_b \\ i_c \\ i_f \end{bmatrix} + \begin{bmatrix} e_a \\ e_b \\ e_c \\ e_{af} \end{bmatrix} \quad (3.1)$$

where v_{an}, v_{bn} and v_{cn} are the phase voltage. i_a, i_b and i_c are the phase current. i_s is the circulating current in the shorted path. e_a, e_b and e_c are the back-EMF generated by the permanent magnet on three phase winding. Subscription h and f denote the remaining healthy turns and shorted turns, respectively. R_s, L_{ss} and M_s are stator resistance per phase, self-inductance per phase and mutual inductance between phases, respectively. A fault index η is defined as the ratio of number of

shorted turns over number of turns of one phase winding. It is designed for stator winding connected in series, where the number of turns of one phase windings is equal to the product of number of coils per phase and number of turns per coil. The back-EMF and resistance are assumed to change linearly regarding to the fault index η. Furthermore, the stator winding is assumed to be symmetrical and the ITSC fault has identical impact on other healthy windings. Therefore, the mutual inductance between different phases are identical in this model.

Assuming that PMSM has N_s turns have been shorted out of N_h in a coil of phase A, which has N_c coils in series, then the self-inductance of phase A under fault condition is given as in (3.2). The mutual inductance between coils within the same phase winding is neglected.

$$\begin{aligned} L_{sh} + L_{sf} + 2M_{sh-sf} &= \frac{(N_c - 1)L_{ss}}{N_c} + \frac{(N_h - N_s)^2}{N_h^2}\frac{L_{ss}}{N_c} + \frac{N_s^2}{N_h^2}\frac{L_{ss}}{N_c} + 2\times\frac{N_s(N_h - N_s)}{N_h^2}\frac{L_{ss}}{N_c} \\ &= \frac{(N_c - 1)L_{ss}}{N_c} + \frac{N_h^2}{N_h^2}\frac{L_{ss}}{N_c} \\ &= L_{ss} \end{aligned} \tag{3.2}$$

In order to simplify the overall analysis, it is also assumed that the ITSC fault has symmetrical effect on the other phase windings. Thus, the relationship between the mutual inductances can be given as in (3.3).

$$\begin{aligned} M_{sh-s} + M_{s-sf} &= \frac{N_c N_h - N_s}{N_c N_h} M_s + \frac{N_s}{N_c N_h} M_s \\ &= M_s \end{aligned} \tag{3.3}$$

By substituting (3.2) and (3.3) into (3.1) and defining index $\eta = N_s/N_c N_h$, the three phase equivalent circuit model can be simplified as in (3.4).

$$\begin{bmatrix} v_{an} \\ v_{bn} \\ v_{cn} \\ 0 \end{bmatrix} = \begin{bmatrix} R_s & 0 & 0 & \eta R_s \\ 0 & R_s & 0 & 0 \\ 0 & 0 & R_s & 0 \\ \eta R_s & 0 & 0 & \eta R_s + R_f \end{bmatrix} \begin{bmatrix} i_a \\ i_b \\ i_c \\ -i_s \end{bmatrix} + \begin{bmatrix} L_{ss} & M_s & M_s & \eta L_{ss} \\ M_s & L_{ss} & M_s & \eta M_s \\ M_s & M_s & L_{ss} & \eta M_s \\ \eta L_{ss} & \eta M & \eta M & L_{ssf} \end{bmatrix} \frac{d}{dt} \begin{bmatrix} i_a \\ i_b \\ i_c \\ -i_s \end{bmatrix} + \begin{bmatrix} e_a \\ e_b \\ e_c \\ e_{af} \end{bmatrix} \quad (3.4)$$

The behavior of short circuit loop is given by the last row in (3.1). It can be seen that the short circuit current is highly dependent on the fault index, which is a key prerequisite of this study. Based on previous literature, it can be calculated in stationary condition based on current injection and real time condition based on certain fault signatures.

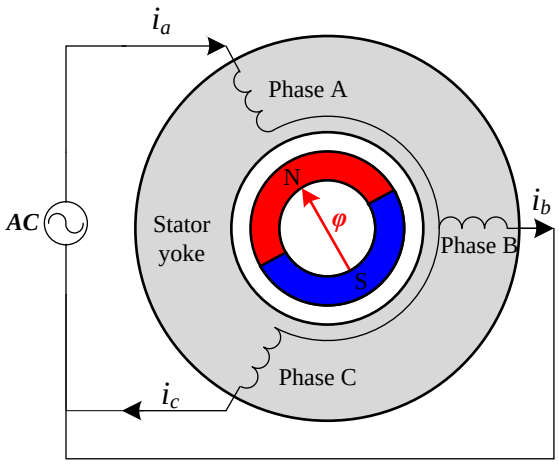

Figure 3.1. AC excitation at standstill condition with 0° electrical angle.

3.3 Analysis of Voltage Variation during AC Excitation at Standstill Condition

The fault severity estimation algorithm is developed based on the parameter identification method at standstill condition, which is mentioned in [35], [90] and [32]. It was originally used to detect the machine failure by the parameter variation. In this algorithm, initially the rotor is aligned to phase A winding, as shown in Figure 3.1. The alignment is achieved by providing identical DC

voltage across terminals A&B and A&C, and shorting terminals B&C. When the rotor is stationary, the AC excitation is applied in similar way, where a sinusoidal AC current is injected form A towards B and C, as shown in Figure 3.1. If the frequency is high enough and the amplitude is relatively low, the injected current does not cause any rotor movement. Thus the back-EMF can be neglected. Based on the voltage command and current response, the synchronous impedance is estimated and hence used to detect the ITSC fault. According to [75], the phase winding with ITSC fault can be identified by comparing the impedance with rotor alignments and directions of the injected currents.

Since the impact of ITSC fault on other healthy phase windings is assumed to be symmetrical, the phase B and phase C current will be identical, if the motor with ITSC fault in phase A is excited as shown in Figure 3.1. Thus, based on (3.4), the corresponding line voltage equation can be derived as following,

$$v_{ab} = R_s i_a + \left(L_{ss} - M_s\right)\frac{di_a}{dt} + \frac{R_s}{2} i_a + \left(\frac{L_{ss}}{2} - \frac{M_s}{2}\right)\frac{di_a}{dt} - \eta R_s i_s - \eta\left(L_{ss} - M_s\right)\frac{di_s}{dt} \quad (3.5)$$

For the surface mounted PMSM, the synchronous inductance L_s is equal to L_{ss} - M_s. Therefore, the above equation can be simplified to,

$$v_{ab} = \frac{3}{2}\left(R_s i_a + L_s \frac{di_a}{dt}\right) - \eta\left(R_s i_s + L_s \frac{di_s}{dt}\right) \quad (3.6)$$

According to (3.6), the equivalent circuit of the fault motor consists of two parts. One is excited by the phase current and is exactly the same as the healthy stator windings. The other one, which introduces the voltage variation, is excited by the short circuit current i_s. However, its impedance is proportional to the healthy one with the rate same as the fault severity index η. In order to simplify the analysis, only the fundamental component is taken into account, which has the same

frequency as the injected sinusoidal current and other harmonics are removed. Thus, equation (3.6) can be rewritten in phasors.

$$\vec{\mathbf{V}}_{ab} = \frac{3}{2}\vec{\mathbf{Z}}_h\vec{\mathbf{I}}_a - \eta\vec{\mathbf{Z}}_h\vec{\mathbf{I}}_s \quad (3.7)$$

where $\vec{\mathbf{Z}}_h$ is the synchronous impedance whose amplitude is equal to $|R_s + j\omega_e L_s|$ and the phase shift is θ_Z. $\vec{\mathbf{I}}_a$, $\vec{\mathbf{I}}_s$ and $\vec{\mathbf{V}}_{ab}$ are phasors of phase A current, short circuit current and line voltage, respectively.

At the same time, the voltage equation of the short circuit loop can be given by (3.8).

$$\eta\left(R_s i_a + L_s\frac{di_a}{dt}\right) - \left[\left(R_f + \eta r_s\right)i_s + L_{ssf}\frac{di_s}{dt}\right] = 0 \quad (3.8)$$

Similarly, it can be expressed by the fundamental component phasors as follows,

$$\eta\vec{\mathbf{Z}}_h\vec{\mathbf{I}}_a - \vec{\mathbf{Z}}_f\vec{\mathbf{I}}_s = 0 \quad (3.9)$$

where, $\vec{\mathbf{Z}}_f$ is the total impedance of the short circuit loop. The amplitude is equal to $|R_f + \eta R_s + j\omega_e L_{ssf}|$ and the phase shift is θ_{zf}.

Since the self-inductance of the shorted turns L_{ssf} is less than the synchronous inductance L_s multiplied by the fault severity index η (detailed in the following part), the short circuit current i_s leads the phase current. The corresponding phasor diagram of voltage and current for fault condition is given in Figure 3.2. Here, the red triangle describes the phasor equation given in (3.7) and the blue phasors describe the phasor equation of short circuit loop shown in (3.9). The phase shift in line to line voltage is θ_v and the angle difference between the actual line to line voltage and the voltage across the stator winding excited by phase current is δ. Since the phase current, line-to-line voltage and synchronous impedance are all accessible, the voltage variance $-\eta\vec{\mathbf{Z}}_h\vec{\mathbf{I}}_s$ can

easily be calculated based on (3.7). Since the synchronous impedance is known, the voltage variation can be simplified to a new phasor, $\vec{\mathbf{K}}$, which is given by (3.10).

$$\vec{\mathbf{K}} = \eta \vec{\mathbf{I}}_s \quad (3.10)$$

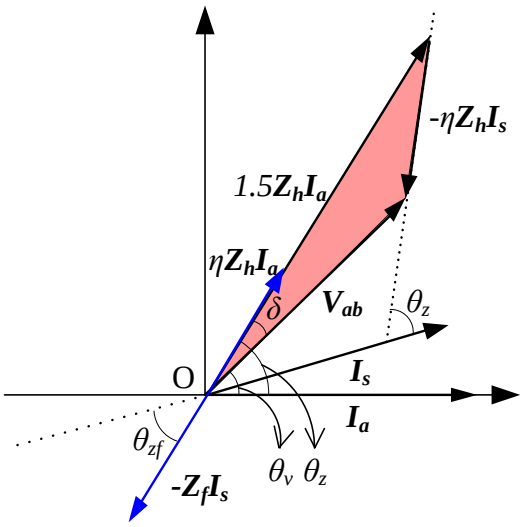

Figure 3.2. Phasor diagram of the equivalent circuit with AC excitation.

3.4 Estimation of Number of Shorted Turns

Following the voltage variance calculation, the product of fault index and short circuit current can be obtained, yet another step is needed to solve η. By substituting (3.10) into (3.9), the following equation can be obtained.

$$\eta^2 \vec{\mathbf{Z}}_h \vec{\mathbf{I}}_a - \vec{\mathbf{Z}}_f \vec{\mathbf{K}} = 0 \quad (3.11)$$

However, the total impedance of the short circuit loop includes two unknown parameters, fault resistance R_f and the self-inductance of shorted turns L_{ssf}. In order to solve η, these two parameters should properly be approximated. In a real application, when the ITSC fault occurs, two conductors

contact directly. Thus the fault resistance in the short circuit loop usually has a very low value. Therefore, it is reasonable to assume that the fault resistance is roughly zero.

In order to estimate the self-inductance of the shorted turns, first, the self-inductance of a single coil must be obtained. There are several methods that can be used to calculate the self-inductance of one coil precisely such as FEA based methods, winding functions and equivalent magnetic circuit.

However, these methods require relatively long computation and detailed input parameter information, like winding topology and motor cross section dimensions which are not easy to obtain. Because the PMSM is designed to have 120° phase shift between the flux generated by each phase winding, the self-inductance of one phase (considering no mutual inductance between the coils of the same phase) is equal to two third of the synchronous inductance. Therefore, the self-inductance of the shorted turns can be derived as follows:

$$L_{ssf} = \frac{2N_s^2}{3N_c N_h^2} L_s = \frac{2N_c}{3} \eta^2 L_s \quad (3.12)$$

However, this approximation may not be valid in the machines with non-overlap fractional-slot concentrated winding. According to [91], the fractional-slot concentrated winding can exhibit very low mutual inductance between phases. In this case, it is recommended to obtain the self-inductance value of single coil via FEA simulations or equivalent magnetic circuit calculation.

According to (3.12), the self-inductance of the shorted turns and the synchronous inductance has the following relationship.

$$\frac{L_{ssf}}{\eta L_s} = \frac{2N_s}{3N_h} \quad (3.13)$$

Under ITSC fault, the number of shorted turns is always less than the number of turns in a healthy coil. Hence, L_{ssf} is always smaller than ηL_s in (3.13). It means that, the reactance of $\vec{\mathbf{z}}_f$ is less than the reactance of $_{\eta}\vec{\mathbf{z}}_h$ in (3.9). Therefore, the short circuit current will be phase leading the phase current.

Based on the approximation of self-inductance L_{ssf}, equation (3.11) can be re-written as,

$$r_f = \eta^2 \sqrt{\frac{\left[R_s^2 + \left(2\pi f L_s\right)^2\right] \times \left|\vec{\mathbf{I}}_a\right|^2}{\left|\vec{\mathbf{K}}\right|^2} - \left(\frac{4\pi f N_c}{3} L_s\right)^2} - \eta R_s \quad (3.14)$$

Hence, assuming that the fault resistance is zero, the fault index can be derived as,

$$\eta = \frac{R_s}{\sqrt{\frac{\left[R_s^2 + \left(2\pi f L_s\right)^2\right] \times \left|\vec{\mathbf{I}}_a\right|^2}{\left|\vec{\mathbf{K}}\right|^2} - \left(\frac{4\pi f N_c}{3} L_s\right)^2}} \quad (3.15)$$

As given in (3.14) and (3.15), high non-zero fault resistance is one of the major factors that could affect the performance of proposed method. Zero fault resistance is possible only in an ideal case for the ITSC fault. In practice, once the current conduction starts and progresses, the fault resistance between the conductors converges to zero, typically in the order of milli-ohm or micro-ohm [92], [93].

If the fault resistance is relatively large, the proposed method is not able to estimate the number of shorted turns accurately. The large fault resistance may exist in an incipient fault condition, where the broken conductors are not fully conducted. It is beyond the focus of this study and need more studies.

However, a non-zero fault resistance is inevitable in the lab experiments due to the taps, sensors and extra wires. Therefore, the fault resistance in the setup may be much larger than real

application, and may results in misleading results if the actual fault resistance value is not used in the model. One should note that the possible shorted turns number are integral series from 1 to N_h. Due to the non-zero fault resistance and system errors, the estimation of the number of shorted turns can be calculated by rounding $\eta N_c N_h$ up towards closest positive integer in order to reduce the error.

3.5 Validation in FEA Based System Simulation

In order to verify the proposed method, the FEA based system simulation mentioned in previous section is used for analysis. The same machine is tested at standstill condition.According to the simulation, the average value of synchronous inductance is 1.8337mH. Meanwhile, the self-inductance of one single coil in healthy condition can be calculated by 2/(3N_c) L_s, which is 0.1746 mH.

The actual self-inductance of one single coil is calculated in the FEA simulation and its average value is 0.1676 mH. It can be seen that the estimated self-inductance of one single coil is very close to the actual self-inductance. Furthermore, the simulation result of shorted turns' self-inductance calculated by (3.12) are 0.0022 mH, 0.0086 mH and 0.0539 mH for 1 turn, 2 turns and 5 turns short circuit fault, respectively. On the other hand, in the simulation, the average values of actual self-inductance for 1 turn, 2 turns and 5 turns short circuit fault are 0.0020 mH, 0.0080 mH and 0.0501 mH, respectively.

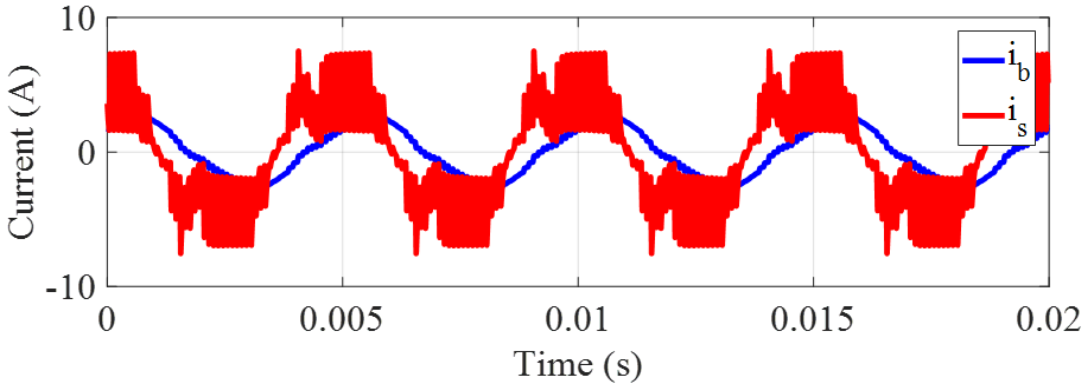

(a)

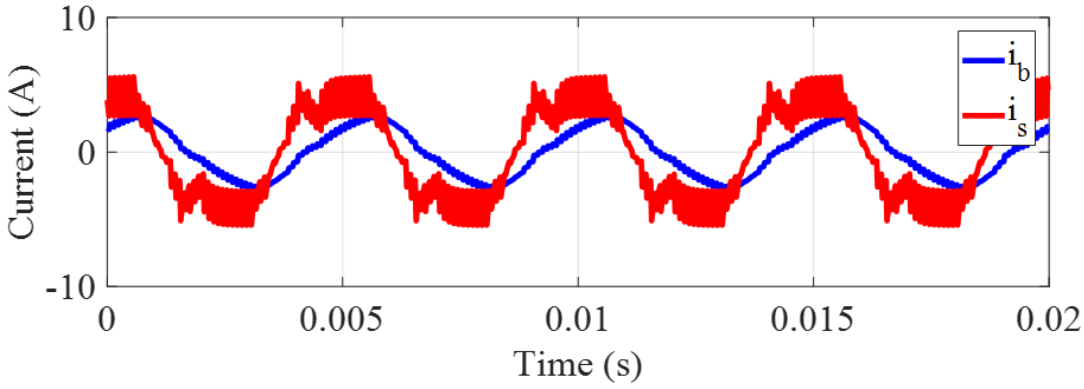

(b)

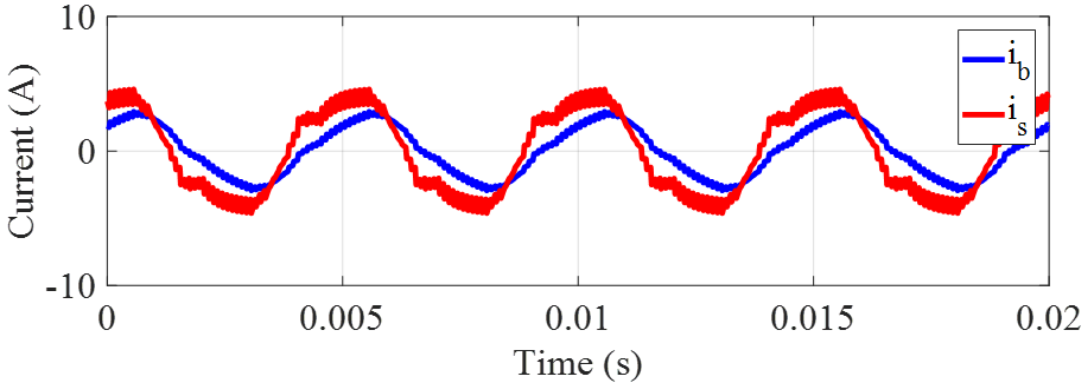

(c)

Figure 3.3. Simulation results of phase current and short circuit current with zero fault resistance. a) 1 turn short circuit case, b) 2 turns short circuit case, c) 5 turn short circuit case.

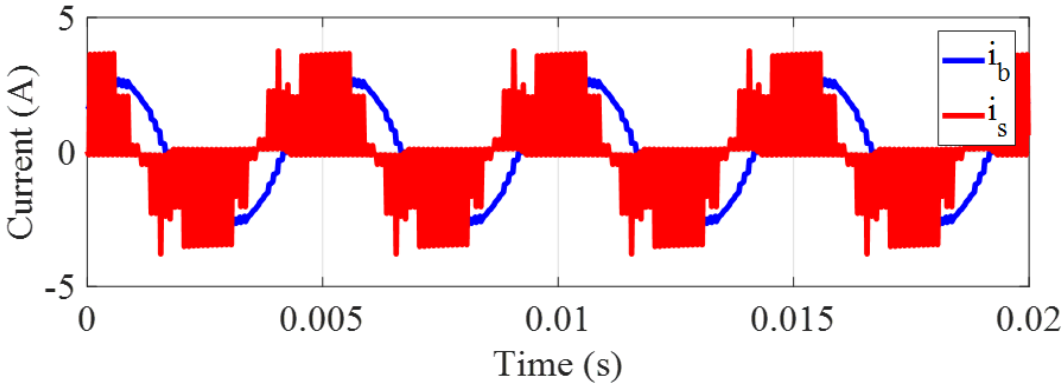

(a)

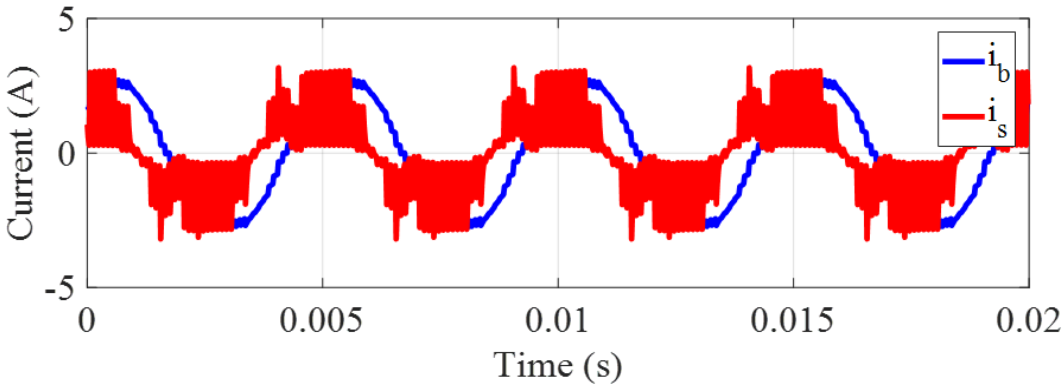

(b)

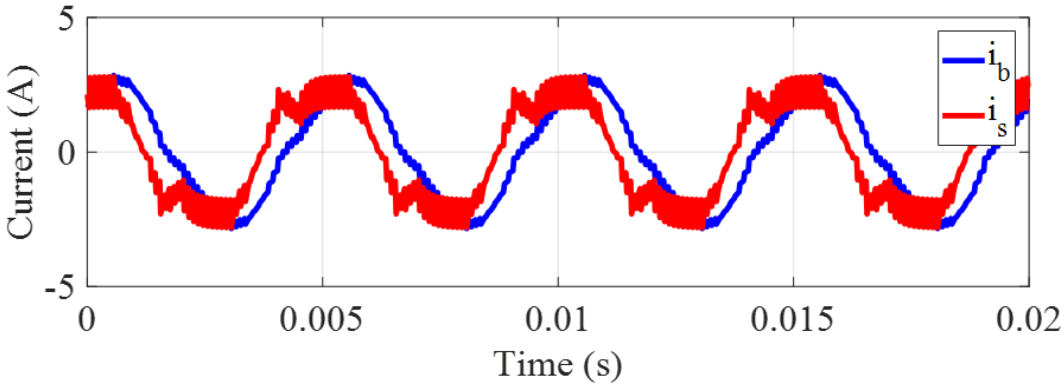

(c)

Figure 3.4. Simulation results of phase current and short circuit current with 0.1 Ohm fault resistance, a) 1 turn short circuit case, b) 2 turns short circuit case, c) 5 turn short circuit case.

In the system simulation, the voltage command is a sine voltage on d-axis and the electrical angle is fixed at 120°. The inverter is controlled to generate 10V, 200Hz line voltage from terminal A to B and C. The system simulation current waveforms are given in Figure 3.3 (sampling frequency is 50 kHz). One can notice that the short circuit current i_s leads the phase current i_b by certain degrees under all fault conditions. In practice, the ITSC fault may have non-zero fault resistance. Therefore, the same simulation is also carried out with 0.1 Ohm resistance and the corresponding current waveform is given in Figure 3.4. It can be seen that the short circuit current is suppressed by the non-zero fault resistance. Furthermore, due to the non-zero fault resistance, the time constant of short circuit loop decreases and a larger current ripple can be observed in the current waveform.

The results of the fault severity estimation are given in Table 3.1. The fault index can be obtained precisely under different fault conditions as well. The number of shorted turns can be calculated by rounding the product of η, N_c and N_h. From the simulation results, one can notice that the phase current slightly increases as the number of shorted turns increase. However, under the same excitation conditions, the short circuit current decreases when the number of shorted turns increases. This is caused by the zero fault resistance. When R_f is equal to zero, the voltage equation of short circuit loop can be simplified to,

$$\left(R_s i_a + L_s \frac{di_a}{dt}\right) = \left(R_s i_s + \frac{2N_c}{3}\eta L_s \frac{di_s}{dt}\right) \quad (3.16)$$

Equation (3.16) reveals the relationships between the short circuit current and phase current inside the short circuit loop without fault resistance. Under the same current excitation, the short circuit current decreases when the fault index increases.

Table 3.1. Simulation results with zero fault resistance

Frequency 200 Hz	1 turn short circuit fault	2 turn short circuit fault	5 turn short circuit fault
Amplitude of line to line Voltage (V)	10.1703	10.1553	10.0065
Amplitude of phase B current (A)	2.4978	2.5305	2.6174
Amplitude of Short Circuit current (A)	4.4784	4.4207	4.1387
Phase shift δ (°)	0.8870	1.5616	2.5275
Synchronous impedance (Ohm)	2.7421	2.7421	2.7421
Amplitude of voltage variation caused by fault (V)	0.1891	0.3774	0.8866
Estimated $\left\|\vec{\mathbf{K}}\right\|$	0.0690	0.1376	0.3233
Actual $\left\|\vec{\mathbf{K}}\right\|$	0.0711	0.1403	0.3285
Actual η	0.0159	0.0317	0.0794
Estimated η	0.0157	0.0314	0.0794
Estimated shorted turns	1	2	5

3.6 Experimental results

In order to verify the practicability of the proposed method, the same prototype ITSC fault PMSM and motor drive system are tested in the experiment. The proposed method requires that the AC excitation is aligned with faulty phase winding, which might not be guaranteed in real applications. Therefore, it is necessary to detect the fault location at first. This can be accomplished by algorithms detecting the occurrence and location of ITSC fault [35]. After locating the ITSC fault, the proposed method can be implemented to estimate the number of shorted turns. Similar to the simulation, the inverter applies sinusoidal line voltage to the motor. Since the fault location is phase B winding, the electrical angle of voltage command is also fixed to 120°. The amplitude of the applied voltage is limited to 10 V so that the short circuit current can be kept in a safe range, which reduces the thermal impact on the estimation as well. However, in actual applications, it can be selected based on the resolution of the voltage measurement. The frequency of applied voltage is set to 200 Hz. If this frequency is low, the rotor may not hold at standstill for long enough time. The non- stationary rotor generates back-EMF, which lets the proposed algorithm fail. Furthermore, the proposed calculation is based on the voltage variation introduced by the short circuit. Due to the small number of shorted turns, voltage variation is very small. If the applied signal has low frequency, the voltage variation cannot be captured. On the other hand, if the frequency of line voltage is too high, the estimation error of the shorted turn self-inductance affects the results. Since it may be very difficult to obtain the accurate self-inductance of shorted turns in real application, the frequency of applied AC signal cannot be calculated in advance. Therefore, based on the above considerations, the phase angle of the synchronous impedance is used as the reference of AC excitation. The impedance angle close to 45° is preferred which can generate

enough voltage variation and avoid the influence of self-inductance estimation error. During the experiment, the frequency is set to 200 Hz, where the phase angle of the synchronous impedance is around 51°.

The current waveforms are given in Figure 3.5, where the short circuit current leads. However, there are some differences between the amplitude of short circuit current in the simulation versus experimental results. From Figure 3.5, one can notice that the amplitude of the short circuit current increase as the fault index η increases, whereas the amplitude decreases in the simulation. This is caused by the non-zero fault resistance R_f. Since the short circuit fault in the tested motor is made artificially, fault resistances are added into the short circuit loop by the taps, current sensors and extra wires. Thus the ideal condition described in (3.16) is no longer valid in this situation even without external resistances. The fault resistance of the experiment setup is around 0.1 Ohms. On the other hand, based on the estimation of L_{ssf}, the total impedance of short circuit loop at 200 Hz frequency are 0.0773 Ohm, 0.1049 Ohm and 0.1959 Ohm for 1 turn, 2 turns and 5 turns short circuit fault respectively. Referring to (3.9), the amplitude of short circuit current can be calculated by,

$$\left|\vec{\mathbf{I}}_s\right| = \frac{\eta}{\left|\vec{\mathbf{Z}}_f\right|}\left|\vec{\mathbf{Z}}_h\right|\left|\vec{\mathbf{I}}_a\right| \quad (3.17)$$

where the value of η over is equal to 0.2054, 0.3025 and 0.4054 for 1 turn, 2 turns and 5 turns short circuit fault respectively. One can notice that this value increases as the fault index increases. Thus, under the same current excitation, the amplitude of short circuit current increases as the number of shorted turns increases.

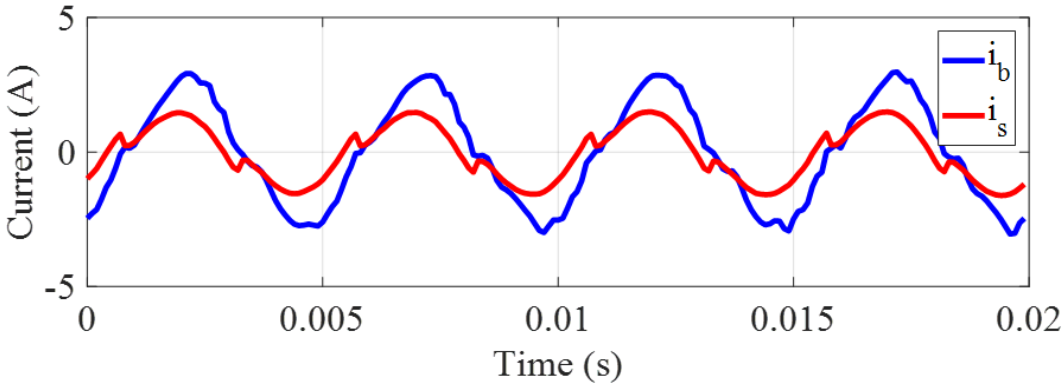

(a)

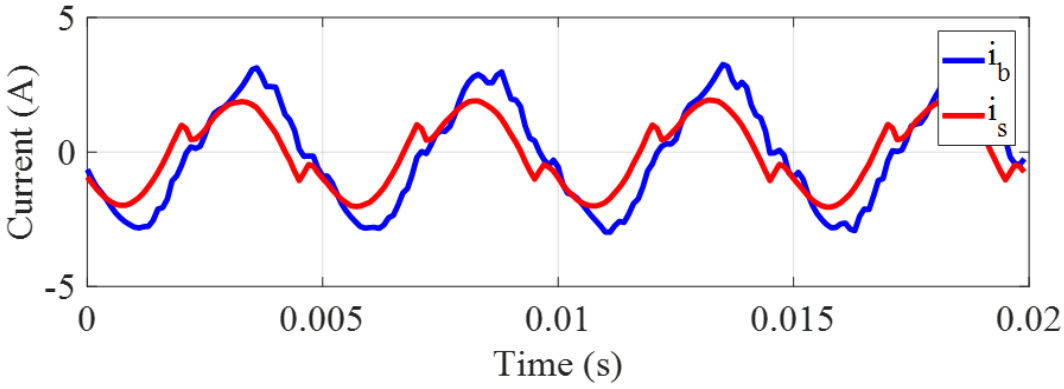

(b)

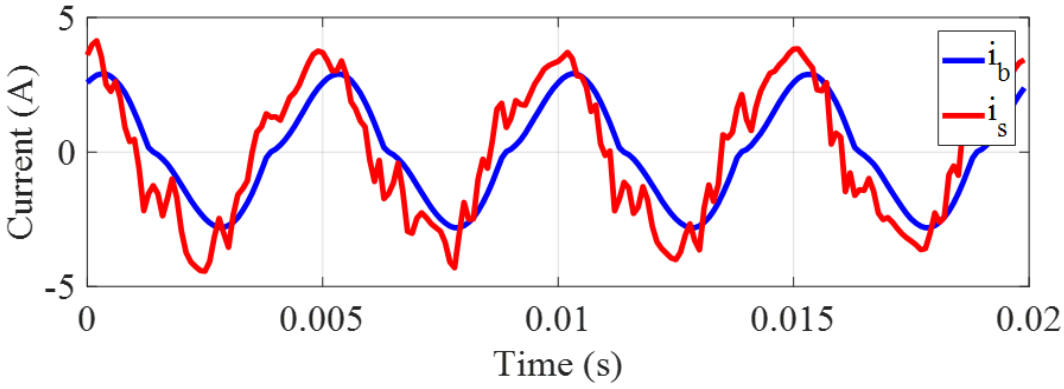

(c)

Figure 3.5. Experimental results of phase current and short circuit current. a) 1 turn short circuit case, b) 2 turns short circuit case, c) 5 turn short circuit case.

Table 3.2. Experimental results of fault index estimation

Frequency 200 Hz	1 turn short circuit fault	2 turn short circuit fault	5 turn short circuit fault
Amplitude of line to line Voltage (V)	10.0702	10.1123	10.1005
Amplitude of phase B current (A)	2.5126	2.5363	2.6414
Amplitude of Short Circuit current (A)	1.7192	2.0679	2.7851
Phase shift δ (°)	0.5149	0.6103	1.9705
Synchronous impedance (Ohm)	2.6756	2.6756	2.6756
Voltage variation caused by fault (V)	0.0917	0.1272	0.6139
Estimated $\left\|\vec{\mathbf{K}}\right\|$	0.0343	0.0475	0.2295
Actual $\left\|\vec{\mathbf{K}}\right\|$	0.0273	0.0656	0.2210
Actual η	0.0159	0.0317	0.0794
Estimated η	0.0088	0.0120	0.0586
Estimated shorted turns	1	1	4

The fault index estimation is given in Table 3.2. The synchronous impedance is measured when all the taps are disconnected. In a real application, it can be measured at the very beginning and stored as reference value. According to Table 3.2, the number of shorted turns can be estimated successfully, but 1 turn error. Compared to the simulation results, this error is caused by the non-zero fault resistance. Referring to (3.14), the fault resistance can be calculated by presuming the fault index. By sweeping the number of shorted turns from 1 to 9, the estimated fault resistance can be plotted as in Figure 3.6. Another simulation is carried out for the same fault resistance and the result is shared in Figure 3.7. It can be noticed that, in the 2 turn and 5 turn short circuit case, the fault resistance can be calculated accurately and it is consistent with the simulation results shown in Figure 3.6. On the other hand, it means that the number of shorted turns can be estimated precisely by considering the non-zero fault resistance as well. However, in 1 turn short circuit fault, the fault resistance estimation is not as precise as the other two cases. This is because the amplitude of voltage variation is too low to measure accurately. In Table 3.2, one can find that the voltage variation of 1 turn and 2 turns short circuit fault are so small and can be affected by measurement noise easily. Furthermore, the imperfect manufacture may also affect the estimation in this scenario. However, the results are still in an acceptable range. Here, note that the non-zero fault resistance is introduced mainly by the extra wires and soldering which are necessary in the experiments but don't necessarily exist in real application. Therefore, the actual fault resistances are much lower in real ITSC fault and the proposed method can have better performance than the experimental results presented here.

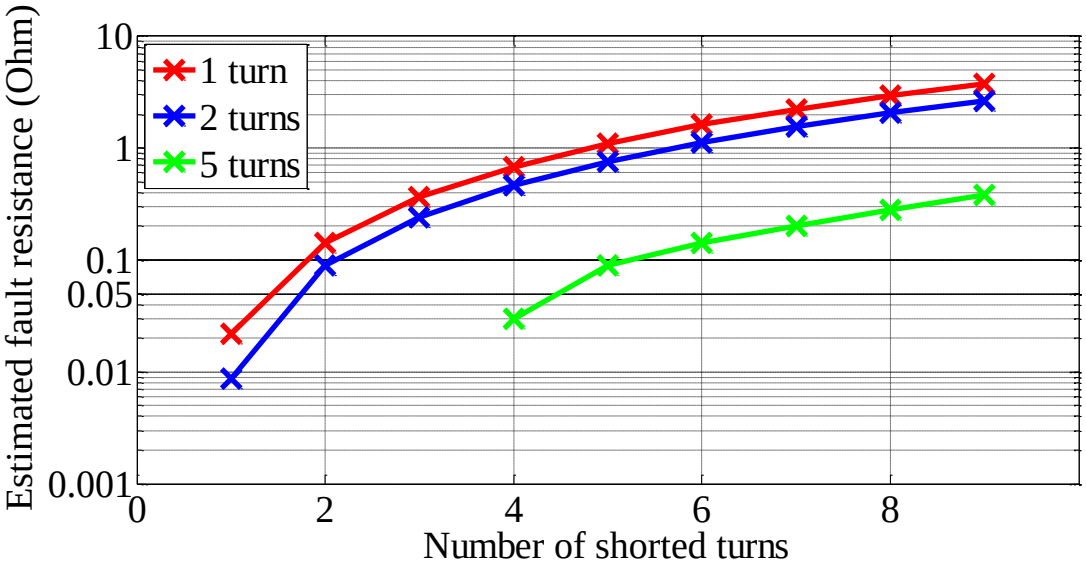

Figure 3.6 Experimental results of fault resistance estimation.

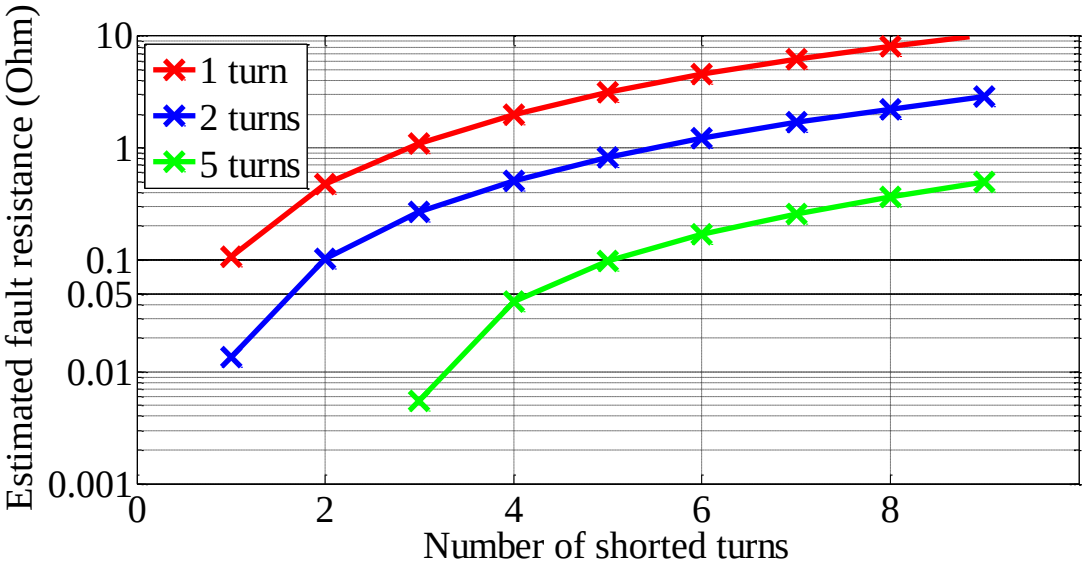

Figure 3.7. Simulation results of fault resistance estimation.

3.7 Conclusion

This study presents a novel method to estimate the faulty severity of ITSC fault in PMSMs. The proposed method is developed based on a parameter identification algorithm at standstill

conditions. Instead of using fault characterization database obtained by the exhaustive experimental results, this method requires synchronous impedance, number of coils and turns of the tested machine. More importantly, instead of searching a relationship between the fault signature and number of shorted turns, this approach provides the number of shorted turns directly. Therefore, it eliminates the need for prototype with artificial fault to characterize motor ITSC fault. On the other hand, the results from this study can be used for ITSC fault mitigation and post fault operation. For example, it can be deployed to optimize current mitigation methods, like field weakening control to suppress the short circuit current. Also, as the number of shorted turns is obtained, it is relatively easy to estimate the short circuit current and define a safe operation area for faulty motor.

CHAPTER 4

SHORT CIRCUIT CURRENT ESTIMATION[4]

4.1 Background

Following the studies on fault detection, the topic of ITSC fault mitigation is the next important step to avoid catastrophic faults. The stator fault mitigation algorithms were first analyzed based on multi-phase PM machines, which have better fault tolerance compared to three phase machine [94] [95]. During the fault condition, multi-phase PM machines exhibit better immunity due to phase windings which generate desired rotating flux for maintaining torque output. In [96], P. Arumugam, C. Gerada and T. Hamiti give a review of mitigation methods of ITSC fault on PM machines. For multi-phase PM machines, the ITSC fault can be mitigated by terminal shorting method, if each phase winding is excited by separate H-bridge inverter. Under ITSC fault condition, the faulty phase can be shorted by the inverter and the short circuit current can be kept in a safe range by proper designs, such as high winding impedance and high current capacity. Phase current injection is an alternative algorithm that can suppress the short circuit current [97]. The principle of this method is to inject predetermined current waveform in remaining healthy windings to nullify the flux associated with the shorted turns. Moreover, the ITSC fault can also be mitigated by specific fault tolerance designs, such as the slot wedge shunt [96]. By using magnetic wedges, it is possible to decouple the rotor flux from the stator windings and reduce the back-EMF in shorted winding. The magnetic wedges can be mechanical shunt and electrical shunt, which are driven by mechanical springs and control windings, respectively. For three phase PM

[4] Reprinted with permission from Y. Qi, M. Zafarani, V. Gurusamy and B. Akin, "Advanced Severity Monitoring of Inter Turn Short Circuit Fault on PMSMs." (to be submitted)

machine, an ITSC fault mitigation algorithm is developed upon field weakening technique in [87]. The concept of this method is injecting negative d-axis current to reduce the magnetic flux coupled with shorted turns. Compared to normal operation, the current injection method can suppress the short circuit current by maintaining the same speed, but the trade-off is decreased torque output.

According to studies on fault mitigation mentioned before, it is worth noting that short circuit current is the key element in ITSC fault, since it is the main reason of causing winding damage after ITSC fault initialized. Therefore, the fault severity is considerably dependent on short circuit current level. However, in the studies of ITSC fault detection, the fault severity is usually defined as the number of shorted turns, which cannot comprehensively evaluate ITSC fault during normal operation.

Thus, this study proposed an advanced fault severity monitoring method, which provides short circuit current estimation for ITSC fault on PMSM. As one of the key advantages, the ITSC fault severity can be quantified in a better way of evaluating the damage on the machine. Furthermore, proper post-fault operation command can be made upon the current capacity of stator windings and short circuit current estimation results. The short circuit current can be reduced in a moderate level by decreasing the speed and torque output in a purposeful manner, instead of tuning blindly. Furthermore, it can also be used to examine the performance of fault mitigation algorithms by observing short circuit current level.

4.2 Short Circuit Current Estimation Algorithm for ITSC Fault PMSM

In this section, the theoretical basis of proposed method is presented in detail. Initially, the ITSC fault is analyzed in a three phase equivalent circuit model. Following the analysis, the characteristic of ITSC fault is investigated and a back-EMF estimator is applied to calculate the voltage variation

caused by ITSC fault. Based on the machine parameters, the short circuit current can be derived, which is introduced in the last part.

4.2.1 Analysis of Voltage Variation Caused by ITSC

As shown in Figure 2.2, the ITSC fault equivalent circuit model can be used as a normal three phase machine, where the short circuit current is injected into certain turns. Thus, the three phase model can be divided into two parts: the healthy three phase winding and the disturbance introduced by short circuit current, as shown in (4.1). The last two terms in (4.1) denotes the voltage variation caused by ITSC fault and the rest terms are same as the healthy stator winding. However, it is inconvenient to analyze this equation in real application, since the neutral point voltage cannot be accessed in Y connected windings with disconnected neutral point. Thus, it is difficult to determine the phase voltage under ITSC fault condition.

$$\begin{bmatrix} v_{an} \\ v_{bn} \\ v_{cn} \end{bmatrix} = \begin{bmatrix} R_s & 0 & 0 \\ 0 & R_s & 0 \\ 0 & 0 & R_s \end{bmatrix} \begin{bmatrix} i_a \\ i_b \\ i_c \end{bmatrix} + \begin{bmatrix} L_{ss} & M_s & M_s \\ M_s & L_{ss} & M_s \\ M_s & M_s & L_{ss} \end{bmatrix} \frac{d}{dt} \begin{bmatrix} i_a \\ i_b \\ i_c \end{bmatrix} + \begin{bmatrix} e_a \\ e_b \\ e_c \end{bmatrix} - \begin{bmatrix} \eta r_s \\ 0 \\ 0 \end{bmatrix} i_s - \begin{bmatrix} \eta L_{ss} \\ \eta M_s \\ \eta M_s \end{bmatrix} \frac{di_s}{dt} \quad (4.1)$$

$$\begin{bmatrix} v_\alpha \\ v_\beta \end{bmatrix} = \begin{bmatrix} R_s & 0 \\ 0 & R_s \end{bmatrix} \begin{bmatrix} i_\alpha \\ i_\beta \end{bmatrix} + \begin{bmatrix} L_s & 0 \\ 0 & L_s \end{bmatrix} \frac{d}{dt} \begin{bmatrix} i_\alpha \\ i_\beta \end{bmatrix} + \begin{bmatrix} e_\alpha \\ e_\beta \end{bmatrix} - \frac{2}{3} \begin{bmatrix} \eta R_s \\ 0 \end{bmatrix} i_s - \frac{2}{3} \begin{bmatrix} \eta L_s \\ 0 \end{bmatrix} \frac{di_s}{dt} \quad (4.2)$$

In order to simplify the analysis, the alpha-beta transformation is applied and the voltage equation can be transformed into (4.2), where v_α and v_β are voltage in alpha-beta reference frame and can be calculated based the terminal voltage of three phase winding. In (4.2), the self-inductance and mutual inductance are replaced by synchronous inductance L_s, which can be measured in healthy condition and used as reference for the estimation. It is worth noting that the voltage variation caused by ITSC fault only appears in alpha-axis and the voltage equation of beta-axis is not

affected. If the fault locates at phase B or C, this analysis can be performed by aligning the transformation matrix to the faulty phase. Thus, the fault has to be located before the analysis. In [49] and [85], different methods of fault location detection are introduced for online and offline diagnosis. Furthermore, the above analysis indicates that it is possible to calculate the short circuit current when the fault index is known. According to [16], the fault index can be calculated based on the k-nearest neighbor (KNN) method.

Based on the studies mentioned above, the short circuit current estimation can be performed. It requires precise measurement of the healthy back-EMF waveform, which is used as the reference in calculating short circuit current. However, the back-EMF measurement is usually difficult in real application, since it needs additional actuator to drive the PM machine for measurement. Fortunately, the back-EMF can also be accessed by closed loop estimator, which is widely used in sensorless control. In this study, the back-EMF estimator is applied parallel to the control loop. The output of the estimator is not feedback to speed controller but used for observing the back-EMF and short circuit current estimation.

If the back-EMF estimator is performed based on the parameters in healthy condition, the estimator cannot identify the voltage variation caused by ITSC fault. Therefore, the estimated back-EMF will include both the voltage variation and actual back-EMF.

This study only focuses on the fundamental component of short circuit current, since it is dominant and makes the most contributions to the heat. The fundamental component of estimated back-EMF under ITSC fault can be given by,

$$\vec{\mathbf{e}}_{\alpha}^{*} = \vec{\mathbf{e}}_{\alpha} - \frac{2}{3}\eta\vec{\mathbf{Z}}_{h}\vec{\mathbf{i}}_{s} \quad (4.3)$$

$$\vec{\mathbf{e}}_{\beta}^{*} = \vec{\mathbf{e}}_{\beta} \quad (4.4)$$

where $\vec{\mathbf{e}}_{\alpha}^{*}$ and $\vec{\mathbf{e}}_{\beta}^{*}$ are the estimated back-EMF of alpha-axis and beta-axis, respectively. $\vec{\mathbf{Z}}_{h}$ is the stator winding impedance under healthy condition.

It can be seen that the estimated back-EMF on alpha-axis is equal to the actual value subtracted by the voltage variation, which is related to fault index, stator winding impedance and short circuit current. The estimated back-EMF on beta-axis is equal to the actual value, since it is affected by ITSC fault. For healthy PMSM, $\vec{\mathbf{e}}_{\alpha}$ has identical amplitude and 90° phase lead compared to $\vec{\mathbf{e}}_{\beta}$. Thus, the short circuit current can be calculated by,

$$\vec{\mathbf{i}}_{s} = \frac{3}{2}\frac{j\vec{\mathbf{e}}_{\beta}^{*} - \vec{\mathbf{e}}_{\alpha}^{*}}{\eta\vec{\mathbf{Z}}_{h}} \quad (4.5)$$

Based on above analysis, the procedure of short circuit current estimation can be described as following. First, the synchronous impedance of PMSM has to be identified in healthy condition and used as a reference. When the ITSC fault is detected during normal condition, the faulty phase should be located and the fault index has to be calculated. Following that, the faulty machine can continue to operae and back-EMF estimator is used for calculating the voltage variance caused by ITSC fault. Based on the estimated fault index and voltage variance, the short circuit current can be estimated from above analysis.

4.2.2 Back-EMF Estimation

Based on above analysis, in order to calculate the short circuit current, the back-EMF must be estimated correctly. The back-EMF can be calculated by (4.2), where the variables, including voltage, current and impedance, are all accessible. However, the calculation requires

differentiation of the current. It makes the calculation vulnerable, since the differentiation process will amplify the current noise significantly. Thus, in order to avoid differentiation of the measured current, a close loop observer is needed for back-EMF calculation. There are several types of observers can be used in the back-EMF estimation, such as sliding mode observer [98], extended state observer (ESO) [31] and Luenberger observer.

In this study, the back-EMF is estimated by a proportional-integral (PI) observer [99], which was designed for the estimation of system disturbance and unknown input.

The differential equation of stator winding in alpha-beta reference frame is given by.

$$\frac{d}{dt}\begin{bmatrix} i_\alpha \\ i_\beta \end{bmatrix} = -\frac{R_s}{L_s}\begin{bmatrix} i_\alpha \\ i_\beta \end{bmatrix} - \frac{1}{L_s}\begin{bmatrix} e_\alpha^* \\ e_\beta^* \end{bmatrix} + \frac{1}{L_s}\begin{bmatrix} v_\alpha \\ v_\beta \end{bmatrix} \quad (4.6)$$

where e_α^* and e_β^* are the estimated back-EMF of alpha-axis and beta-axis, respectively.

The PI controllers is applied to calculate the back-EMF based on the error of actual current and estimated current. Since the differential equation of alpha-axis is the same as the one of beta-axis, the PI observer for different axis are identical. In order to analyze the dynamic of the system, the output of the integrator is extended to a new state variable f_α, which denotes the system unknown input. f_α is described by,

$$f_\alpha = -\frac{e_\alpha}{L_s} \quad (4.7)$$

The structure of PI observer of alpha-axis is given by Figure 4.1

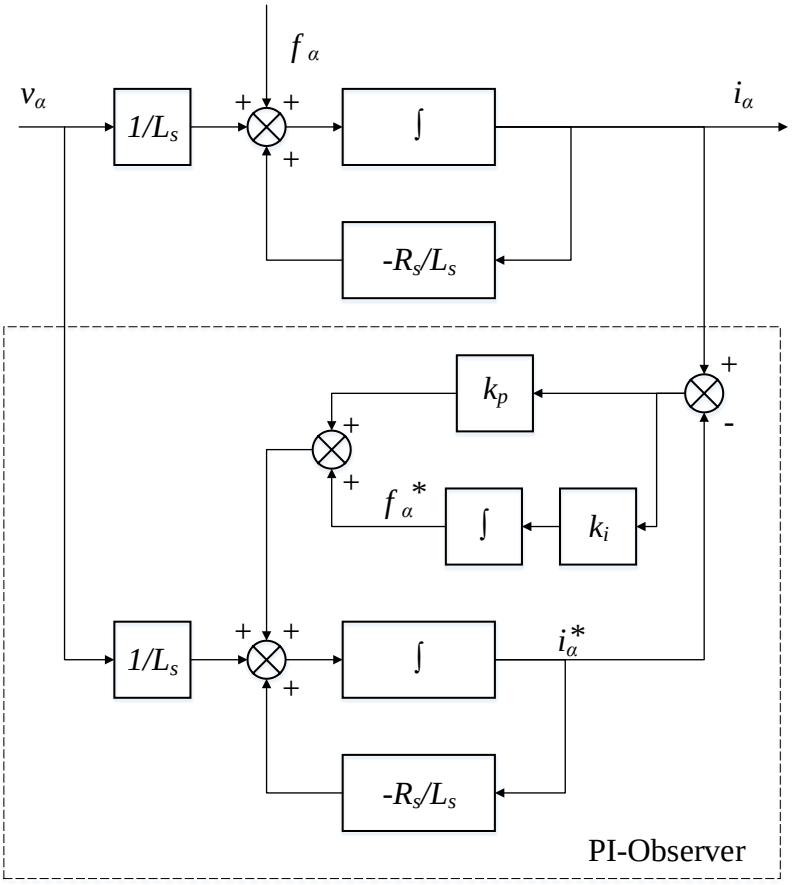

Figure 4.1. Structure of PI observer.

Based on Figure 4.1, the dynamic of PI observer of alpha-axis are described by,

$$\begin{bmatrix} \dot{i}_\alpha^* \\ \dot{f}_\alpha^* \end{bmatrix} = \begin{bmatrix} -\frac{R_s}{L_s} & 1 \\ 0 & 0 \end{bmatrix} \begin{bmatrix} i_\alpha^* \\ f_\alpha^* \end{bmatrix} + \begin{bmatrix} \frac{1}{L_s} \\ 0 \end{bmatrix} v_\alpha + \begin{bmatrix} k_p \\ k_i \end{bmatrix} \left(i_\alpha - i_\alpha^* \right) \quad (4.8)$$

where i_α^* is the estimated value of i_α. k_p and k_i are the proportional gain and integral gain, respectively. f_α^* is the estimated unknown input. According to (4.8), the estimated unknown input can be used to describe the estimated back-EMF.

Equation (4.8) can be simplified to (4.9), which is given by,

$$\begin{bmatrix} \dot{i}_\alpha^* \\ \dot{f}_\alpha^* \end{bmatrix} = \begin{bmatrix} -\frac{R_s}{L_s} - k_p & 1 \\ -k_i & 0 \end{bmatrix} \begin{bmatrix} i_\alpha^* \\ f_\alpha^* \end{bmatrix} + \begin{bmatrix} \frac{1}{L_s} \\ 0 \end{bmatrix} v_\alpha + \begin{bmatrix} k_p \\ k_i \end{bmatrix} i_\alpha \quad (4.9)$$

Based on (4.9), the characteristic polynomial of the PI observer can be given by,

$$p(s) = s^2 + \left(\frac{R_s}{L_s} + k_p \right) s + k_i \quad (4.10)$$

Based on (4.10), the design of PI observer is simplified to find the characteristic polynomial by selecting proper k_p and k_i for the PI controller. The simplified method of finding characteristic polynomial can be achieved by assuming to have two identical negative real pole of (4.10). Thus, the integral gain can be determined by,

$$k_i = \frac{1}{4} \left(\frac{R_s}{L_s} + k_p \right)^2 \quad (4.11)$$

Hence, the characteristic polynomial is simplified to,

$$p(s) = \left(s + \frac{R_s}{2L_s} + \frac{k_p}{2} \right)^2 \quad (4.12)$$

Thus, the system bandwidth is determined by the poles given by (4.12) and it can be selected based on the operating speed and switching frequency. In this study, the observer bandwidth is designed around 1 kHz, which is 10 times lower than the switching frequency.

4.3 Validation in FEA Based Simulation

In order to verify the proposed algorithm, the systematic simulation method referred in chapter 2 is carried out in this study. The system overview is shown in Figure 4.2. In system simulation, the PMSM operates under speed regulation with FOC. The PMSM is driven by a voltage source

inverter with pulse width modulation (PWM). Therefore, a low pass filter is used for terminal voltage measurement and corresponding compensation is applied for fundamental component.

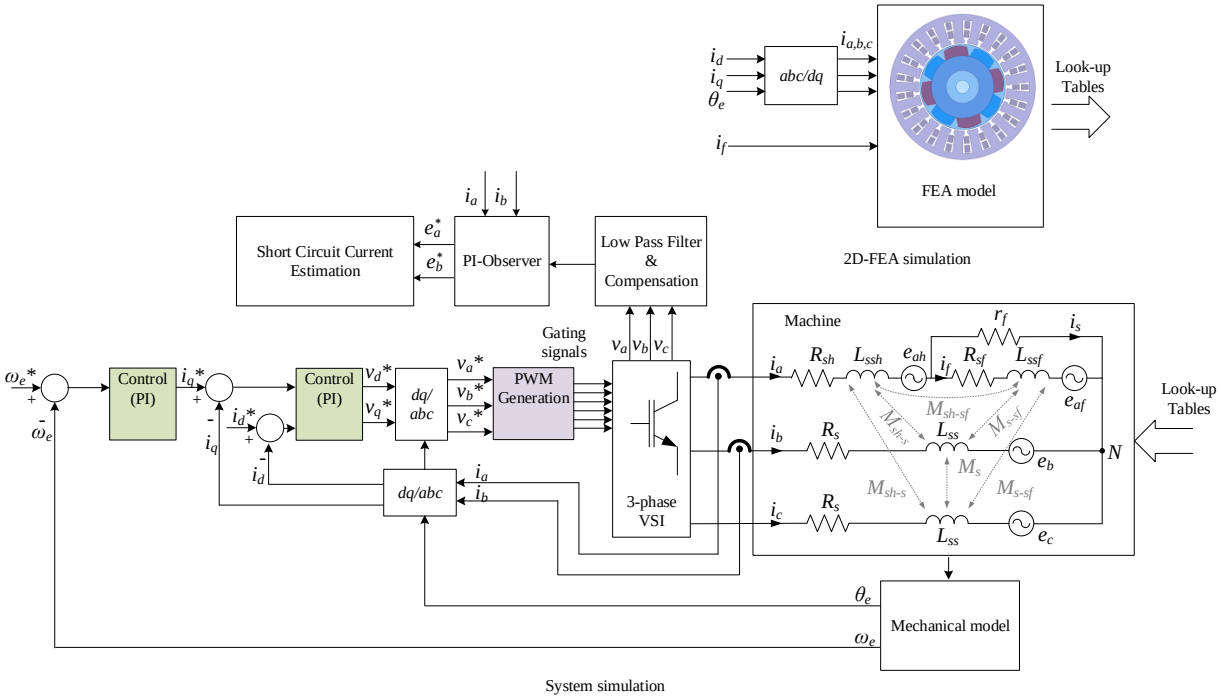

Figure 4.2. Block diagram of FEA supported system simulation.

The proposed algorithm is performed parallel to the control loop with 10 kHz sampling frequency. The machine parameter is listed in Table 2.1 and zero fault resistance is applied in the simulation. In order to maintain the short circuit current in a reasonable range, the PMSM is operated at low speed, which is 1200 RPM.

The simulation results in 1 turn short circuit condition are given in Figure 4.3 to Figure 4.5 and the numerical analysis of different fault conditions is given in Table 4.1. As shown in Figure 4.3, the estimated back-EMF waveform is close to the actual back-EMF waveform. There is a small phase shift between the estimated value and measured value, which is caused by the delay of PI observer. However, it doesn't affect the short circuit current results, since phase shift are identical in the two

axis and hence the relative phase shift of between estimated back-EMF in alpha-beta frame doesn't change. The estimated back-EMF of alpha-axis and beta-axis have very close amplitude and the phase shift is around 90°. It means that the voltage variance caused by ITSC fault has limited effect. The main reason is the small number of turns involved in the ITSC fault compared to the total number of turns in one phase. According to (4.3), the amplitude of voltage variation caused by ITSC fault is related with the fault index and short circuit current. Although the short circuit current is several times higher than rated current, it is still limited by the impedance of the shorted turns. However, the fault index is extremely low in this case. Therefore, the voltage variation is not obvious compared to the back-EMF of entire winding. The measured current and estimated current waveforms are shown in Figure 4.4. It can be seen that the proposed PI observer can drive to the estimation error to zero successfully. The short circuit current waveform is also shown in Figure 4.5. One can see that the amplitude of short circuit current is much higher than rated current even when the motor is running at low speed condition. This over rated current can greatly increase the electrical and thermal stress on fault winding and hence cause severe damage. However, according to the results given in Table 4.1, the short circuit current amplitude doesn't change too much regarding different number of shorted turns. This is mainly caused by zero fault resistance and low operating speed. Assuming a linear change in resistance and back-EMF, the equation of short circuit loop with zero fault resistance can be modified as,

$$R_s i_s + \frac{L_{ssf} di_s}{\eta dt} = R_s i_a + L_{ss} \frac{di_a}{dt} + M_s \frac{di_b}{dt} + M_s \frac{di_c}{dt} + e_a \quad (4.13)$$

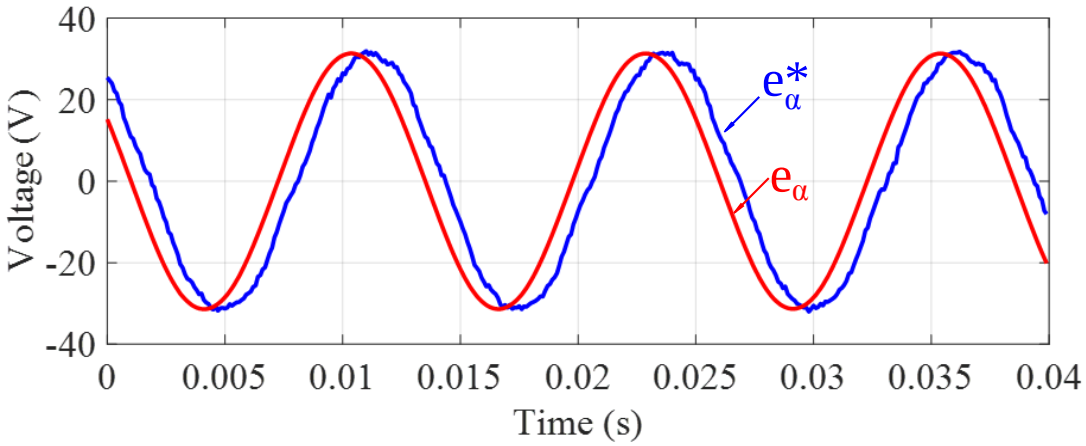

(a)

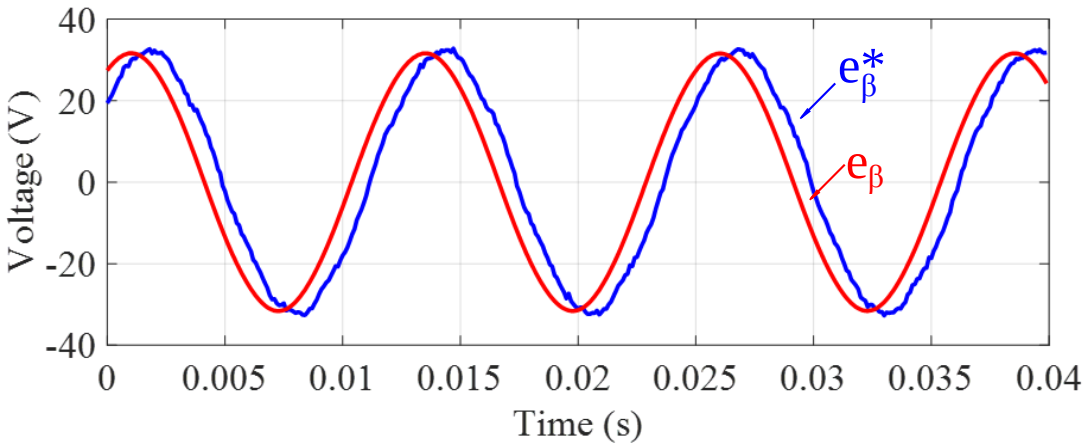

(b)

Figure 4.3. Simulation result of back-EMF in 1 turn short circuit fault condition. a) estimated back-EMF and measured back-EMF in alpha-axis, b) estimated back-EMF and measured back-EMF in beta-axis.

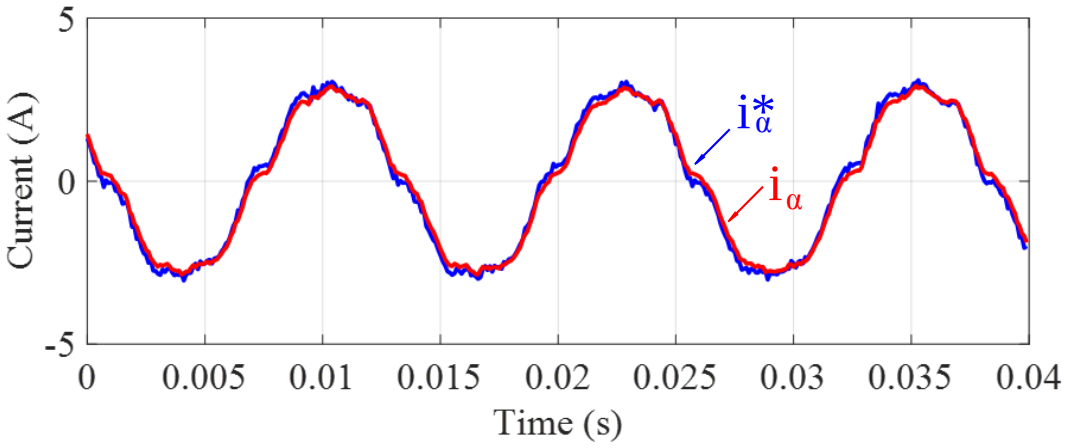

(a)

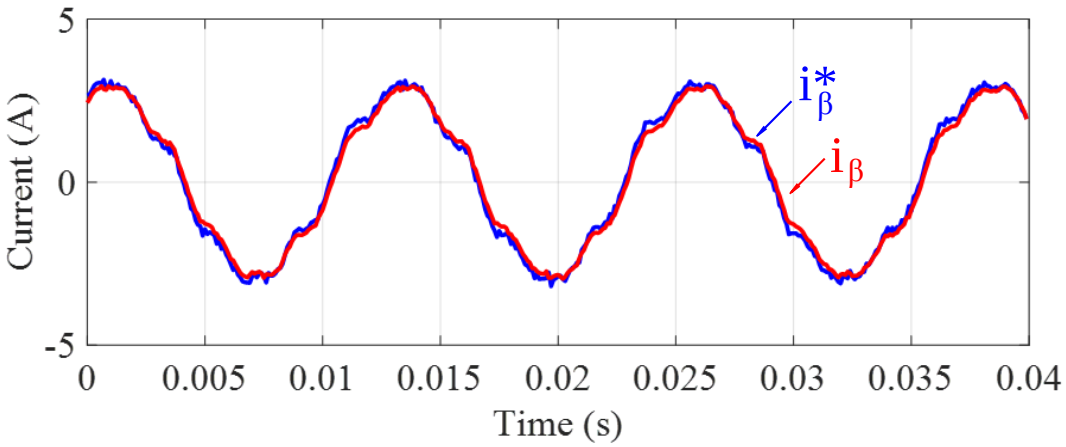

(b)

Figure 4.4. Simulation result of stator current in 1 turn short circuit fault condition. a) estimated current and measured current in alpha-axis, b) estimated current and measured current in beta-axis.

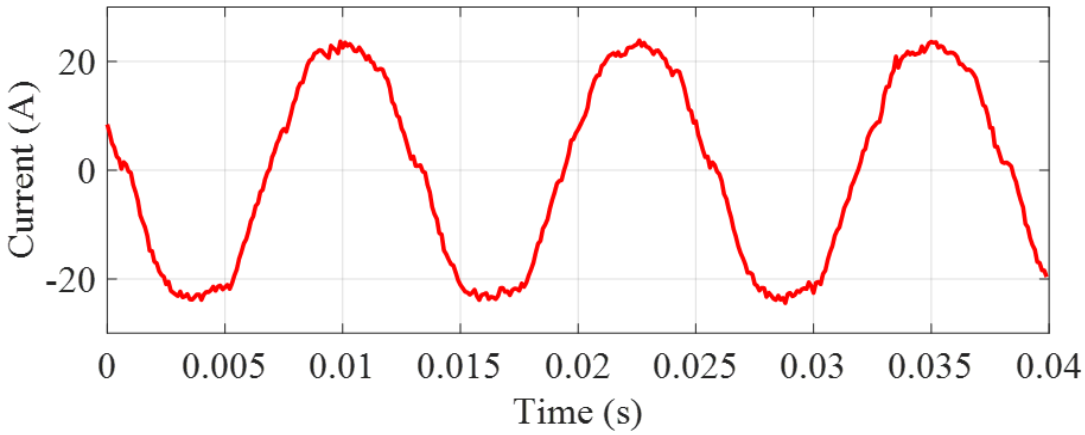

Figure 4.5. Simulation result of short circuit current in 1 turn short circuit fault condition.

Compared to (3.4), it can be seen that the fault index is cancelled out, except the differential term of short circuit current. Since the self-inductance of shorted turns is proportional to the power of number of shorted turns, the increasing fault index will decrease the short circuit current under this scenario. However, when the motor operates at low speed, this differential term has limited effect. Therefore, in this case, the short circuit current doesn't change significantly regarding to the fault index. But one can still see the amplitude of short circuit current decreases slightly as the fault index increasing, as shown in Table 4.1.

As listed in Table 4.1, the error between estimated short circuit current and actual value is in an acceptable range. The error may be due to the back-EMF estimator errors and inaccurate estimation of inductance. Consider 5 turns short circuit fault as an example. The mutual inductance between shorted turns and phase A winding is -15.4 μH and the mutual inductance between shorted turns and phase C winding is -42.2 μH. It means that the ITSC fault has different influence on other healthy windings. Thus, when the alpha-beta transformation is applied, there is also voltage variation on beta-axis. Therefore, the system accuracy is affected.

Table 4.1. Simulation results of short circuit current estimation with zero fault resistance

Speed 1200 RPM	1 turn short circuit fault	2 turn short circuit fault	5 turn short circuit fault
$\left\|\vec{\mathbf{e}}_{\alpha}\right\|$ (V)	31.4741	31.4705	31.4600
$\left\|\vec{\mathbf{e}}_{\beta}\right\|$ (V)	31.5004	31.5061	31.4972
$\angle\vec{\mathbf{e}}_{\alpha}-\angle\vec{\mathbf{e}}_{\beta}$ (°)	90.0530	89.0244	90.2770
$\left\|\vec{\mathbf{e}}_{\alpha}^{*}\right\|$ (V)	31.6028	31.2696	30.2259
$\left\|\vec{\mathbf{e}}_{\beta}^{*}\right\|$ (V)	31.9479	31.9440	31.9211
$\angle\vec{\mathbf{e}}_{\alpha}^{*}-\angle\vec{\mathbf{e}}_{\beta}^{*}$ (°)	89.5018	89.0122	87.6984
Actual $\left\|\vec{\mathbf{i}}_{s}\right\|$ (A)	24.3938	24.4231	24.3616
Estimated $\left\|\vec{\mathbf{i}}_{s}\right\|$ (A)	23.1659	22.7157	22.0594

4.4 Experimental Results

In order to verify the proposed method in real application, the proposed method is tested on the prototype ITSC fault PMSM and motor drive system mentioned in Chapter 2. The machine parameters are obtained based on signal injection algorithm at standstill condition. Since it is surface mounted PMSM, the synchronous inductance is determined by the d-axis inductance.

The line voltage is accessed via a resistor divider circuit and a RC filter. Proper compensation on fundamental component is applied in the software. The FOC is applied for speed regulation, where

the motor operates at constant speed with constant load. Since the excessive short circuit current can permanently damage the winding, the operating speed is limited to 1200 RPM and load torque is limited to 1 Nm, in order to limit the current amplitude.

The experimental results of different fault conditions are shown in Figure 4.6 to Figure 4.8, where the PMSM runs at 1200 RPM. According to the results, the error of measured current and estimated current is nearly zero, which proves the functionality of PI observer.

The experimental results of estimated current and back-EMF are close to the results given in the simulation. Due to the manufacturing imperfections and environment noise, there are certain distortions in the experimental results of estimated values, especially in the 5 turns short circuit case, which has the most number of turns shorted and highest short circuit current. However, compared to simulation results, the short circuit current amplitude decreases greatly under the same operating condition. It is caused by the non-zero fault resistance in the short circuit loop. Due to imperfect soldering and extra wires for measurement, there is 0.1 Ohm inherent resistance between the shorted nodes. Furthermore, one can notice that as the fault index increasing, the short circuit current increases. This phenomena is also caused by the non-zero fault resistance, which is considerable compared to the impedance of shorted turns. According to the analysis in previous section, the short circuit current is inversely proportional to the fault index when the fault resistance is zero. However, when the fault resistance is notably large, the increasing fault index will make short circuit current rise based on (3.4).

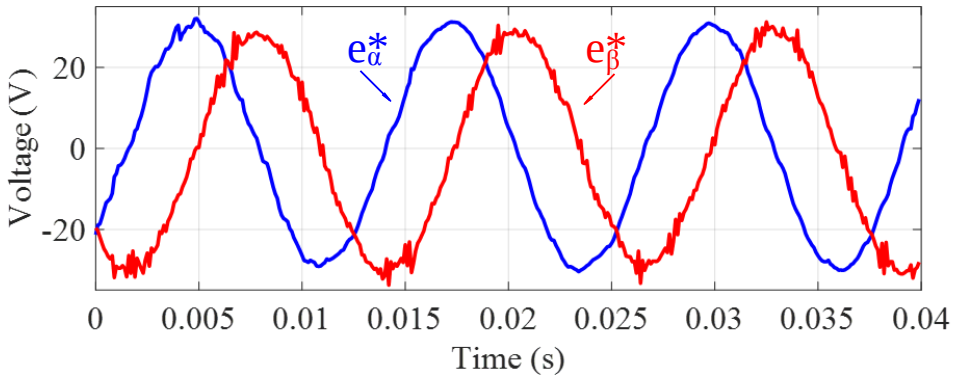

(a)

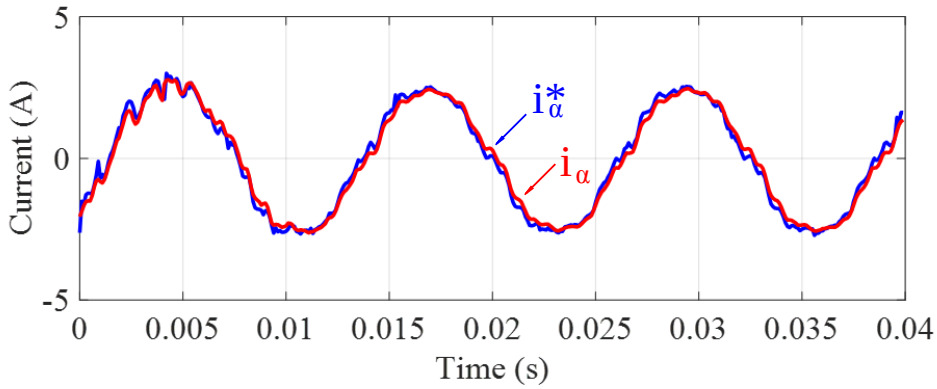

(b)

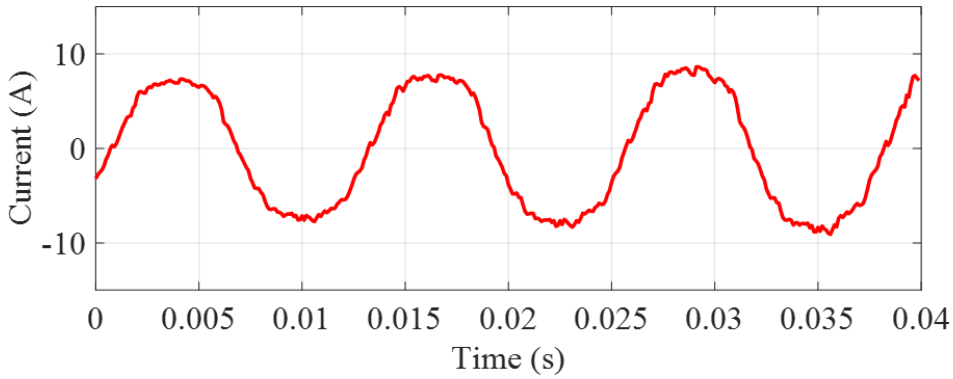

(c)

Figure 4.6. Experimental result of 1 turn short circuit fault condition at 1200 RPM. a) estimated back-EMF in alpha-beta reference frame, b) estimated current and measured current in alpha-axis, c) short circuit current is.

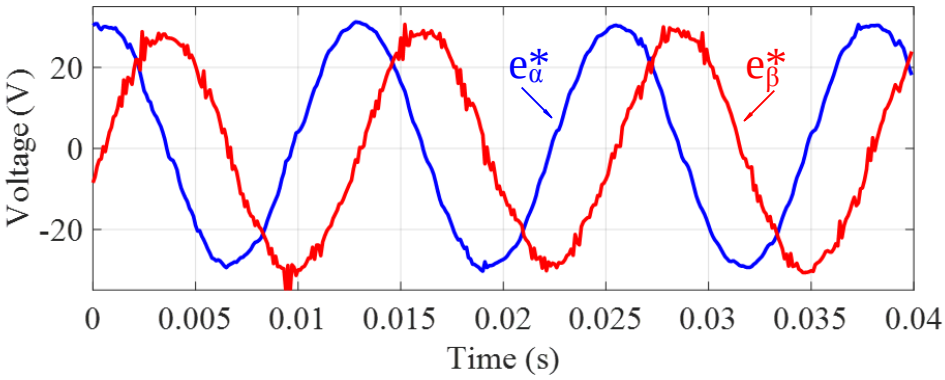

(a)

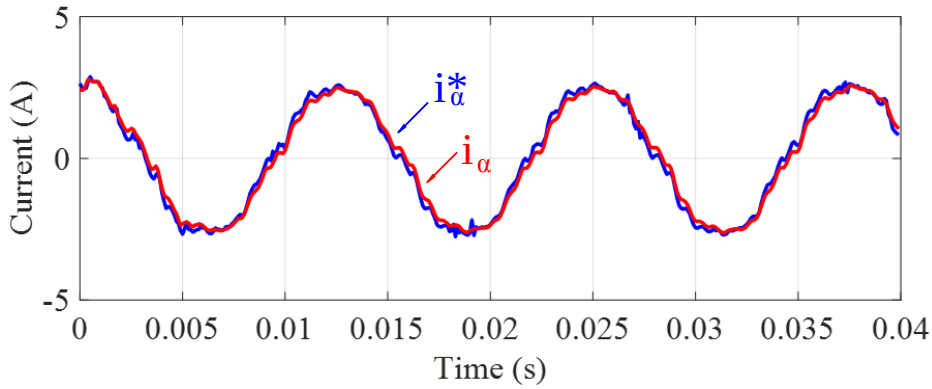

(b)

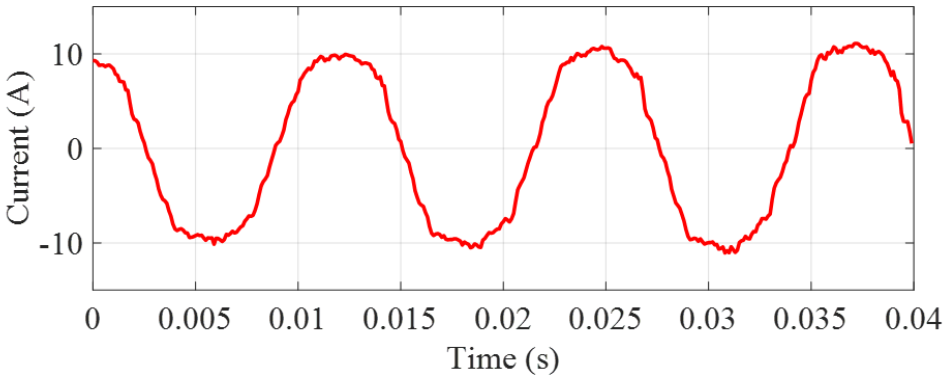

(c)

Figure 4.7. Experimental result of 2 turn short circuit fault condition at 1200 RPM. a) estimated back-EMF in alpha-beta reference frame, b) estimated current and measured current in alpha-axis, c) short circuit current is.

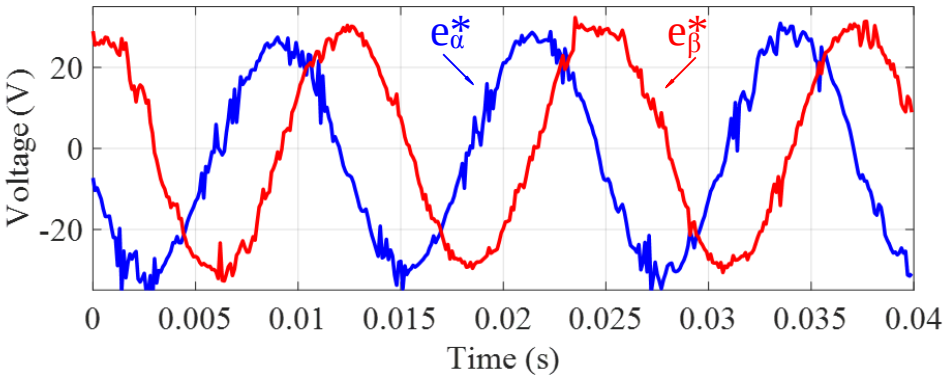

(a)

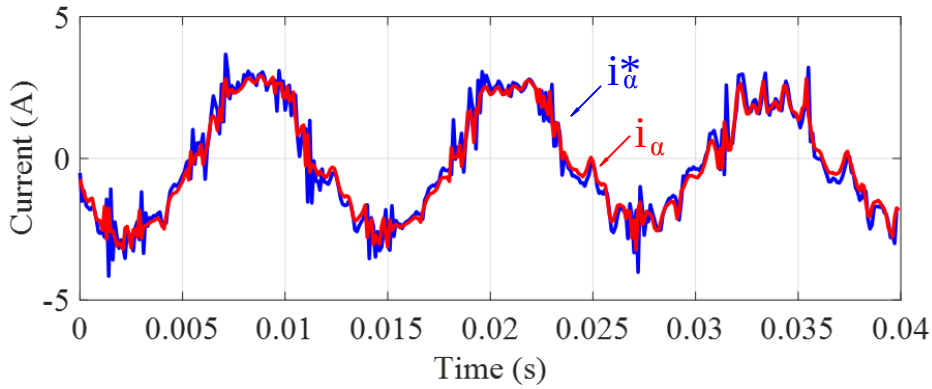

(b)

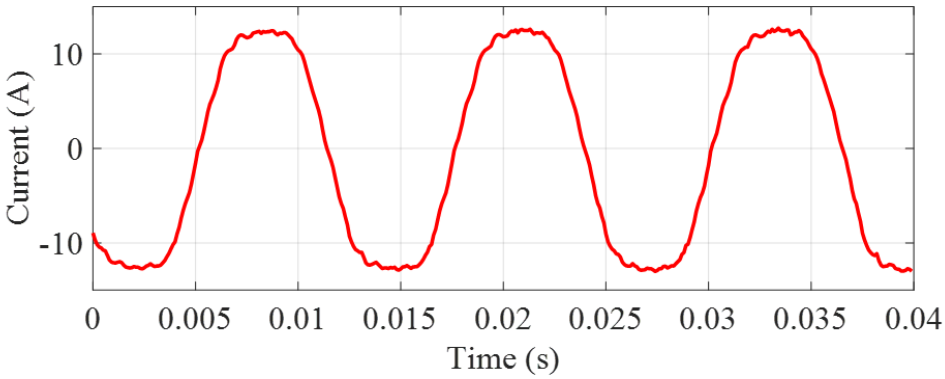

(c)

Figure 4.8. Experimental result of 5 turn short circuit fault condition at 1200 RPM. a) estimated back-EMF in alpha-beta reference frame, b) estimated current and measured current in alpha-axis, c) short circuit current is.

Table 4.2. Experimental results of short circuit current estimation with zero fault resistance at 1200 RPM

Speed 1200 RPM	1 turn short circuit fault	2 turn short circuit fault	5 turn short circuit fault
$\left\|\vec{\mathbf{e}}_{\alpha}^{*}\right\|$ (V)	30.0899	29.2387	22.4811
$\left\|\vec{\mathbf{e}}_{\beta}^{*}\right\|$ (V)	30.1991	29.4985	23.4587
$\angle\vec{\mathbf{e}}_{\alpha}^{*} - \angle\vec{\mathbf{e}}_{\beta}^{*}$ (°)	89.7844	89.4275	88.7496
Actual $\left\|\vec{\mathbf{i}}_{s}\right\|$ (A)	6.6939	9.1959	10.8729
Estimated $\left\|\vec{\mathbf{i}}_{s}\right\|$ (A)	7.8217	9.7321	10.9119
Speed 1200 RPM	1 turn short circuit fault	2 turn short circuit fault	5 turn short circuit fault
$\left\|\vec{\mathbf{e}}_{\alpha}^{*}\right\|$ (V)	30.0899	29.2387	22.4811
$\left\|\vec{\mathbf{e}}_{\beta}^{*}\right\|$ (V)	30.1991	29.4985	23.4587

Table 4.3. Experimental results of short circuit current estimation with zero fault resistance at 900 RPM

Speed 900 RPM	1 turn short circuit fault	2 turn short circuit fault	5 turn short circuit fault
$\left\|\vec{\mathbf{e}}_{\alpha}^{*}\right\|$ (V)	22.7081	22.4173	18.3123
$\left\|\vec{\mathbf{e}}_{\beta}^{*}\right\|$ (V)	22.8693	22.6787	19.1920
$\angle\vec{\mathbf{e}}_{\alpha}^{*} - \angle\vec{\mathbf{e}}_{\beta}^{*}$ (°)	89.7260	89.2831	88.9709
Actual $\left\|\vec{\mathbf{i}}_{s}\right\|$ (A)	5.4951	7.5511	9.5996
Estimated $\left\|\vec{\mathbf{i}}_{s}\right\|$ (A)	10.0857	9.9640	9.7617
Speed 900 RPM	1 turn short circuit fault	2 turn short circuit fault	5 turn short circuit fault
$\left\|\vec{\mathbf{e}}_{\alpha}^{*}\right\|$ (V)	22.7081	22.4173	18.3123
$\left\|\vec{\mathbf{e}}_{\beta}^{*}\right\|$ (V)	22.8693	22.6787	19.1920

The estimation results are given in Table 4.2. Due to the distortion, the fundamental component of back-EMF of 5 turns short circuit case decreases dramatically. However, it can be seen that the proposed estimation algorithms has good performance, especially in high short circuit current scenario. When the short circuit current is low, as in the 1 turn short circuit case, the estimation error is high. In this case, the voltage variation and back-EMF phase shift caused by ITSC fault are extremely small. As a result, it is difficult to estimate the short circuit current accurately with low short circuit current. In order to analyze the accuracy of the proposed method, an experimental is also carried out at 900 RPM and the results are given in Table 4.3. It can be seen that, the accuracy of the proposed method decreases from 5 turns fault to 1 turn fault, where the short circuit current drops from 9.5996 A to 5.4951 A. In 1 turn short circuit fault case, the estimation algorithm completely fails due to low short circuit current. However, in real application, the short circuit current is usually high due to the high operating speed and low fault resistance. As a result, it makes the voltage variation and phase shift more obvious and easy to be estimated accurately. On the other hand, the fault mitigation method requires precise estimation of short circuit current even in moderate conditions. Therefore, the threshold of voltage variation and back-EMF phase shift caused by ITSC fault must be defined properly based on machine parameters and system capability, in order to fulfill the requirement of fault mitigation algorithms.

4.5 Conclusion

This study proposes a novel method of estimating short circuit current for surface mounted PMSM with ITSC fault. The proposed method provides a new approach for fault severity monitoring in ITSC faults. By estimating and monitoring the short circuit current, the potential dangers of ITSC fault can be evaluated more effectively based on the current capacity of stator winding. It is more

meaningful than the algorithms considering only the number of shorted turns, because the stator winding and motor performance are affected by number of shorted turns and short circuit current simultaneously.

On the other hand, the proposed algorithm is beneficial for fault mitigation methods, which focus on suppressing short circuit current. It is important to obtain the short circuit current for evaluating the performance of mitigation. Furthermore, the monitoring the short circuit current can also help define the safe operating area, where the faulty machine is allowed to finish its duty with limited performance. However, in order to fulfill the requirement of these purposes, the accuracy of proposed method must be improved so that the short circuit current can be estimated successful in moderate fault condition.

CHAPTER 5

SUMMARY

In the past few years, PMSM has been extensively used in many industry applications, such as traction and auxiliary machine market, due to their high efficiency and high torque density. However, as the requirement of torque density increases, the PMSMs will be exposed to higher mechanical, thermal and electrical stress, which can increase the possibility of machine failures. Moreover, the uncontrolled permanent magnet excitation can further increase the potential of stator related fault in harsh operating environment. Therefore, the stator related fault of PMSMs should be taken care of with more effort.

The ITSC fault is one of the most critical stator related fault, since it is hard to be noticed and can easily transform to severe failures without proper treatment. Due to the small number of turns involved, the ITSC fault doesn't have obvious signatures and have little impact on machine performance. However, the low impedance and uncontrolled excitation of permanent magnet can generate excessive short circuit current, which can increase the thermal stress heavily on nearby turns. Without proper treatment, the insulation can be further damaged by the short circuit current and more turns can be involved. As a result, the ITSC can turn into phase to phase short circuit fault, phase to ground short circuit fault or open circuit fault, which can make the motor tripped over. In order to avoid the unexpected stop, the topic of ITSC fault detection has been analyzed extensively in many studies. Meanwhile, it also raises the demand of characterization and mitigation of ITSC fault for mission critical and safety critical system. In those applications, the unexpected maintenance and replacement is costly and need to be minimized. Therefore, proper

mitigation algorithm should be applied to drive the fault machine to finish the task with limited performance.

In this study, the behavior of short circuit current is analyzed in terms of number of shorted turns and fault resistance. It reveals that, under zero fault resistance condition, the short circuit current can be times of rated current even in low speed condition. Thus, in order to ensure the SOA, it is important to have the access to short circuit current that makes the most contributions to the insulation damage. Following the analysis, this study proposed a method to estimate the number of shorted turns. Compared to other methods, the proposed method eliminates the need for data collecting on artificial ITSC fault machine, which requires extra effort on re-winding and is not convenient for most applications. After the number of shorted turns is obtained, the short circuit current estimation algorithm is proposed based on the PI observer, which is used to calculate voltage variance caused by ITSC fault in back-EMF. According to the simulation and experimental result, the short circuit current level can be estimated successfully in the tested motor drive system. By the results of short circuit current estimation, the ITSC fault motor can be controlled to operate in SOA, which can minimize the risk of expanding existing fault severity. Moreover, the short circuit current estimation is also compatible with existing mitigation methods, which focus on suppressing the short circuit current. Through the estimation of short circuit current, the efficiency and effectiveness of mitigation algorithms can be further improved. As a result, the lifetime of ITSC fault machine can be extended.

REFERENCES

[1] B.-G. Gu, J.-H. Choi, and I.-S. Jung, "Development and Analysis of Interturn Short Fault Model of PMSMs With Series and Parallel Winding Connections," *IEEE Trans. Power Electron.*, vol. 29, no. 4, pp. 2016–2026, Apr. 2014.

[2] J. A. Rosero, L. Romeral, J. Cusido, A. Garcia, and J. A. Ortega, "On the short-circuiting Fault Detection in a PMSM by means of Stator Current Transformations," in *2007 IEEE Power Electronics Specialists Conference*, 2007, pp. 1936–1941.

[3] M. Khan and M. A. Rahman, "Development and Implementation of a Novel Fault Diagnostic and Protection Technique for IPM Motor Drives," *IEEE Trans. Ind. Electron.*, vol. 56, no. 1, pp. 85–92, Jan. 2009.

[4] G. Espinosa, J. A. Rosero, J. Cusido, L. Romeral, and J. A. Ortega, "Fault Detection by Means of Hilbert–Huang Transform of the Stator Current in a PMSM With Demagnetization," *IEEE Trans. Energy Convers.*, vol. 25, no. 2, pp. 312–318, Jun. 2010.

[5] J. Hang, J. Zhang, M. Cheng, and Z. Wang, "Fault diagnosis of mechanical unbalance for permanent magnet synchronous motor drive system under nonstationary condition," in *2013 IEEE Energy Conversion Congress and Exposition*, 2013, pp. 3556–3562.

[6] J.-K. Park and J. Hur, "Detection of Inter-Turn and Dynamic Eccentricity Faults Using Stator Current Frequency Pattern in IPM-Type BLDC Motors," *IEEE Trans. Ind. Electron.*, vol. 63, no. 3, pp. 1771–1780, Mar. 2016.

[7] S.-T. Lee and J. Hur, "Detection technique for stator inter-turn faults in BLDC motors based on third harmonic components of line currents," in *2015 IEEE Energy Conversion Congress and Exposition (ECCE)*, 2015, pp. 1899–1904.

[8] P. S. Barendse and P. Pillay, "A New Algorithm for the Detection of Faults in Permanent Magnet Machines," in *IECON 2006 - 32nd Annual Conference on IEEE Industrial Electronics*, 2006, pp. 823–828.

[9] O. Ogidi, P. S. Barendse, and M. A. Khan, "The detection of interturn short circuit faults in axial-flux permanent magnet machine with concentrated windings," in *2015 IEEE Energy Conversion Congress and Exposition (ECCE)*, 2015, pp. 1810–1817.

[10] Zhang, F. Wang, Z. Wang, and J. Yang, "Analysis of stator winding inter-turn short circuit fault of PMSM for electric vehicle based on finite element simulation," in *2014 IEEE Conference and Expo Transportation Electrification Asia-Pacific (ITEC Asia-Pacific)*, 2014, pp. 1–6.

[11] K.-H. Kim, B.-G. Gu, and I.-S. Jung, "Online fault-detecting scheme of an inverter-fed

permanent magnet synchronous motor under stator winding shorted turn and inverter switch open," *IET Electr. Power Appl.*, vol. 5, no. 6, p. 529, 2011.

[12] K.-H. Kim, "Simple Online Fault Detecting Scheme for Short-Circuited Turn in a PMSM Through Current Harmonic Monitoring," *IEEE Trans. Ind. Electron.*, vol. 58, no. 6, pp. 2565–2568, Jun. 2011.

[13] Y. Li and Y. Liang, "A comparative study on inter-tern short circuit fault of PMSM using finite element analysis and experiment," in *2015 International Conference on Advanced Mechatronic Systems (ICAMechS)*, 2015, pp. 290–294.

[14] Z. Qi and Y. Liang, "Evaluating the stator winding inter-tern short circuit fault of permanent magnet motor using FEA combined with experiment," in *2014 17th International Conference on Electrical Machines and Systems (ICEMS)*, 2014, pp. 1034–1038.

[15] M. A. S. Nejad and M. Taghipour, "Inter-turn stator winding fault diagnosis and determination of fault percent in PMSM," in *2011 IEEE Applied Power Electronics Colloquium (IAPEC)*, 2011, pp. 128–131.

[16] B. M. Ebrahimi and J. Faiz, "Feature Extraction for Short-Circuit Fault Detection in Permanent-Magnet Synchronous Motors Using Stator-Current Monitoring," *IEEE Trans. Power Electron.*, vol. 25, no. 10, pp. 2673–2682, Oct. 2010.

[17] J. A. Rosero, L. Romeral, J. A. Ortega, and E. Rosero, "Short-Circuit Detection by Means of Empirical Mode Decomposition and Wigner–Ville Distribution for PMSM Running Under Dynamic Condition," *IEEE Trans. Ind. Electron.*, vol. 56, no. 11, pp. 4534–4547, Nov. 2009.

[18] C. Wang, X. Liu, and Z. Chen, "Incipient Stator Insulation Fault Detection of Permanent Magnet Synchronous Wind Generators Based on Hilbert–Huang Transformation," *IEEE Trans. Magn.*, vol. 50, no. 11, pp. 1–4, Nov. 2014.

[19] Z. A. Ping, Y. Juan, and W. Ling, "Fault Detection of Stator Winding Interturn Short Circuit in PMSM Based on Wavelet Packet Analysis," in *2013 Fifth International Conference on Measuring Technology and Mechatronics Automation*, 2013, pp. 566–569.

[20] A. Mohammed, Z. Liu, S. Liu, and N. Y. Abed, "Internal Short Circuit Fault Diagnosis for PM Machines Using FE-Based Phase Variable Model and Wavelets Analysis," *IEEE Trans. Magn.*, vol. 43, no. 4, pp. 1729–1732, Apr. 2007.

[21] W. G. Zanardelli, E. G. Strangas, and S. Aviyente, "Identification of Intermittent Electrical and Mechanical Faults in Permanent-Magnet AC Drives Based on Time–Frequency Analysis," *IEEE Trans. Ind. Appl.*, vol. 43, no. 4, pp. 971–980, 2007.

[22] E. G. Strangas, S. Aviyente, and S. S. H. Zaidi, "Time–Frequency Analysis for Efficient Fault Diagnosis and Failure Prognosis for Interior Permanent-Magnet AC Motors," *IEEE Trans. Ind. Electron.*, vol. 55, no. 12, pp. 4191–4199, Dec. 2008.

[23] J. Yang, M. Dou, Z. Dai, J. Yang, M. Dou, and Z. Dai, "Modeling and Fault Diagnosis of Interturn Short Circuit for Five-Phase Permanent Magnet Synchronous Motor," *J. Electr. Comput. Eng.*, vol. 2015, pp. 1–9, 2015.

[24] F. Cira, M. Arkan, and B. Gumus, "A new approach to detect stator fault in permanent magnet synchronous motors," in *2015 IEEE 10th International Symposium on Diagnostics for Electrical Machines, Power Electronics and Drives (SDEMPED)*, 2015, pp. 316–321.

[25] Y. Nyanteh, C. Edrington, S. Srivastava, and D. Cartes, "Application of Artificial Intelligence to Real-Time Fault Detection in Permanent-Magnet Synchronous Machines," *IEEE Trans. Ind. Appl.*, vol. 49, no. 3, pp. 1205–1214, May 2013.

[26] Y. D. Nyanteh, S. K. Srivastava, C. S. Edrington, and D. A. Cartes, "Application of artificial intelligence to stator winding fault diagnosis in Permanent Magnet Synchronous Machines," *Electr. Power Syst. Res.*, vol. 103, pp. 201–213, Oct. 2013.

[27] Jeong, B. J. Hyon, and K. Nam, "Dynamic Modeling and Control for SPMSMs With Internal Turn Short Fault," *IEEE Trans. Power Electron.*, vol. 28, no. 7, pp. 3495–3508, Jul. 2013.

[28] Hang, S. Ding, J. Zhang, M. Cheng, W. Chen, and Q. Wang, "Detection of Interturn Short-Circuit Fault for PMSM With Simple Fault Indicator," *IEEE Trans. Energy Convers.*, vol. 31, no. 4, pp. 1697–1699, Dec. 2016.

[29] Yang, M. Dou, Z. Dai, D. Zhao, and Z. Zhang, "Modeling and fault diagnosis of inter-turn short circuit for five-phase PMSM based on Particle Swarm Optimization," in *2016 IEEE Applied Power Electronics Conference and Exposition (APEC)*, 2016, pp. 3134–3139.

[30] A. Mazzoletti, G. R. Bossio, C. H. De Angelo, and D. R. Espinoza-Trejo, "A Model-Based Strategy for Interturn Short-Circuit Fault Diagnosis in PMSM," *IEEE Trans. Ind. Electron.*, pp. 1–1, 2017.

[31] B. Du, S. Wu, S. Han, and S. Cui, "Interturn Fault Diagnosis Strategy for Interior Permanent-Magnet Synchronous Motor of Electric Vehicles Based on Digital Signal Processor," *IEEE Trans. Ind. Electron.*, vol. 63, no. 3, pp. 1694–1706, Mar. 2016.

[32] R. Z. Haddad and E. G. Strangas, "Detection of static eccentricity and turn-to-turn short circuit faults in permanent magnet synchronous AC machines," in *2015 IEEE 10th International Symposium on Diagnostics for Electrical Machines, Power Electronics and Drives (SDEMPED)*, 2015, pp. 277–283.

[33] K.-T. Kim, J. Hur, and G.-H. Kang, "Inter-turn fault analysis of IPM type BLDC motor using fault impedance modeling," in *8th International Conference on Power Electronics - ECCE Asia*, 2011, pp. 2216–2224.

[34] J.-K. Park, C.-L. Jeong, S.-T. Lee, and J. Hur, "Early Detection Technique for Stator Winding Inter-Turn Fault in BLDC Motor Using Input Impedance," *IEEE Trans. Ind. Appl.*, vol. 51, no. 1, pp. 240–247, Jan. 2015.

[35] Y. Qi, M. Zafarani, B. Akin, and S. Fedigan, "Analysis and Detection of Inter Turn Short Circuit Fault through Extended Self-Commissioning," *IEEE Trans. Ind. Appl.*, pp. 1–1, 2016.

[36] Leboeuf, T. Boileau, B. Nahid-Mobarakeh, N. Takorabet, F. Meibody-Tabar, and G. Clerc, "Estimating Permanent-Magnet Motor Parameters Under Inter-Turn Fault Conditions," *IEEE Trans. Magn.*, vol. 48, no. 2, pp. 963–966, Feb. 2012.

[37] Leboeuf, T. Boileau, B. Nahid-Mobarakeh, N. Takorabet, F. Meibody-Tabar, and G. Clerc, "Inductance Calculations in Permanent-Magnet Motors Under Fault Conditions," *IEEE Trans. Magn.*, vol. 48, no. 10, pp. 2605–2616, Oct. 2012.

[38] B. Vaseghi, N. Takorabet, and F. Meibody-Tabar, "Fault Analysis and Parameter Identification of Permanent-Magnet Motors by the Finite-Element Method," *IEEE Trans. Magn.*, vol. 45, no. 9, pp. 3290–3295, Sep. 2009.

[39] B. Vaseghi, B. Nahid-mobarakh, N. Takorabet, and F. Meibody-Tabar, "Inductance Identification and Study of PM Motor With Winding Turn Short Circuit Fault," *IEEE Trans. Magn.*, vol. 47, no. 5, pp. 978–981, May 2011.

[40] Z. Liu, O. A. Mohammed, and S. Liu, "FE-based physical phase variable model of PM synchronous machines under stator winding short circuit faults," *IET Sci. Meas. Technol.*, vol. 1, no. 1, pp. 12–16, Jan. 2007.

[41] W. Tang, G. Liu, and J. Ji, "Winding turn-to-turn faults detection of five-phase fault-tolerant permanent-magnet machine based on parametric model - IEEE Xplore Document," in *Electrical Machines and Systems (ICEMS), 2012 15th International Conference on*, 2012, pp. 1–6.

[42] S. Mezani, C. Gerada, L. Belguerras, J. Arellano-Padilla, P. Arumugam, and T. Hamiti, "Non-linear circuit based model of permanent magnet synchronous machine under inter-turn fault: a simple approach based on healthy machine data," *IET Electr. Power Appl.*, vol. 10, no. 6, pp. 560–570, Jul. 2016.

[43] J. Arellano-Padilla, M. Sumner, and C. Gerada, "On-line detection of stator winding short-circuit faults in a PM machine using HF signal injection," in *2008 18th International Conference on Electrical Machines*, 2008, pp. 1–8.

[44] J. Arellano-Padilla, M. Sumner, and C. Gerada, "Winding condition monitoring scheme for a permanent magnet machine using high-frequency injection," *IET Electr. Power Appl.*, vol. 5, no. 1, p. 89, 2011.

[45] S.-C. Yang, "On-Line Turn Fault Detection of Interior Permanent Magnet Machines Using the Pulsating-Type Voltage Injection," in *2015 IEEE Energy Conversion Congress and Exposition (ECCE)*, 2015, pp. 2200–2207.

[46] J. Arellano-Padilla, C. Gerada, and M. Sumner, "Condition monitoring approach for permanent magnet synchronous motor drives based on the INFORM method," *IET Electr. Power Appl.*, vol. 10, no. 1, pp. 54–62, Jan. 2016.

[47] H. S. and L. R. J. C. Urresty, J. R. Riba, "Detection of inter-turns short circuits in permanent magnet synchronous motors operating under transient conditions by means of the zero sequence voltage - IEEE Xplore Document," in *2011 14th European Conference on Power Electronics and Applications*, 2011, pp. 1–9.

[48] Y. Fan, W. Zhu, X. Zhang, and L. Zhang, "Stator winding inter-turn short circuit faults severity detection controlled by OW-SVPWM without CMV of five-phase FTFSCW-IPM," in *2015 18th International Conference on Electrical Machines and Systems (ICEMS)*, 2015, pp. 1192–1197.

[49] J. Hang, J. Zhang, M. Cheng, and J. Huang, "Online Interturn Fault Diagnosis of Permanent Magnet Synchronous Machine Using Zero-Sequence Components," *IEEE Trans. Power Electron.*, vol. 30, no. 12, pp. 6731–6741, Dec. 2015.

[50] M. van der Geest, H. Polinder, J. A. Ferreira, A. Veltman, J. Wolmarans, and N. Tsiara, "Analysis and neutral voltage based detection of inter-turn faults in high-speed permanent magnet machines with parallel strands," *IEEE Trans. Ind. Electron.*, vol. 62, no. 6, pp. 1–1, 2015.

[51] Y. Lee and T. G. Habetler, "An On-Line Stator Turn Fault Detection Method for Interior PM Synchronous Motor Drives," in *APEC 07 - Twenty-Second Annual IEEE Applied Power Electronics Conference and Exposition*, 2007, pp. 825–831.

[52] T. Boileau, N. Leboeuf, B. Nahid-Mobarakeh, and F. Meibody-Tabar, "Synchronous Demodulation of Control Voltages for Stator Interturn Fault Detection in PMSM," *IEEE Trans. Power Electron.*, vol. 28, no. 12, pp. 5647–5654, Dec. 2013.

[53] M. A. Awadallah, M. M. Morcos, S. Gopalakrishnan, and T. W. Nehl, "Detection of stator short circuits in VSI-fed brushless DC motors using wavelet transform," *IEEE Trans. Energy Convers.*, vol. 21, no. 1, pp. 1–8, Mar. 2006.

[54] M. Khov, J. Regnier, and J. Faucher, "Monitoring of turn short-circuit faults in stator of PMSM in closed loop by on-line parameter estimation," in *2009 IEEE International*

Symposium on Diagnostics for Electric Machines, Power Electronics and Drives, 2009, pp. 1–6.

[55] M. Khov, J. Regnier, and J. Faucher, "Detection of turn short-circuit faults in stator of PMSM by on-line parameter estimation," in *2008 International Symposium on Power Electronics, Electrical Drives, Automation and Motion*, 2008, pp. 161–166.

[56] H. Obeid, T. Boileau, and B. Nahid-Mobarakeh, "Modeling and diagnostic of incipient inter-turn faults for a three phase permanent magnet synchronous motor using wavelet transform," in *2015 IEEE Industry Applications Society Annual Meeting*, 2015, pp. 1–8.

[57] K.-T. Kim, S.-T. Lee, and J. Hur, "Diagnosis Technique Using a Detection Coil in BLDC Motors With Interturn Faults," *IEEE Trans. Magn.*, vol. 50, no. 2, pp. 885–888, Feb. 2014.

[58] J. Chai, J. Wang, K. Atallah, and D. Howe, "Performance Comparison and Winding Fault Detection of Duplex 2-Phase and 3-Phase Fault-Tolerant Permanent Magnet Brushless Machines," in *2007 IEEE Industry Applications Annual Meeting*, 2007, pp. 566–572.

[59] S.-T. Lee, K.-T. Kim, and J. Hur, "Diagnosis technique for stator winding inter-turn fault in BLDC motor using detection coil," in *2015 9th International Conference on Power Electronics and ECCE Asia (ICPE-ECCE Asia)*, 2015, pp. 2925–2931.

[60] M. Q. Zhang and K. J. Tseng, "An approach for on-line electrical machine winding inter-turn fault detection," in *2014 IEEE PES General Meeting | Conference & Exposition*, 2014, pp. 1–5.

[61] Y. Da, X. Shi, and M. Krishnamurthy, "A New Approach to Fault Diagnostics for Permanent Magnet Synchronous Machines Using Electromagnetic Signature Analysis," *IEEE Trans. Power Electron.*, vol. 28, no. 8, pp. 4104–4112, Aug. 2013.

[62] J. Ojeda, J. Boisson, and M. Gabsi, "5-phase flux switching machine insulation failure detection using vibration monitoring," in *2014 17th International Conference on Electrical Machines and Systems (ICEMS)*, 2014, pp. 1039–1043.

[63] Z. Yang, X. Shi, and M. Krishnamurthy, "Vibration monitoring of PM synchronous machine with partial demagnetization and inter-turn short circuit faults," in *2014 IEEE Transportation Electrification Conference and Expo (ITEC)*, 2014, pp. 1–6.

[64] T. Boileau, B. Nahid-Mobarakeh, and F. Meibody-Tabar, "Back-EMF Based Detection of Stator Winding Inter-turn Fault for PM Synchronous Motor Drives," in *2007 IEEE Vehicle Power and Propulsion Conference*, 2007, pp. 95–100.

[65] H. Saavedra, J.-R. Riba, and L. Romeral, "Inter-turn fault detection in five-phase pmsms. Effects of the fault severity," in *2013 9th IEEE International Symposium on Diagnostics for Electric Machines, Power Electronics and Drives (SDEMPED)*, 2013, pp. 520–526.

[66] J.-C. Urresty, J.-R. Riba, and L. Romeral, “Diagnosis of Interturn Faults in PMSMs Operating Under Nonstationary Conditions by Applying Order Tracking Filtering,” *IEEE Trans. Power Electron.*, vol. 28, no. 1, pp. 507–515, Jan. 2013.

[67] R. Z. Haddad and E. G. Strangas, “On the Accuracy of Fault Detection and Separation in Permanent Magnet Synchronous Machines Using MCSA/MVSA and LDA,” *IEEE Trans. Energy Convers.*, vol. 31, no. 3, pp. 924–934, Sep. 2016.

[68] F. Immovilli, C. Bianchini, E. Lorenzani, A. Bellini, and E. Fornasiero, “Evaluation of Combined Reference Frame Transformation for Interturn Fault Detection in Permanent-Magnet Multiphase Machines,” *IEEE Trans. Ind. Electron.*, vol. 62, no. 3, pp. 1912–1920, Mar. 2015.

[69] C. Bianchini, F. Immovilli, E. Lorenzani, A. Bellinil, and E. Fomasicro, “Experimental evaluation of combined reference frames transformation for stator fault detection in multi-phase machines,” in *2013 9th IEEE International Symposium on Diagnostics for Electric Machines, Power Electronics and Drives (SDEMPED)*, 2013, pp. 491–496.

[70] C. Bianchini, E. Fornasiero, T. N. Matzen, N. Bianchi, and A. Bellini, “Fault detection of a five-phase Permanent-Magnet machine,” in *2008 34th Annual Conference of IEEE Industrial Electronics*, 2008, pp. 1200–1205.

[71] Y. Li and Y. Liang, “The correlation analysis of PM inter-turn fault based on stator current and vibration signal,” in *2015 IEEE International Conference on Mechatronics and Automation (ICMA)*, 2015, pp. 1733–1737.

[72] Y. Liang, “Diagnosis of inter-turn short-circuit stator winding fault in PMSM based on stator current and noise,” in *2014 IEEE International Conference on Industrial Technology (ICIT)*, 2014, pp. 138–142.

[73] S. S. Refaat, H. Abu-Rub, M. S. Saad, E. M. Aboul-Zahab, and A. Iqbal, “Discrimination of stator winding turn fault and unbalanced supply voltage in permanent magnet synchronous motor using ANN,” in *4th International Conference on Power Engineering, Energy and Electrical Drives*, 2013, pp. 858–863.

[74] Min Dai, A. Keyhani and T. Sebastian, "Fault analysis of a PM brushless DC Motor using finite element method," in *IEEE Transactions on Energy Conversion*, vol. 20, no. 1, pp. 1-6, March 2005.

[75] B. G. Gu, Jun-Hyuk Choi and I. S. Jung, "A dynamic modeling and a fault detection scheme of a PMSM under an inter turn short," *2012 IEEE Vehicle Power and Propulsion Conference*, Seoul, 2012, pp. 1074-1080.

[76] H. Qian, H. Guo and X. Ding, "Modeling and Analysis of Interturn Short Fault in Permanent Magnet Synchronous Motors With Multistrands Windings," in *IEEE Transactions on Power Electronics*, vol. 31, no. 3, pp. 2496-2509, March 2016.

[77] F. Wu, P. Zheng and T. M. Jahns, "Analytical modeling of inter-turn short circuit for multiphase fault-tolerant PM machines with fractional-slot concentrated windings," *2015 IEEE Energy Conversion Congress and Exposition (ECCE)*, Montreal, QC, 2015, pp. 6970-6977.

[78] Z. Sun, J. Wang, D. Howe and G. Jewell, "Analytical Prediction of the Short-Circuit Current in Fault-Tolerant Permanent-Magnet Machines," in *IEEE Transactions on Industrial Electronics*, vol. 55, no. 12, pp. 4210-4217, Dec. 2008.

[79] L. Romeral, J. C. Urresty, J. R. Riba Ruiz and A. Garcia Espinosa, "Modeling of Surface-Mounted Permanent Magnet Synchronous Motors With Stator Winding Interturn Faults," in *IEEE Transactions on Industrial Electronics*, vol. 58, no. 5, pp. 1576-1585, May 2011.

[80] A. Sarikhani and O. A. Mohammed, "Inter-Turn Fault Detection in PM Synchronous Machines by Physics-Based Back Electromotive Force Estimation," in *IEEE Transactions on Industrial Electronics*, vol. 60, no. 8, pp. 3472-3484, Aug. 2013.

[81] K. H. Kim, D. U. Choi, B. G. Gu and I. S. Jung, "Fault model and performance evaluation of an inverter-fed permanent magnet synchronous motor under winding shorted turn and inverter switch open," in *IET Electric Power Applications*, vol. 4, no. 4, pp. 214-225, April 2010.

[82] T. Kim, H. W. Lee and S. Kwak, "The Internal Fault Analysis of Brushless DC Motors Based on the Winding Function Theory," in *IEEE Transactions on Magnetics*, vol. 45, no. 5, pp. 2090-2096, May 2009.

[83] Z. Gao, S. X. Ding and C. Cecati, "Real-time fault diagnosis and fault-tolerant control," *IEEE Transactions on Industrial Electronics*, vol. 62, no. 6, pp. 3752-3756, June 2015.

[84] M. Zafarani, E. Bostanci, Y. Qi, T. Goktas and B. Akin, "Inter-turn Short Circuit Faults in Permanent Magnet Synchronous Machines: An Extended Review and Comprehensive Analysis," *IEEE Journal of Emerging and Selected Topics in Power Electronics*, vol. 6, no. 4, pp. 2173-2191, Dec. 2018.

[85] Y. Qi, M. Zafarani and B. Akin, "A Diagnosis Procedure in Standstill Mode for Inter Turn Short Circuit Faults of PMSMs Through Modified Self-Commissioning," *2016 IEEE Energy Conversion Congress and Exposition (ECCE)*, Milwaukee, WI, 2016, pp. 1-7.

[86] Y. Qi, E. Bostanci, V. Gurusamy and B. Akin, "A Comprehensive Analysis of Short Circuit Current Behavior in PMSM Inter Turn Short Circuit Faults," IEEE Transactions on Power Electronics, vol. 33, no. 12, pp. 10784-10793, Dec. 2018.

[87] J. G. Cintron-Rivera, S. N. Foste and E. G. Strangas, "Mitigation of Turn-to-Turn Faults in Fault Tolerant Permanent Magnet Synchronous Motors," *IEEE Transactions on Energy Conversion*, vol. 30, no. 2, pp. 465-475, June 2015.

[88] R. M. Tallam, T. G. Habetler and R. G. Harley, "Transient model for induction machines with stator winding turn faults," in *IEEE Transactions on Industry Applications*, vol. 38, no. 3, pp. 632-637, May-June 2002.

[89] A. Berzoy, A. A. S. Mohamed and O. Mohammed, "Complex-Vector Model of Interturn Failure in Induction Machines for Fault Detection and Identification," in *IEEE Transactions on Industry Applications*, vol. 53, no. 3, pp. 2667-2678, May-June 2017.

[90] J. Hong *et al*., "Detection and Classification of Rotor Demagnetization and Eccentricity Faults for PM Synchronous Motors," *IEEE Transactions on Industry Applications*, vol. 48, no. 3, pp. 923-932, May-June 2012.

[91] A. M. EL-Refaie, "Fractional-Slot Concentrated-Windings Synchronous Permanent Magnet Machines: Opportunities and Challenges," *IEEE Transactions on Industrial Electronics*, vol. 57, no. 1, pp. 107-121, Jan. 2010.

[92] M. Andruşcă, M. Adam, R. Burlica, A. Munteanu and A. Dragomir, "Considerations regarding the influence of contact resistance on the contacts of low voltage electrical equipment," *2016 International Conference and Exposition on Electrical and Power Engineering (EPE)*, Iasi, 2016, pp. 123-128.

[93] C. M. Gheorghiţă, M. Adam, M. Andruşcă, A. Munteanu and A. Dragomir, "About contact resistance of the electrical equipment," *2017 International Conference on Modern Power Systems (MPS)*, Cluj-Napoca, 2017, pp. 1-4.

[94] A. Mohammadpour and L. Parsa, "A Unified Fault-Tolerant Current Control Approach for Five-Phase PM Motors with Trapezoidal Back EMF under Different Stator Winding Connections," IEEE Transactions on Power Electronics, vol 28, pages 3517-3527, 2013.

[95] A. Mohammadpour and L. Parsa, "Global Fault-Tolerant Control Technique for Multiphase Permanent-Magnet Machines," in IEEE Transactions on Industry Applications, vol. 51, no. 1, pp. 178-186, Jan.-Feb. 2015.

[96] P. Arumugam, T. Hamiti and C. Gerada, "Turn–turn short circuit fault management in permanent magnet machines," in *IET Electric Power Applications*, vol. 9, no. 9, pp. 634-641, 11 2015.

[97] A. Welchko, J. Wai, T. M. Jahns and T. A. Lipo, "Magnet-fluxing control of interior PM Machine drives for improved steady-state response to short-circuit faults", *Industry Applications IEEE Transactions* on, vol. 42, pp. 113-120, 2006.

[98] H. Kim, J. Son and J. Lee, "A High-Speed Sliding-Mode Observer for the Sensorless Speed Control of a PMSM," in *IEEE Transactions on Industrial Electronics*, vol. 58, no. 9, pp. 4069-4077, Sept. 2011.

[99] D. Söffker, T. J. Yu and P. C. Müller, "State estimation of dynamical systems with nonlinearities by using proportional-integral observer", *International Journal of Systems Science* 26 (9), 1571-1582, 1995.

BIOGRAPHICAL SKETCH

Yuan Qi received his B.E. degree in automation from Shandong University, Jinan, China, in 2013 and M.S. degree in electrical engineering from The University of Texas at Dallas, Richardson, in 2015. He is currently working toward the Ph.D. degree at The University of Texas at Dallas Richardson, TX, USA. In 2014, he joined the Power Electronics and Drives Laboratory in the Engineering and Computer Science Department at The University of Texas at Dallas. His research interests include variable speed motor drives and fault diagnoses in PM motors.

CURRICULUM VITAE

Yuan Qi

EDUCATION & PROFESSIONAL DEVELOPMENT

Ph.D. in Electrical Engineering, The University of Texas at Dallas (GPA: 3.8/4)

Sept. 2015 – Dec. 2018 (Expected)

Dissertation: Diagnosis of Inter Turn Short Circuit Fault in Permanent Magnet Synchronous Machines

M.S in Electrical Engineering, The University of Texas at Dallas (GPA: 3.8/4)

Sept. 2013 – May. 2015

Thesis: Parameter Identification and Automatic Loop tuning for Permanent Magnet Synchronous Motors

B.S. in Automation, Shandong University, China (GPA: 84/100)

Sept. 2009 - Jun. 2013

RELEVANT EXPERIENCE (SELECTED)

Student Worker & Research Assistant at Power Electronics Lab, The University of Texas at Dallas **Jan. 2014 - Present**

- Health Monitoring and Diagnostics for PMSM (sponsored by Schlumberger Technology Corporation)
    - PMSM modeling with stator fault in FEM simulation (Ansys Maxwell) and motor drive modeling in system simulation (Ansys Simpleror)

    - Develop multiple diagnosis algorithms for stator fault on PMSMs, including motor current signature analysis (MCSA) and parameter identification analysis.
    - Comprehensive analysis of proposed detection algorithms on sensitivity, ease of implementation and characteristics in different working conditions.
    - Experimental validation and tests on different platforms
- Automatic Tuning for PMSM Drive System (sponsored by Active-Semi International Inc.)
    - Develop and implement automatic parameter identification methods for PMSMs, including resistance, inductance, back-emf and inertia.
    - Develop and implement automatic PI tuning for FOC based on system pole-zero placement.
- PMSM sensorless control (sponsored by Active Semi)
    - •Build the sliding model back-emf estimator and test in sensorless FOC
    - Inductance characterization of PM machines (sponsored by Texas Instrument)
    - •FEM model development of PM machines with different current levels
    - •Analysis on the saturation effect in terms of machine geometry parameters
    - •Analysis on the spatial harmonics in inductance
- Research in PMSM fault diagnosis
    - Reduce order modeling of PMSM in system simulation with considering saturation effect and parameter variance at different rotor positions
    - Develop advanced fault severity detection method and short circuit current estimation algorithm of stator fault PMSM

- Analytical and experimental investigation of leakage flux on stator fault PMSM with integrated flux gate sensor

Electrical Engineer Intern at Schlumberger Technology Corporation

May. 2018 – Aug. 2018

- Real time Stator Fault Detection for PMSM
  - Reduce order modeling of PMSM with stator fault in Matlab/Simulink environment
  - Develop real-time solutions of motor current signature analysis (MCSA) and provide executable C code
  - Real time test of the proposed methods with Piccolo TMS320F28335 MCU
  - Comprehensive case study of the proposed methods in different operating conditions

PUBLICATIONS

Journal Publication

[1] Y. Qi, M. Zafarani, B. Akin and S. E. Fedigan, "Analysis and Detection of Inter-Turn Short-Circuit Fault Through Extended Self-Commissioning," in *IEEE Transactions on Industry Applications*, vol. 53, no. 3, pp. 2730-2739, May-June 2017.

[2] Y. Qi, E. Bostanci, V. Gurusamy, and B. Akin, " A Comprehensive Analysis of Short Circuit Current Behavior in PMSM Inter Turn Short Circuit Faults," in *IEEE Transactions on Power Electronics* vol. 33, no. 12, pp. 10784-10793, Dec. 2018.

[3] M. Zafarani, E. Bostanci, Y. Qi, T. Goktas and B. Akin, "Inter-turn Short Circuit Faults in Permanent Magnet Synchronous Machines: An Extended Review and Comprehensive Analysis"

in *IEEE Journal of Emerging and Selected Topics in Power Electronics*, vol. 6, no. 4, pp. 2173-2191, Dec. 2018.

[4] Y. Qi, E. Bostanci, M. Zafarani and B. Akin, " Severity Estimation of Inter Turn Short Circuit Fault for PMSM," in *IEEE Transactions on Industry Electronics*. (in press)

Conference Publication

[1] Y. Qi, M. Zafarani and B. Akin, "A diagnosis procedure in standstill mode for inter turn short circuit faults of PMSMs through modified self-commissioning," 2016 IEEE Energy Conversion Congress and Exposition (ECCE),Milwaukee, WI, 2016, pp. 1-7.